Division of Structural and Fire Engineering
Department of Civil, Environmental and Natural Resource Engineering
Luleå University of Technology, Sweden

Post Elastic Behaviour and Moment Redistribution in a Double Span LTP200 Steel Trapezoidal Sheet

Author: Attiq Ur Rahman Dogar

Supervisor: Naveed Iqbal, Ph.D.

European Commission
ERASMUS MUNDUS

Study Program: SUSCOS_M
Academic Year: 2016-18

ACKNOWLEDGEMENT

This dissertation work is done as a partial fulfilment of my Master Degree under the Erasmus Mundus Master Program SUSCOS (Sustainable Constructions under Natural Hazards and Catastrophic Events) for the academic year 2016-18. This thesis work was done under the Division of Structural and Fire Engineering at Luleå University of Technology, Sweden.

I would like to express deepest gratitude to my thesis supervisor, Ph.D. Naveed Iqbal for consulting the Lindab Engineering to make this research possible. His devotion towards helping in research and open door policy had been really helpful and made it easy for me to complete the work in allotted time.

I want to thank Lindab International for providing me the opportunity to do research on one of their products and providing the material for experimental tests. I would give credit to Jan-Christer Mäki, Development Engineer at Lindab International for assisting me throughout the dissertation work. His dedication towards explaining the principles and interpreting the experimental results was exceptional. I want to thank Erik Andersson from LTU Laboratory and Kenneth Palo from Lindab, who along-with Jan-Christer helped me setting up the laboratory test setup.

I want to thank all my Professors and colleagues from SUSCOS program for sharing their knowledge with me and enhancing my skills.

I want to thank my parents and family members for providing me moral support throughout this program and made me believe in myself.

Finally, I am thankful to GOD Almighty ALLAH for everything I have in my life.

ABSTRACT

Cold Formed Steel Trapezoidal sheets are very popular in Sweden as a roofing system for stadiums and arenas. To effectively utilize the span and field moment capacities, Lindab International uses Gerber system of joints for one of their products LTP200 Trapezoidal Profile. In this joint, a hinge is placed in span at a predefined location near the internal support where the bending moment is theoretically zero.

Within the working limit states, this joint works very well as it is not subjected to any moments. But as the section over the mid-support fails, the stiffness of this section decreases dramatically and so does its moment capacity, which is normally the case with cold formed section. As the moment capacity of this section drops, there is a redistribution of bending moments in the whole system and the joint will be subjected to moments in this post elastic scenario.

Previously, the joint was not able to sustain these bending moments. Now, Lindab is modifying the design of this joint by using a combination of screws and sheet overlap. In this design, the joint will work as a hinge in working limit states, but as the section over mid-support fails, contribution of overlap is attained and the joint will now work as continuous sheet. The amount of moments this joint is subjected to; depends on the variation of stiffness of the section over mid-support and reserve capacity of this section.

The aim of this thesis is to study the behaviour of the section over mid-support after its elastic limit and make conclusions about inelastic reserve capacity and stiffness variation. In the end, a moment redistribution diagram will be made for a double span system at ultimate state which will enable the design of joint against the varying internal forces.

Table of Contents

List of Tables

List of Figures

Symbols and Abbreviations

CFS	Cold Formed Steel
FEM	Finite Element Modelling
c/c	Centre to Centre
E	Modulus of Elasticity
K	Stiffness
ε	Strain
kN	kilo-Newton
f_y	Yield Stress
σ	Stress
f_{yb}	Yield stress of the base element
f_u	Ultimate Stress
M_{el}	Elastic Moment
M_{pl}	Plastic Moment
M_c	Moment capacity
r_j	Internal radius of the rounded corner
$\emptyset_j$	Angle between two plane elements
$b_{p,i}$	Notional flat width of plane elements in cross section
A_g	Gross Section properties with rounded corners
A_{red}	Reduced Area
I_g	Gross Section Properties with sharp corners
$A_{g,sc}$	Gross Section properties with rounded corners
$I_{g,sc}$	Gross Section Properties with sharp corners
W	Section Modulus
W_{eff}	Effective Section Modulus
ρ	Reduction Factor for effective width
$\bar{\lambda}_p$	Slenderness of the plane part
χ_d	Reduction Factor for slenderness

1. Introduction

The first chapter of thesis report aims to describe the background of the issue, particular focus of this research work and how it contributes to overall problem. The organization of this thesis report is presented at the end of this chapter.

1.1 Background

In Sweden, a number of roofs made with the corrugated sheets collapsed during the winters of 2009/2010 and 2010/2011. The Swedish National Board of Housing, Building and Planning [Boverket] carried out an extensive study to investigate the reason of this collapse (SJÖLANDER & TIDERMAN, 2016). In their investigation, they found a lot of reasons linked to the design and construction practices for the corrugated sheet, but all the sheets designed with Gerber system failed, that put the a question mark on the validity of this system.
Gerber System also known as cantilever drop-in system uses a hinge in span at the location of theoretical zero bending moment to optimally distribute the bending moment in a continuous beam. This optimal distribution has economic benefits as the section in the span and above the internal support is subjected to reduced internal forces and is thus effectively used. Due to its economy and ease of installation, this system is mostly preferred by the manufacturers.
The problem with the Gerber joint is that it works well under the static loads for which it is designed, but it is very sensitive to uneven distribution of loads which is mostly the case with snow loads. Similarly, this system is also sensitive to redistribution of moments in case of failure of a section in its vicinity as the designed joint is unable to carry the bending moments it is imposed to. Due to its deficiency in aforementioned concerns, this system is prohibited for use in Sweden.

1.2 Purpose of the study

The support for this thesis has been provided by “Luleå University of Technology” and “Lindab International” for the study of a trapezoidal sheet LTP200 manufactured by Lindab International. LTP200 is a single bay trapezoidal steel sheet used for roof decking and was often used together with the Gerber-system which is now prohibited. To use this sheet for a continuous system, a modified joint named as “Maeki-Gerber Joint” is being designed and tested.
The ultimate aim of this thesis is to study the post failure behaviour of LTP200 trapezoidal sheet section over mid-support and its effect on moment redistribution in a two span system to aid in designing the “Maeki-Gerber Joint”.

1.3 Problem Statement

Recent trends in the construction industry show the advancement in the use of cold-formed steel sections due to their numerous advantages over other construction materials. One of the main types of the cold formed steel section is a trapezoidal sheet that is normally employed as roof decking. A lot of manufacturers of these trapezoidal sheeting are present in the market who continue using different techniques to employ these sections effectively. LHP 200 is one of the prominent steel trapezoidal sheets manufactured by Lindab International. LHP 200 profile is used as a roof decking for stadiums, arenas and other large span buildings. To effectively use the material, Gerber system of joint was often employed for the continuous span of this sheet. This Gerber system also known as cantilever drop-in system is a technique in which a hinged joint is located in the span at the desired location instead of over the support due to which the bending moments are optimally distributed in the system (figure 1).

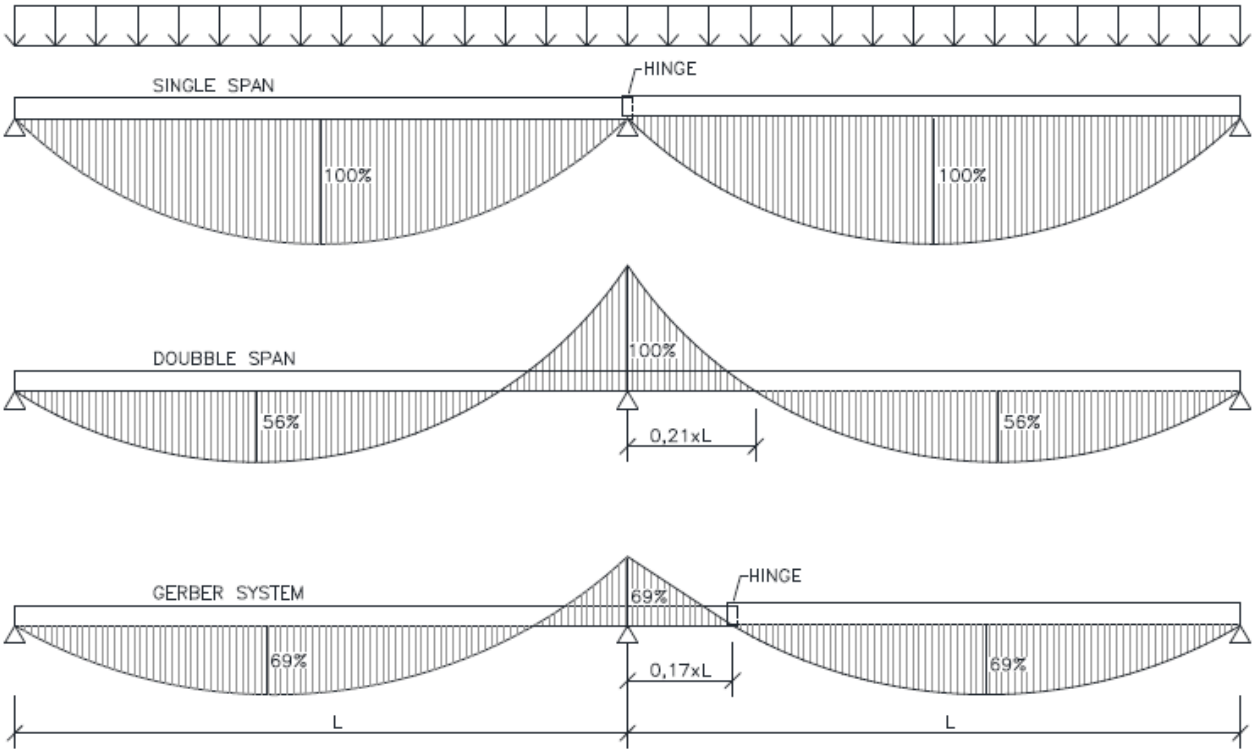

Figure 1. Principle of Gerber joint to optimally distribute bending moments[1]

After the collapse of all the roofs designed using Gerber system of joints, the Gerber system was prohibited to be used. In case of accidental loads i.e. Snow loads, behaving as a pin, this joint is sensitive to collapse over mid-support. The internal forces in the hinged joint depend on the stiffness of the section over the mid-support. Under the working limit state, the section has 100% stiffness and the joint behaves as a perfect hinge and is not subjected to

[1] Document Provided by Jan Christer Mäki

bending moments. As the section over the mid-support fails, the stiffness of the section start varying thus redistributing the moments in the system. Due to this redistribution, the joint will now be subjected to bending moments. To prevent the progressive collapse, the joint must behave as a continuous sheet in case of collapse over mid-support till ultimate capacity of section at support or mid-span. The optimized joint will act as a Gerber joint under normal conditions but as a continuous sheet in case of collapse over mid-support.

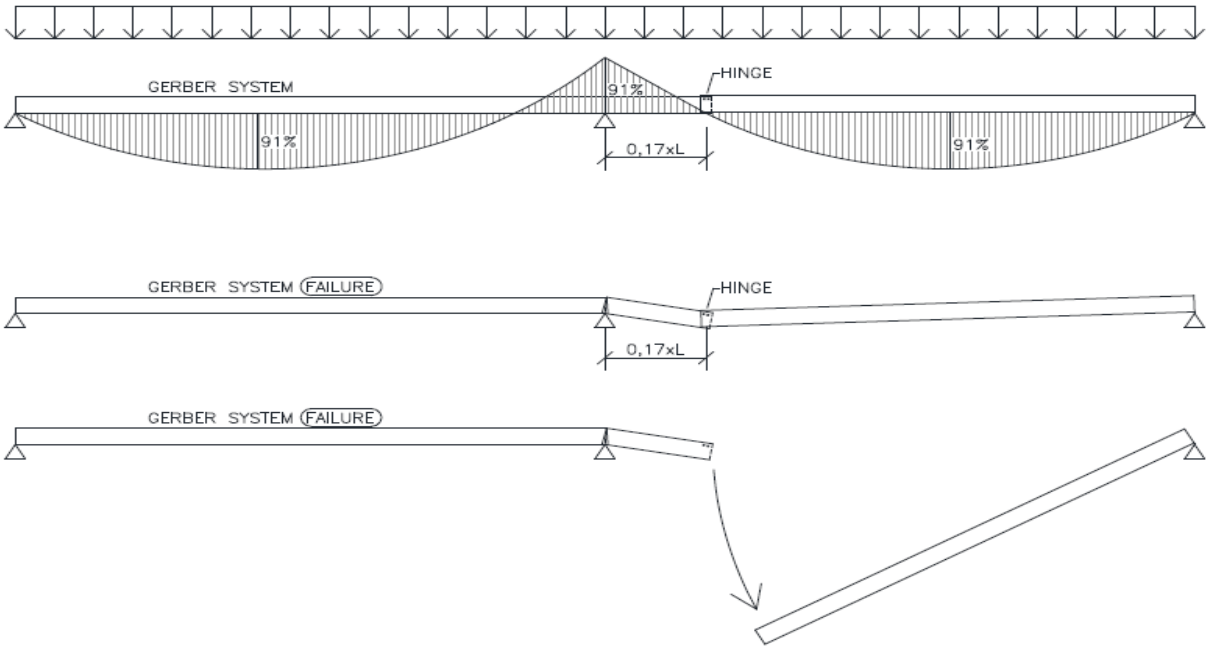

Figure 2. Collapse of Hinge due to Internal Support Failure[2]

1.4 Scope & Objective

The main objective of this thesis is to study the behaviour of the section over mid-support and resulting stiffness variation. This variation of stiffness will enable to evaluate forces the joint is subjected to till the collapse of the system.
The complete aim of the study can be divided into following steps:

- Predicting the load carrying capacity of the section and the associated buckling modes.
- Studying the post yield behaviour and residual moment capacity of the section over mid-support.
- Evaluating the variation of stiffness of the section and make conclusions regarding the moment redistribution in the system after the failure of section over mid-support.

In order to achieve the aforementioned objectives, thesis work will include:

[2] Document Provided by Jan Christer Mäki

- Finite Element Modelling of the system using ABAQUS software
- Theoretical Analysis of the system
- Full Scale Experimental tests
- Comparison and interpretation of results.

1.5 Organization of Report

This dissertation report consists of 6 chapters. The background of problems, study objectives and the scope of work has already been defined in this chapter. The structure of the report has also been outlined below.

Chapter 2 deals with the literature that was reviewed to carry out this work. It includes the details regarding cold formed steel section, problems related with the design of such section and European guidelines to tackle those problems and design rules. It also includes the theory of moment redistribution in cold formed and stockier sections.

Chapter 3 describes the experimental tests that were performed at Luleå University of Technology in detail. The test performed on each sample, the failure modes and the resulting load-displacement diagrams are presented in this chapter.

Chapter 4 includes the development of numerical model to carry out this research. It describes the different modules and the assumptions related to each of them in Abaqus software. At the end of this chapter, the failure modes in the software are compared with those of experimental tests.

Chapter 5 includes the analytical calculations that were carried out from the data obtained from chapter 3 and 4. First, it gives the methodology that was used to calculate the reserve capacities, stiffness variation and in the end, results are shown in the form of redistributed bending moment diagrams.

Chapter 6 gives the conclusions that were made from this thesis and recommendation are also presented for further study.

2. State of the art

2.1 Cold Formed Steel

2.1.1 Trends in usage and manufacture of cold formed sections

The global construction practices are now evolving which in turn demands for use of sophisticated materials. The industry now demands the materials which are environmental friendly and lightweight for the ease of transportation and construction. Due to such dynamic trends, cold formed steel is being utilized more because of its advantages over the other construction materials. However, the design and construction of cold-formed steel structures is quite different because of their weight and thinness. This increased demand and peculiar design characteristics require continuous research and development for their effective use. This chapter will focus on the evolution in shapes, design criteria and failures of trapezoidal sheets only due to the scope of this study.

Cold Formed Steel (CFS) refers to the type of steel products that is made by rolling or bending thin gauges of steel sheets into desired shapes. This bending is done at the room temperature which is its main difference from the other type i.e. hot rolled steel which is normally done at elevated temperatures. The other difference is the thickness of material as CFS is quite thin and lightweight. This manufacturing of cold formed steel sheets can be done by two processes:

- Roll Forming
- Brake Forming

2.1.2 Advantages of the CFS

During the last few decades, construction using CFS is gaining popularity because of the development of design standards and its advantages over other types of construction materials. The main advantages of using CFS are:

- Rolling into the desired shapes and lengths and that too with close tolerances.
- Lightness in weight with very high strength to weight ratio
- Ease of production, transportation and fast and easy erection and installation.
- Ease of detailing and dimensional accuracy
- Durable for a long period of time due to zinc coating applied that can last long
- Impervious to termites and rot
- Highly favoured by green building programs due to its recycling qualities positive Sustainability impacts

2.1.3 Types of CFS

The CFS has quite vast structural and non-structural applications. For structural, CFS is available in a number of shapes depending on the load requirements and location of use within a structure.

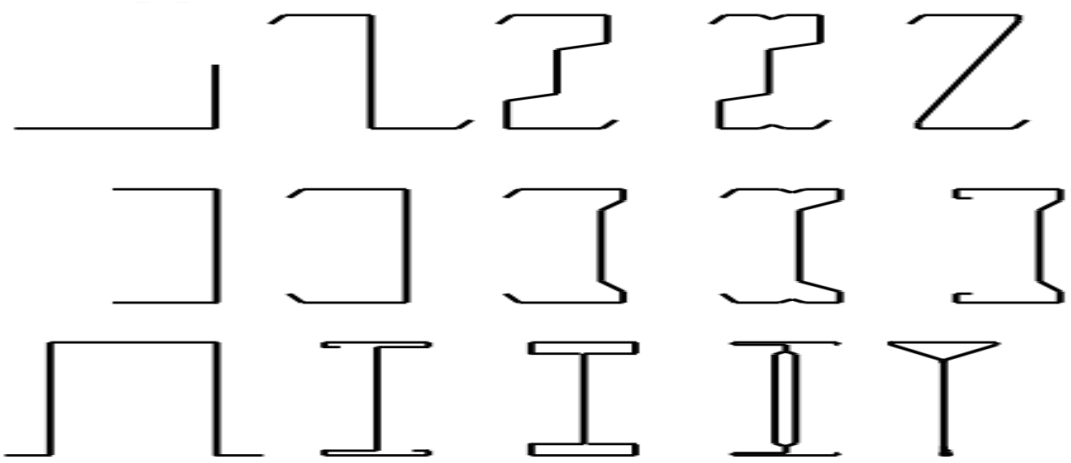

Figure 3. Single Open Cold Formed Section

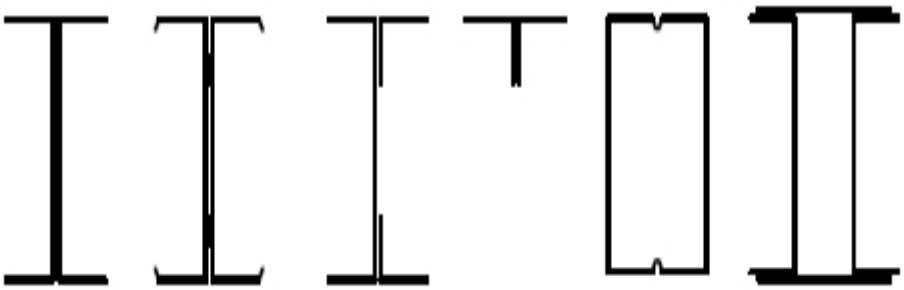

Figure 4. Cold Formed Steel built up sections

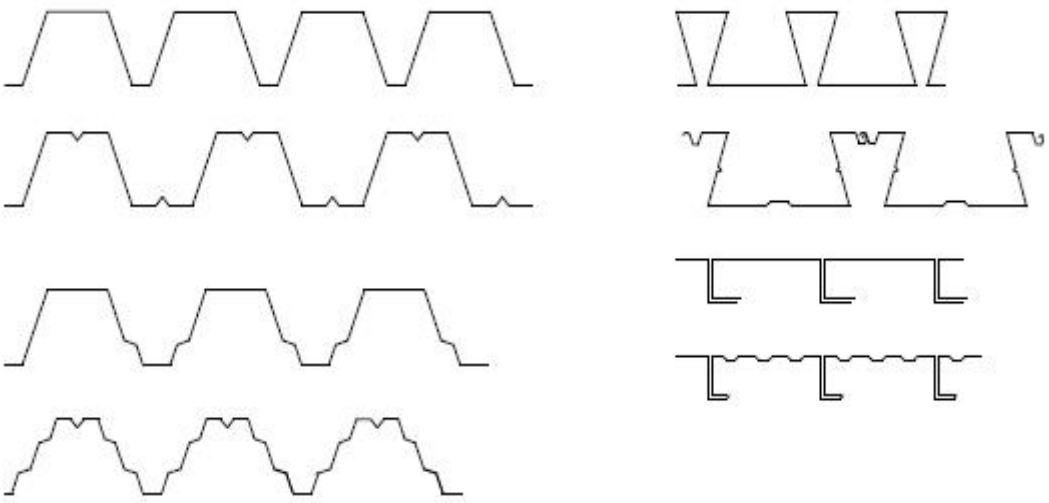

Figure 5. Trapezoidal Profiled Sheets and Liner Trays

2.1.4 Roof Decking Types

Among all these types of Cold Formed Steel sections, profiled sheets (figure 5) are used as roof decking system. Cold Formed Trapezoidal Sheets are manufactured by rolling or press-braking the steel sheets in desired shapes of profiled sheets or liner trays. They are used as

a building envelope where they can either be employed as roofing or wall cladding. The profiled sheets have a very small thickness in the range of 0.4-2mm and the depth of section can be in the range of 20-200mm.

This type of roofing system is gaining importance because of its economic efficiency and quick and safe erection. During the erection stage of construction, this type of roof decking provides a formwork as well as can be used as a working platform. These profiles sheets can be used in either of the two ways mentioned below:

1. Single skin systems:

This type of roofing consists of a single profiled sheet attached to either purlin or the supporting beam (figure 6). It is normally used where no insulation is required but in some cases, insulation is suspended directly beneath the sheeting. These types of systems are mostly used for warehouses, industrial or agricultural buildings.

2. Built-up Double Skin System:

This type of system is built up from their constitutive parts (figure 7). It consists of metal liner, a layer of insulation, spacer system and external metal sheet. This type of system is used where there are insulation requirements.

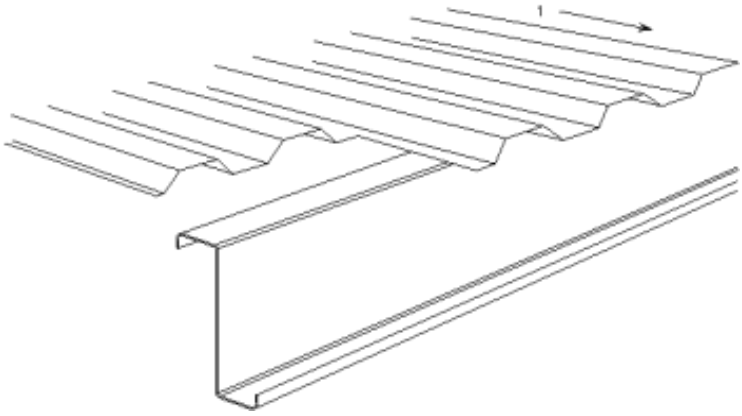

Figure 6. Single skin CFS Trapezoidal Sheets

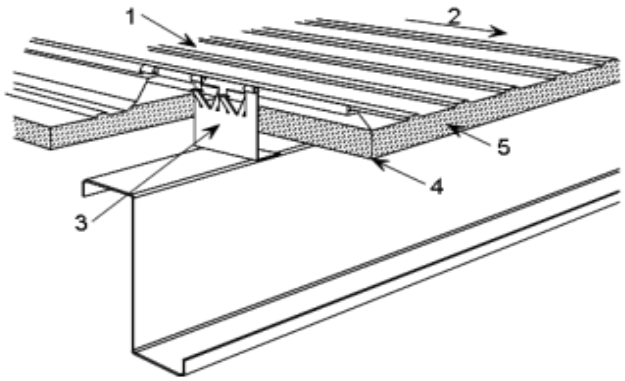

1 Outer sheeting
2 Slope
3 Standing seam clip
4 Inner sheeting
5 Insulation

Figure 7. Built Up double skin CFS sections

The profiled sheets that are available in the market can be divided into three generations depending on their shapes. These shapes affect the load carrying capacity and failure modes consequently deciding the spans the particular generation can be used for.

1. First Generation: The simplest trapezoidal sheets that are made with plane section parts. They are used for the spans ranging 3-6m.
2. Second Generation: The trapezoidal sheets which are stiffened by grooves in the flanges or folds in the webs to improve the load carrying capacity. They are used for the spans ranging 4-8m.
3. Third Generation: The trapezoidal sheets which use combination of longitudinal (flange grooves & web folds) and transversal (grooves) stiffening. They are used for the spans ranging 6-12m.

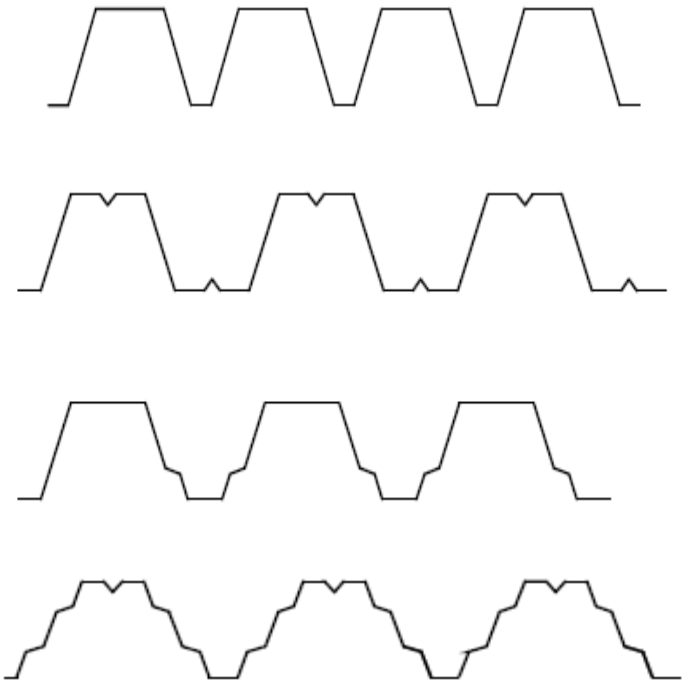

Figure 8. Generations of CFS Trapezoidal Sheets

2.1.5 LTP200 Profile

The types of roof decking differ according to their intended use and the load carrying requirements. Due to which a variety of roof decks are available in the market and their properties vary from manufacture to manufacturer.

The current study aims at the LTP200 profile made by Lindab International. This profile is intended for use in stadiums and arenas and a single section comes with a covering width of 800mm. It is manufactured with 4 different steel sheet thickness i.e. 0.85, 1.00, 1.25, 1.50mm. It is used where insulation is intended and has acoustic properties as well. The section of LTP200 profile is shown in figure 6.

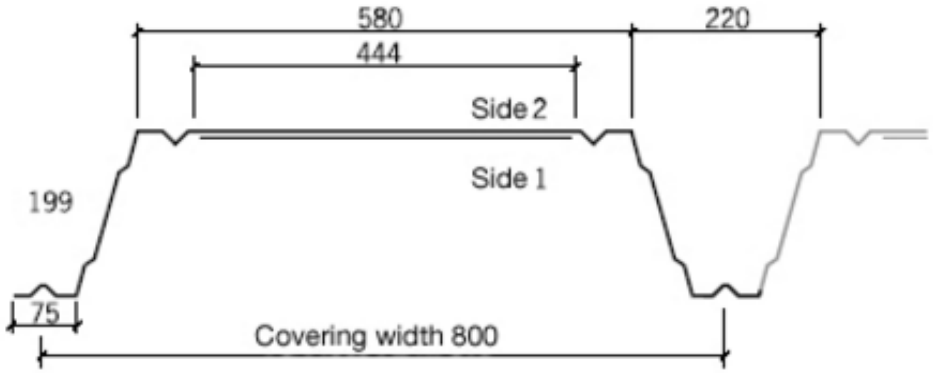

Figure 9. LTP200 Profile Cross Section

Over the supports, support cleats are used in conjunction with LTP200 profile to increase the load bearing capacity.

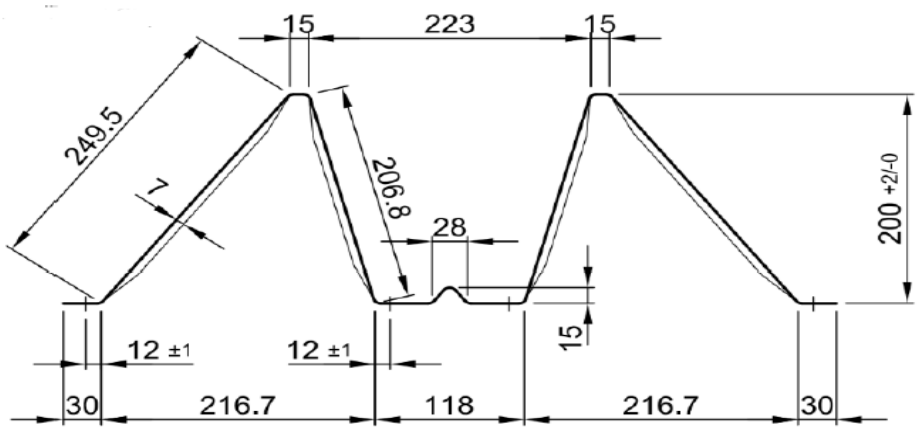

Figure 10. Support Cleat Cross Section

2.2 Behavior of the Cross-Sections

2.2.1 Elastic and Plastic Behavior of the Cross-Section

The behaviour of a member against the applied loads depends on two important factors, (i) Material and (ii) Geometry of the member and applied loads. The non-linearity in both of these factors greatly influences the response of the member and in turn, the behaviour is not linear. The material behaviour is described by a stress-strain curve achieved through direct tensile test performed on the samples of material (figure 11). The typical stress-strain curve for steel is shown in.

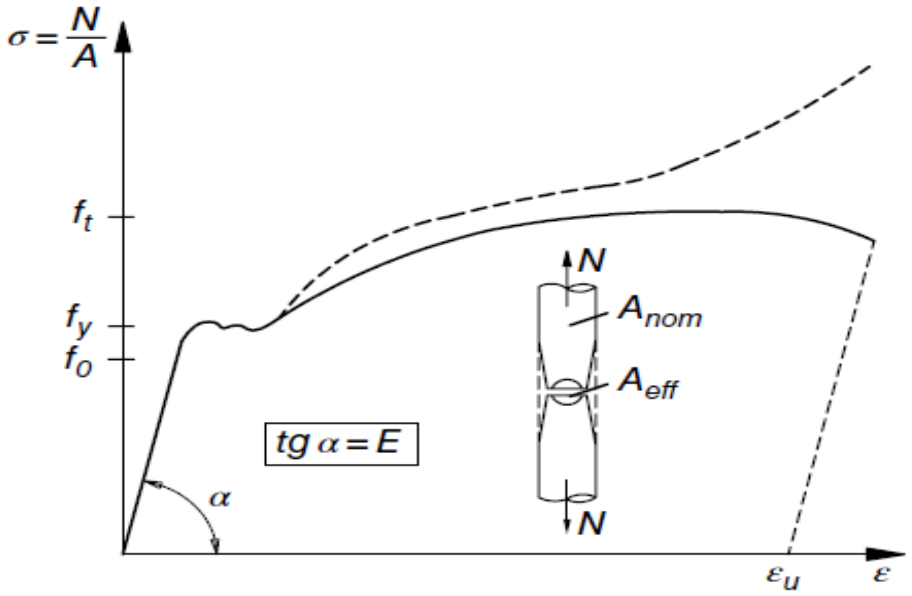

Figure 11. Stress Strain curve for steel (Bernuzzi & Cordova, 2016)

The term on y-axis is the applied tensile stress (σ) on the complete cross sectional area (A_{nom}) of the material. On x-axis, is the strain (ε) caused by the applied stress. Initially, when the stress is applied on the material, it follows the Hooke's law which states that the applied stress is directly proportional to the strain. The slope of the curve in this zone is called modulus of elasticity (E) also known as Young's modulus. When the stress reached the point f_o, the behaviour of the material loses its direct proportionality but the response is still elastic till the yield point termed as f_y. Till the yield stress, the transverse deformations of the section are really small and there is no reduction in the nominal area of the cross-section. After the yield point, the material enters into the plastic range and for a small duration where the strains keep on increasing under the same stress value. From this point on, the transverse deformations of the cross section due to Poisson's effect become significant. If the gross-section section of the material is used in the stress calculation then the solid curve is obtained (Figure 11). This region is known as the strain hardening where the material again starts taking stresses along with continuing deformation. At the end of this region, the transversal deformations start concentrating at a single point in the middle of the section. This phenomenon is known as necking and after this point, the stresses start decreasing until the failure of the material and the stress corresponding to the failure is known as ultimate stress f_u.

This behaviour of the material is quite significant when studying the distribution of the stresses in the cross section and its impact on the distribution in the member. The response of the cross section which is mostly stresses in the member is similar to this stress-strain distribution and that in-turn affect the stress distribution within the whole member. This can be better explained by a point load on the centre of a simply supported beam. As the load is applied on the beam, the triangular distribution of the stresses is obtained with

maximum compression at the top fibre and maximum tension at the bottom fibre. The value of these maximum stresses can be obtained by the formula:

$$\sigma = My / I$$

Where,

M = Bending moment at the cross section location

Y= Distance of the fiber from Neutral Axis

I= Second Moment of Area of the Cross Section

The load is increases till the fibre at the extreme yield, the stress corresponding to this load is called yield stress (f_y) and the moment is known as elastic moment capacity (M_{el}). As the load is increased further, the yielded zone increase further towards the neutral axis and correspondingly the plastic zone of the cross section start increasing. When the whole of the cross section has yielded, the cross section is said to have formed the plastic hinge and the moment corresponding to its formation is known as plastic moment capacity (M_{pl}).

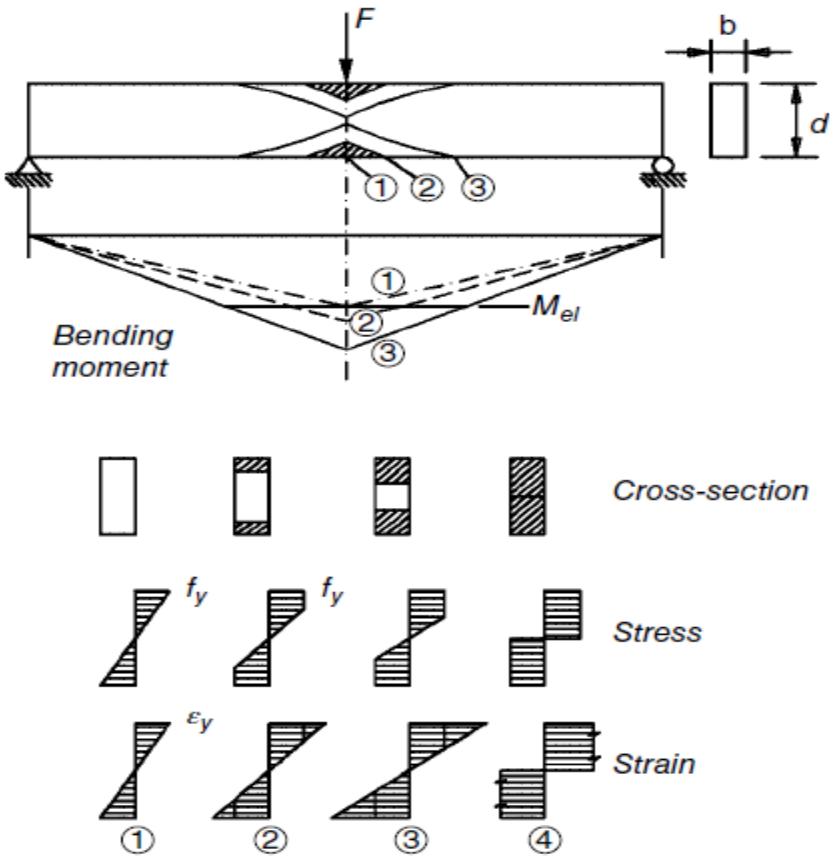

Figure 12. Spread of Plasticity within a cross-section (Bernuzzi & Cordova, 2016)

2.2.2 European Guidelines for Cross Section Behavior

Eurocode classifies the cross-sections in four types depending on the moment-rotation characteristics of a cross section (Dubina, Ungureanu, & Landolfo, 2012). This cross-section classification is the identification of impact of local buckling resistance of the section on its

resistance and rotation capacity. This moment-rotation characteristic of the cross-section depends on width to thickness ratio of the compressed part of compressed parts of cross section. The cross section classes are defined below:

1. Class 1: The type of cross sections which can utilize their full plastic resistance with the rotation capacity without any reduction in strength. These cross sections can develop a plastic hinge (Plastic / Ductile sections);
2. Class 2: These cross sections can utilize their full plastic moment resistance like class 1 sections, but have limited rotational capacity due to buckling phenomena (compact sections);
3. Class3: The type of cross sections which cannot develop their full plastic resistance because of local buckling. However, the stresses in the extreme compressed fibres can reach their yield strength considering elastic distribution of stresses (semi-compact sections);
4. Class 4: The cross section in which local buckling phenomena occurs in one or more parts of the cross-section before the yield stress in the extreme fibres is attained. Most of the cold formed steel sections lie in class 4 (Slender sections);

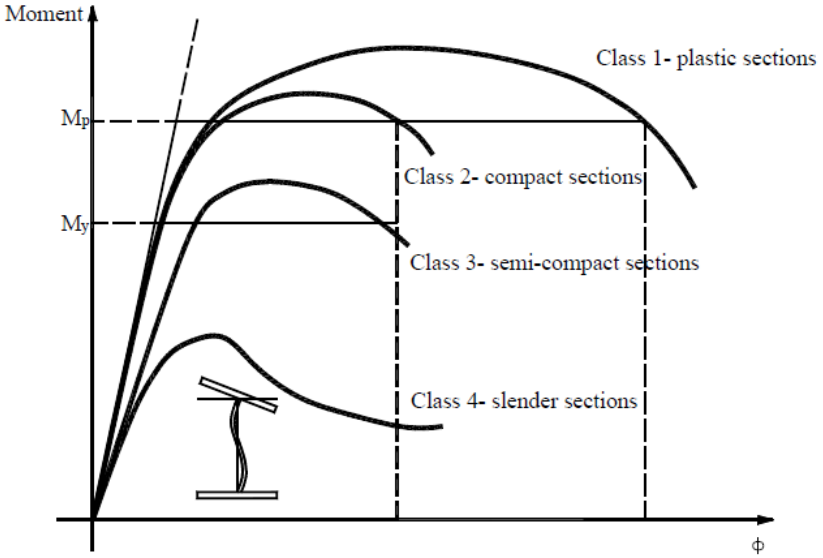

Figure 13. Classification of Cross Section based on Moment-Rotation (Dubina, Ungureanu, & Landolfo, 2012)

2.2.3 Eurocode Guidelines for Trapezoidal Steel Sheeting Cross-Section Behavior

Design rules that are followed for trapezoidal sheeting are almost common with the rules for cold formed steel. However, design of cold Formed steel is typically different from hot-rolled steel members because of their thickness and manufacturing process. There are some restrictions that are particularly essential for cold formed steel members (Eurocode 3 - Design of steel structures - Part 1-3: General rules, 2009).

2.2.3.1 Buckling

The most important concern in determining the load carrying capacity of cold formed steel member is the buckling. The compressed parts of the section may be subjected to instability before the strength of the cross section is fully utilized. To account for this instability, either the strength of the section is reduced or the capacity of the section is calculated based on a reduced area. There are two types of buckling phenomenon particularly related with steel sections which are global and sectional buckling modes (Dubina, Ungureanu, & Landolfo, 2012). However, sectional buckling is more common in cold formed steel sections.
Global buckling, also known as rigid body buckling is the mode in which the entire section moves without any distortion of the cross-section. It can be observed as flexural, flexural torsional and lateral torsional buckling of the members. On the other hand, sectional buckling can either be in the form of local or distortional buckling. Local buckling is the buckling of individual plane elements. Local buckling can be characterized by the short wavelength buckling of the plane element. In distortional buckling, as the name suggests, the fold lines move relative to each other and the whole cross section seems distorted. The wavelength in such case is intermediate between the local and global buckling.

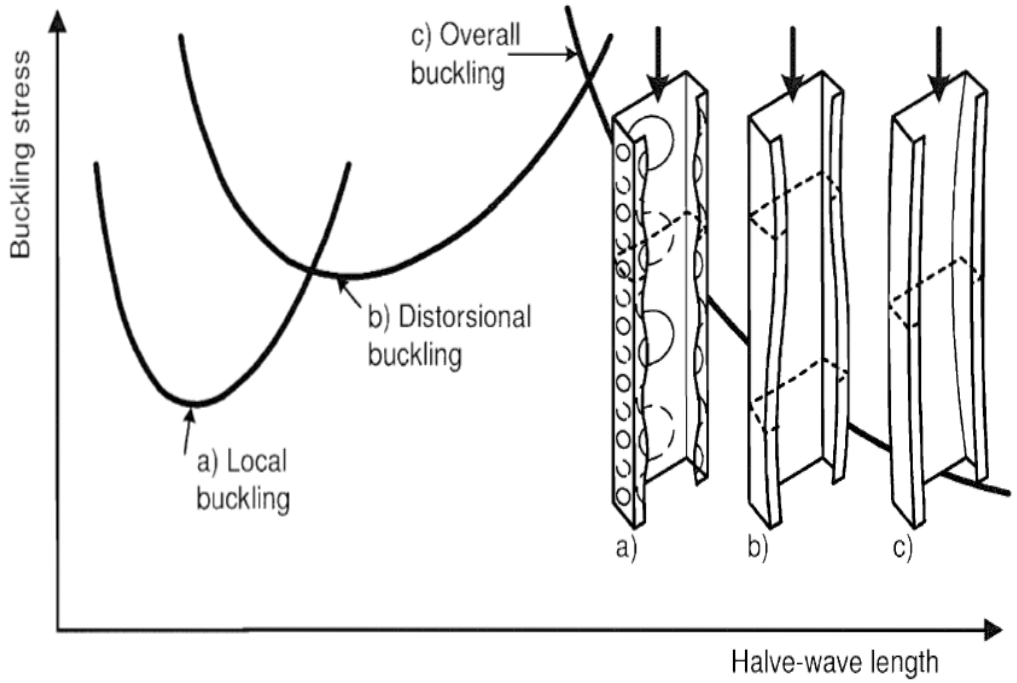

Figure 14. Buckling modes of Cold Formed Steel Sections (Dubina, Ungureanu, & Landolfo, 2012)

2.2.3.2 Eurocode Provision for Design

The steel trapezoidal sheet lies in class-4 cross sections, the design and load carrying capacity of the sheet is governed by its susceptibility to local / distortional buckling. Eurocode 1993-1-3 gives a complete guideline to design and determine the resistance of trapezoidal sheet.

1. Gross cross-section Properties:

The cross section of a steel trapezoidal sheet consists of combination of plane elements and stiffeners. These plane elements and stiffeners are measured based on their nominal dimensions i.e. width, thickness. During the cold-forming process, the corners between the elements themselves and the stiffeners are rounded and their effect must be taken into account. First of all, the notional flat widths of these elements must be measured by replacing the rounded corners with the intersection of mid-lines of the elements (Figure 15).

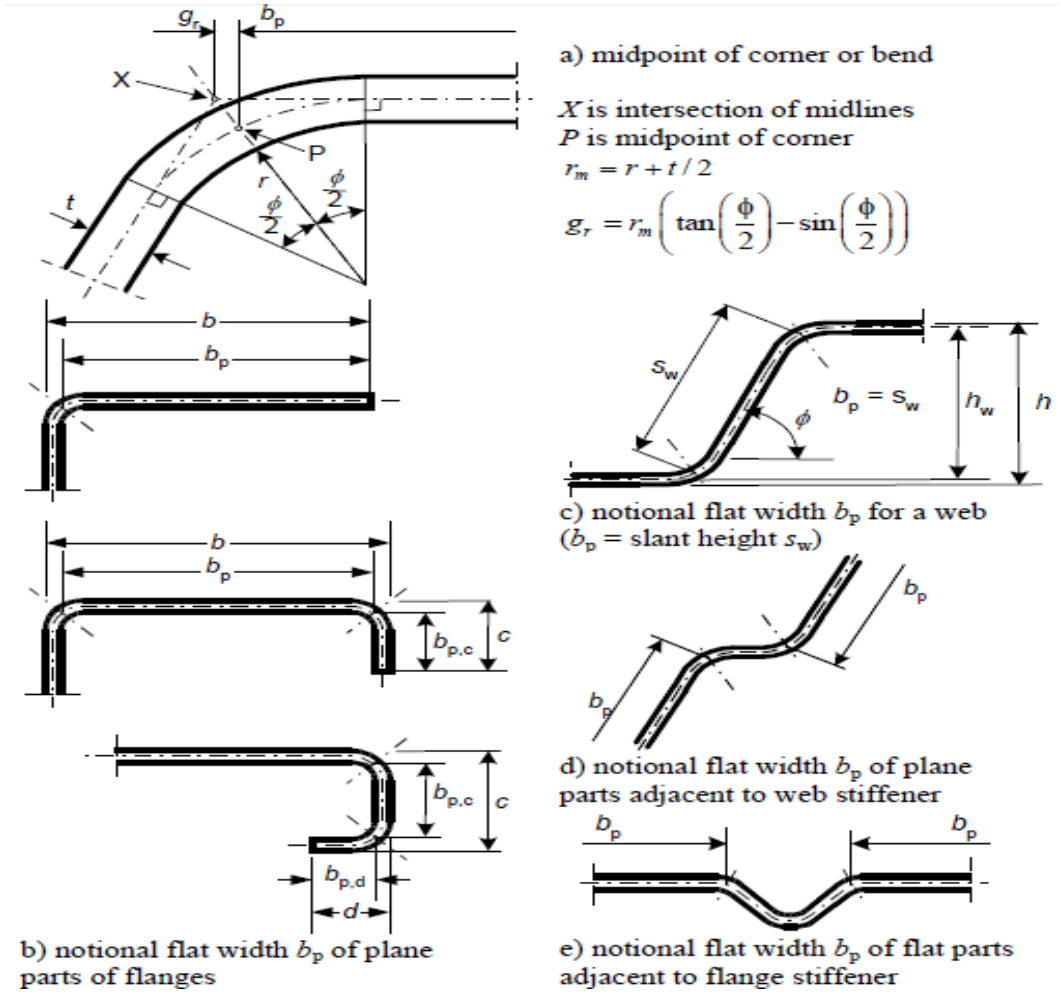

Figure 15. Notional Flat widths of plane parts (Dubina, Ungureanu, & Landolfo, 2012)

After taking into consideration these notional flat widths, the gross section properties of the cross section i.e. area, centroid and moment of inertia can be measured. These are the properties based on the gross section with sharp corners. The next is to take into account the influence of rounded corners in order to avoid the overestimation of these gross section properties, but this influence can be neglected if the internal radii of the rounded is small i.e. r <5 t and r <0.1b_p. Where, b_p is the notional flat width of the plane element. To

consider the influence of rounded corners, equation 5.1d of EN1993-1-3 gives the value of δ which is used to reduce the properties calculated through sharp corners.

$$\delta = 0.43 \frac{\sum_{j=1}^{n} r_j \frac{\emptyset_j}{90}}{\sum_{i=1}^{m} b_{p,i}}$$

r_j Internal radius of the rounded corner
$\emptyset_j$ Angle between two plane elements
$b_{p,i}$ Notional flat width of plane elements in cross section

This factor can be used to reduce the section properties calculated for sharp corners to include the influence of rounded corners.

$$A_g = A_{g,sc}(1 - \delta)$$

$$I_g = I_{g,sc}(1 - 2\delta)$$

A_g, I_g Gross Section properties with rounded corners
$A_{g,sc}, I_{g,sc}$ Gross Section Properties with sharp corners

2. Effective Section Properties:

The cross section of a cold formed trapezoidal sheet can be considered as a section composed by joining different plate elements. In such scenario, the capacity of the cross section is limited by the elastic buckling of one of these plate elements in the compression zone due to which the thin walled elements especially steel trapezoidal sheets lies in class 4 cross-sections. Therefore, allowance must be made to account for the local buckling of the plate elements constituting the cross section as well as the distortional buckling which is the flexural buckling of the stiffener itself. This allowance is made by reducing the area of the compressed part of cross-section and the remaining section is termed as effective cross section.

To begin with the calculation of effective area calculation of the cross section, section 5.5.3.4 of Eurocode 3 part 1-3 gives a complete guideline. The goal of calculation is to compute the reduction factor χ_d which gives the effective area of the section. Eurocode gives a four step to calculate the elastic critical buckling stress and reduction of area to account for these stresses. These four steps are:

1. Elastic Critical buckling stress for the flanges with stiffeners.
2. Elastic Critical buckling stress for the webs with stiffeners.
3. Combination of buckling stress for flanges and webs.
4. Reduction Factor Calculation
5. Load carrying capacity

1. Elastic Critical buckling stress for the flanges with stiffeners

As discussed in previous sections, the compressed parts of the cross section are susceptible to local instabilities which affect the capacity of the section. Eurocode recommends reducing the area of the flange in compression to calculate the elastic buckling stress. This reduced area is calculated by using an effective width of the plane parts adjacent to the flange stiffener.

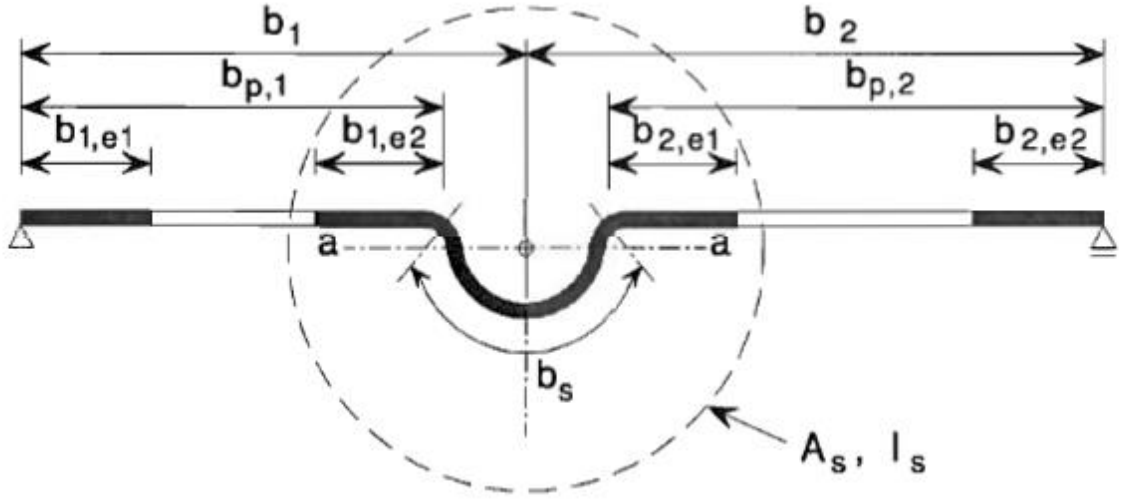

Figure 16. Effective area of flange stiffener (Eurocode 3 - Design of steel structures - Part 1-3: General rules, 2009)

This reduction in the plane part depends on its slenderness and stress distribution in the bottom flange. Initially, each plane part is considered to consist of two plane elements $b_{p,1}$ and $b_{p,}2$ and assumed that these two plane elements are simply supported. Eurocode 3(1-5) section 4.2 gives the procedure to calculate this reduction factor.

$$b_{eff} = \rho\, b_p$$

ρ Reduction Factor

b_p Nominal Width of the adjacent plane part

$$\rho = \frac{\bar{\lambda}_p - 0.055\,(3 + \Psi)}{\bar{\lambda}_p{}^2} \leq 1$$

$\bar{\lambda}_p$ Slenderness of the plane part

Ψ Ratio of stress distribution

$$\bar{\lambda}_p = \frac{\frac{b_p}{t}}{28.4\varepsilon\sqrt{k_\sigma}}$$

$$k_\sigma = f(\Psi) = f(\frac{\sigma_2}{\sigma_1})$$

σ_i Stress at either side of flange

$$\varepsilon = \sqrt{235/f_{yb}}$$

f_{yb} Yield stress of the base element

The elastic critical buckling stress ($\sigma_{cr,s}$) for the flange in stiffener is then calculated by using the reduced area calculated from this effective width. The guidelines for calculating this stress are given in the section 5.5.3.4.2 of Eurocode 3(1-3). Different formulas are recommended based on the number of stiffeners in the flange.

2. Elastic Critical buckling stress for the webs with stiffeners.

The area of part of web in compression must also be reduced as in case of the flange in compression. The web is considered to be composed of active areas in the compressed part of the cross section [Figure 17]. The effective part is calculated by using the centroid of the section with effective flanges and gross webs. Once the effective parts are calculated using this centroid axis, iterations are performed by updating centroid after each iterations since the result starts converging.

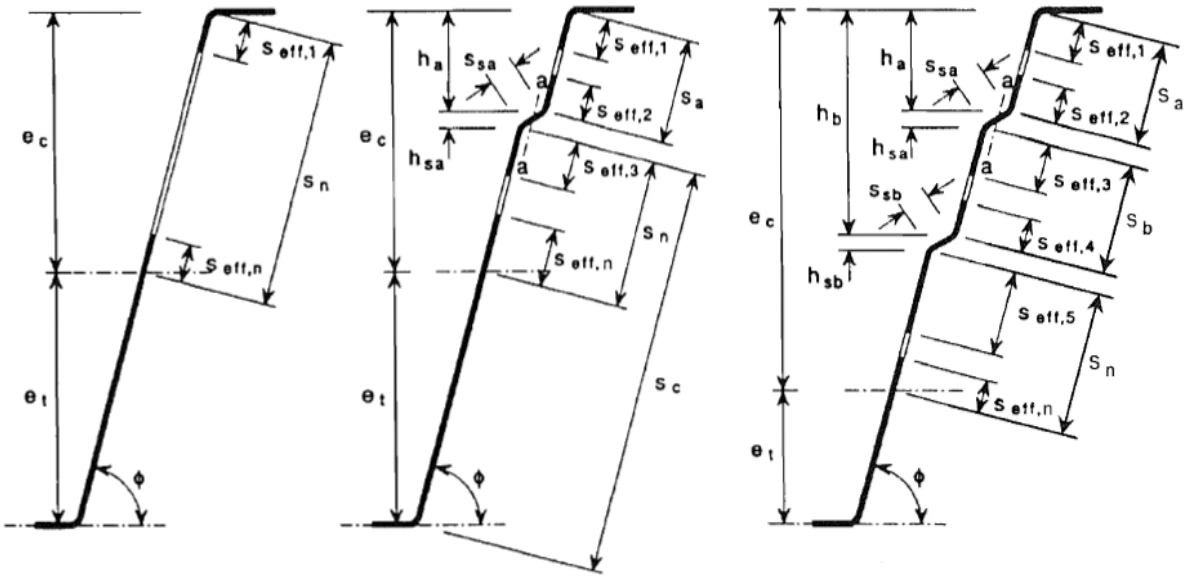

Figure 17 Effective Area of Webs (Eurocode 3 - Design of steel structures - Part 1-3: General rules, 2009)

The reduced area calculated from effective parts of the cross section is used to calculate the elastic critical stress for the web with stiffeners. Eurocode Part 3(1-3) section 5.5.3.4.3 gives formulas for calculating these critical stresses based on the number of stiffeners in a flange.

3. Combination of buckling stress for flanges and webs.

The final cross section of a sheet includes the effective area of the compressed part and gross area of the cross section part in tension (Figure 18). The interaction of elastic critical stresses of both the flange and the web taken into account by using the equation

$$\sigma_{cr,mod} = \frac{\sigma_{cr,s}}{\sqrt[4]{1 + [\beta_s \frac{\sigma_{cr,s}}{\sigma_{cr,sa}}]^4}}$$

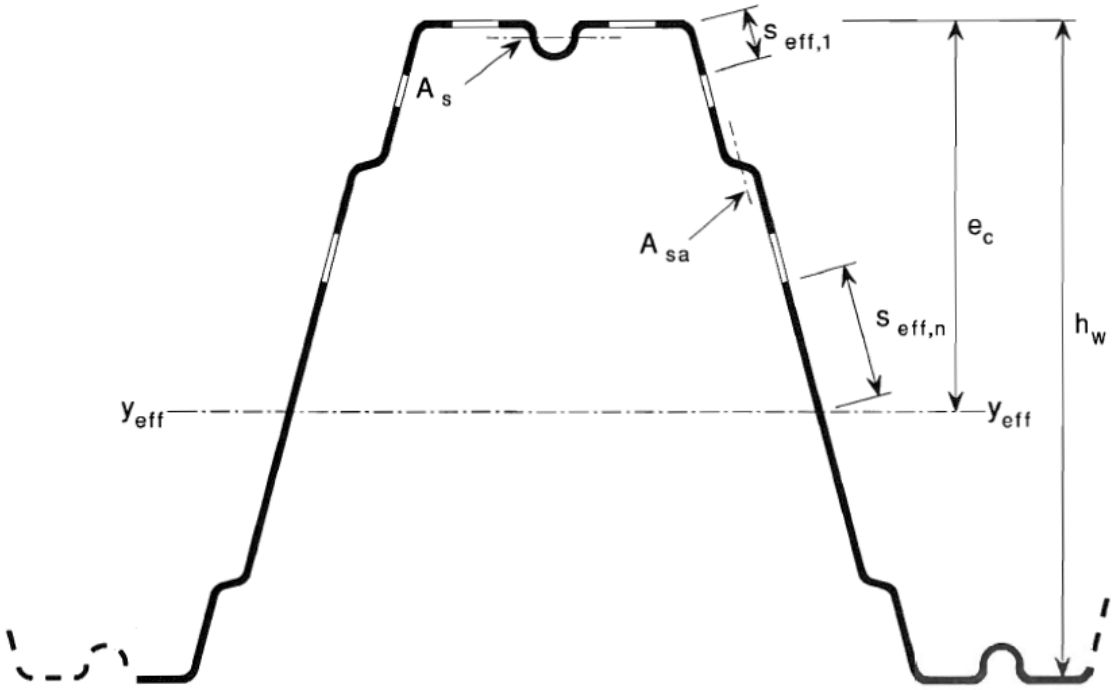

Figure 18 Effective Area of a cross section (Eurocode 3 - Design of steel structures - Part 1-3: General rules, 2009)

4. Reduction Factor Calculation:

Once the elastic critical stress considering the stiffeners in both flanges and webs are calculates, the relative slenderness of the section can be obtained. This relative slenderness ultimately gives the reduction factor for whole cross section.

$$\bar{\lambda}_d = \sqrt{\frac{f_{yb}}{\sigma_{cr,mod}}}$$

This relative slenderness ultimately gives the reduction factor for whole cross section.

$$\chi_d = 1 \qquad if\ \lambda_d \leq 1$$

$$\chi_d = 1.47 - 0.723\lambda_d \qquad if 0.65 < \lambda_d < 1.38$$

$$\chi_d = \frac{0.66}{\lambda_d} \qquad if\ \lambda_d > 1.38$$

5. Load Carrying Capacity:

Once the reduction factor is obtained considering the buckling of parts in compression, the effective section can be obtained. Since the effective section is smaller than the gross section, these cross sections lie in class 4 type cross sections. Based on the type of forces a trapezoidal sheet is subjected to, the relevant load carrying capacity can be calculated using chapter 6 of Eurocode 3 Part 1-3.

2.2.4 Degree of Moment Redistribution

The inelastic capacity of a cross section depends on the material and the slenderness of section and thus, greatly impacts the redistribution of moments in a multi-span system. In case of a two span system, the section at the interior support reaches its elastic capacity first. In the ideal scenario, this cross-section should allow enough rotations beyond its elastic limit so that the moments are redistributed in the system and the section at the mid-span should be able to utilize its full capacity also. This ideal redistribution of bending moment capacity is characterized by the bilinear moment-rotation response of a cross section (Hui, Gardner, & Nethercot, 2015).

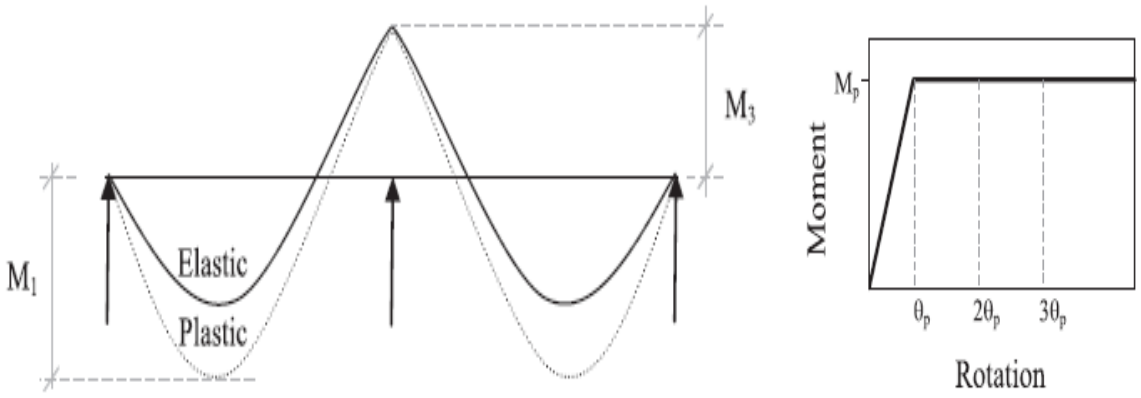

Figure 19. Ideal Redistribution of Moments in Stocky Cross Section (Hui, Gardner, & Nethercot, 2015)

As discussed in the section 2.2.2, the stocky cross-section that lie in the class 1 and 2 exhibit this behaviour. These cross sections, being able to deform plastically, does not show any significant drop in their bending moment capacity and allow the sections in the mid-span to fully utilize their capacities. The moment rotation response of these stockier cross sections is quite similar to the ideal behaviour and the curve has a plateau after the elastic moment capacity of these cross-sections. This plateau indicates that the section is allowing large rotations while maintaining their bending moment capacity. Due to such ideal redistribution

of bending moments, the Eurocode allows to utilize their plastic moment capacity through the procedures given in the relevant parts.

Owing to the thin walled nature of the cold formed sections, they are not able to exhibit this ideal redistribution of bending moment. The local instabilities affect their strength due to which they cannot maintain their capacity while allowing sufficient rotations and their moment-rotation response is characterized by their peaky nature.

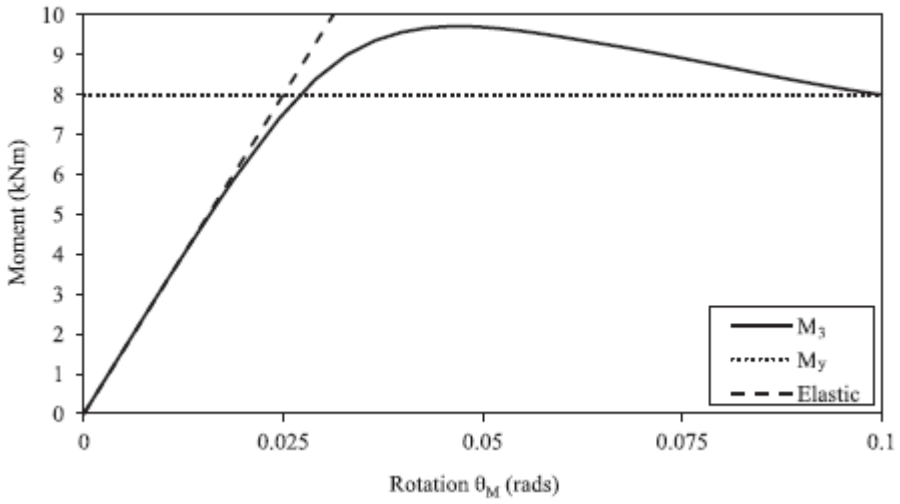

Figure 20 Typical Moment Rotation Curvature of Stockier Cross Sections (Hui, Gardner, & Nethercot, 2015)

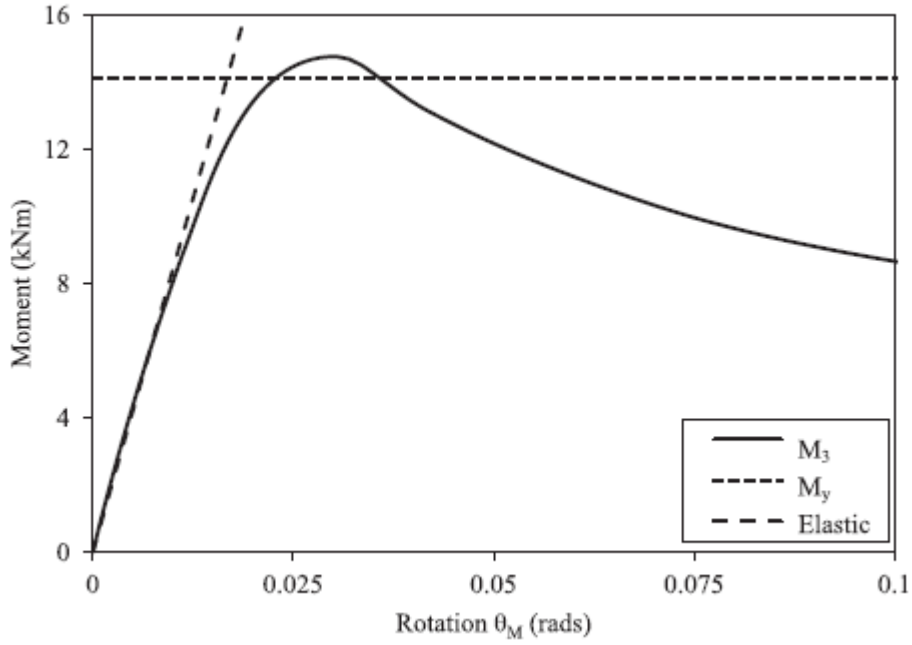

Figure 21. Typical Moment Rotation Curvature of Slender Cross Sections (Hui, Gardner, & Nethercot, 2015)

The research area of this post-elastic behaviour of the cold formed sections particularly trapezoidal sheets is very limited. However, from the tests performed on the cold-formed sections, it has been observed that the cold formed sections have inelastic strength reserve but it depends on a number of factors and the most important of which is cross-section

slenderness. Eurocode also recognizes this inelastic strength reserve but doesn't provide direct guidelines and recommends performing experimental tests to make recommendations about the inelastic strength reserve and degree of moment redistribution.

3. Experimental Tests

Experimental Tests were performed to investigate the behaviour of the section over the mid-support. This behaviour will influence the forces and moments the joint is subjected to. In order to study the behaviour of joint and the forces it is subjected to, two types of test configurations were used. (i) Setup 1 with a Gerber hinge joint and sheets overlap of 500mm. (ii) Setup 1 with a Gerber hinge joint with sheets overlap of 100mm.

3.1 Test Setup

3.1.1 Sheet Samples

A total of 3 samples with different thicknesses were tested during the experiments which are summarized in the Table 1. The width of the total section is 1600mm which is formed by two sections, one full section in the middle with a width of 800mm and two half sections on each side with widths of 400mm each, making a total width of 1600mm. The theoretical load capacity has been calculated as per the section with bottom flange in compression i.e. section over the internal support. This theoretical load capacity is for the section with 1600mm width.

Table 1. Theoretical Load Capacities of Sheets

Sample	Thickness (mm)	Yield Stress (MPa)	Theoretical Capacity (kN)
1	0.85	420	50.51
2	1	420	69.83
3	1.5	350	118.12

3.1.2 Support Mechanism

To support the sheets sections, cleats are provided which connect the underlying support with the outer parts of the top flange. For this experimental setup, support cleats were first screwed in the timber boards. Each timber board contains two support cleats and three supports were prepared for the double span.

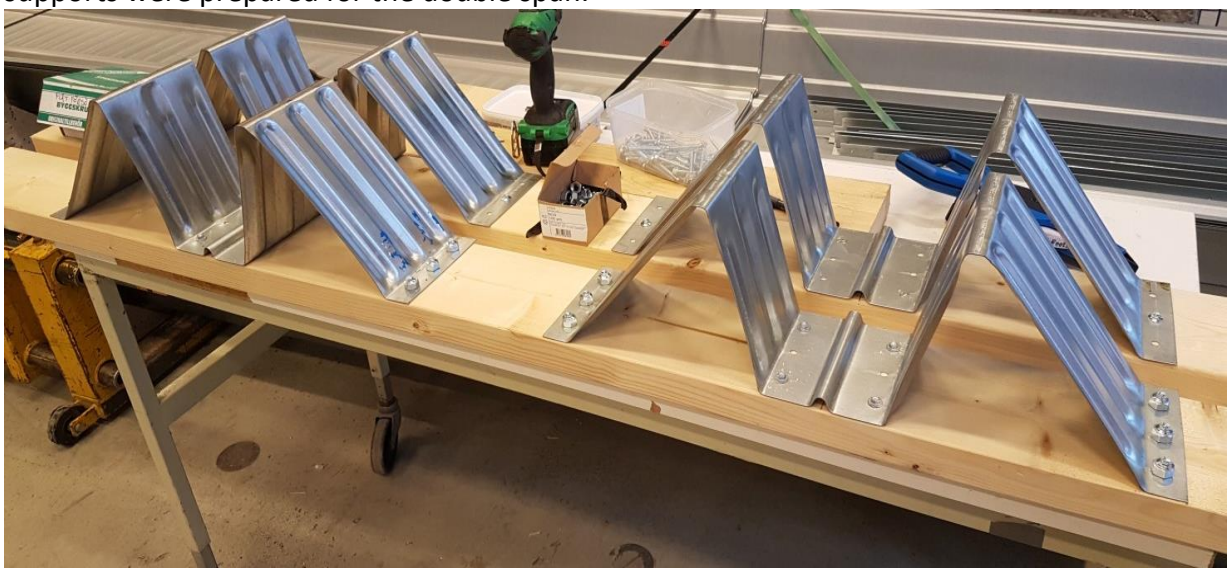

Figure 22. Support cleats attached to timber boards

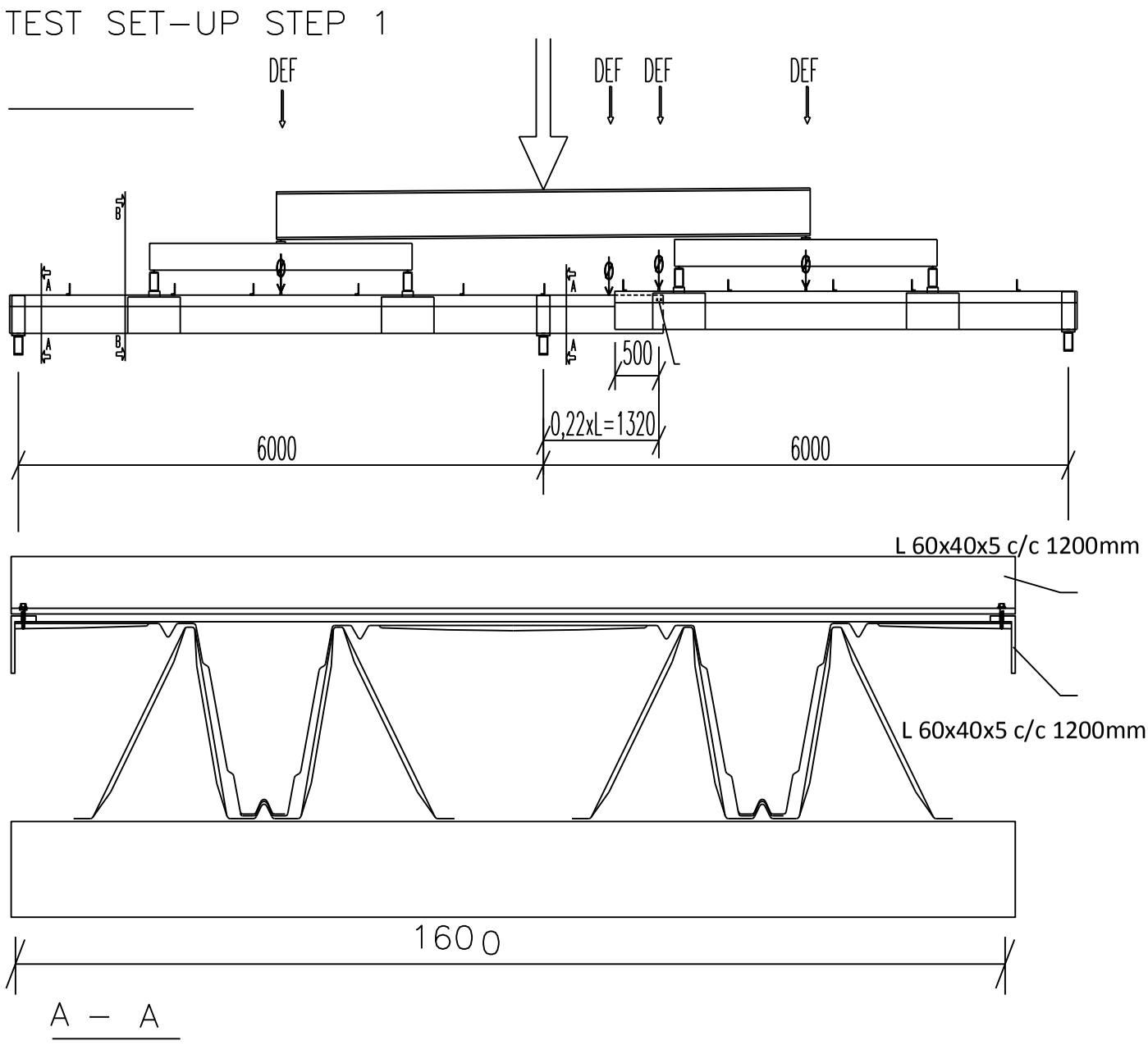

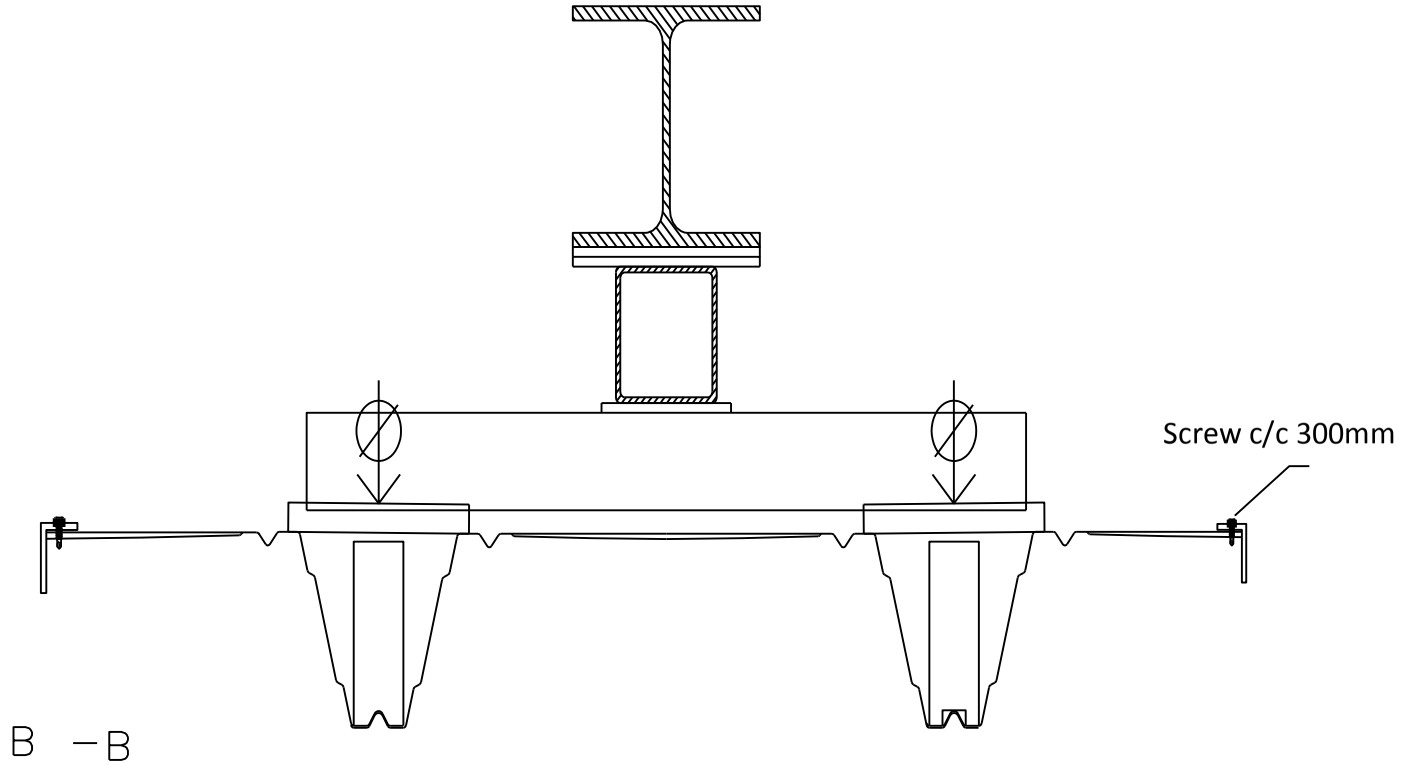

Figure 23. Test Setup-1 Configuration

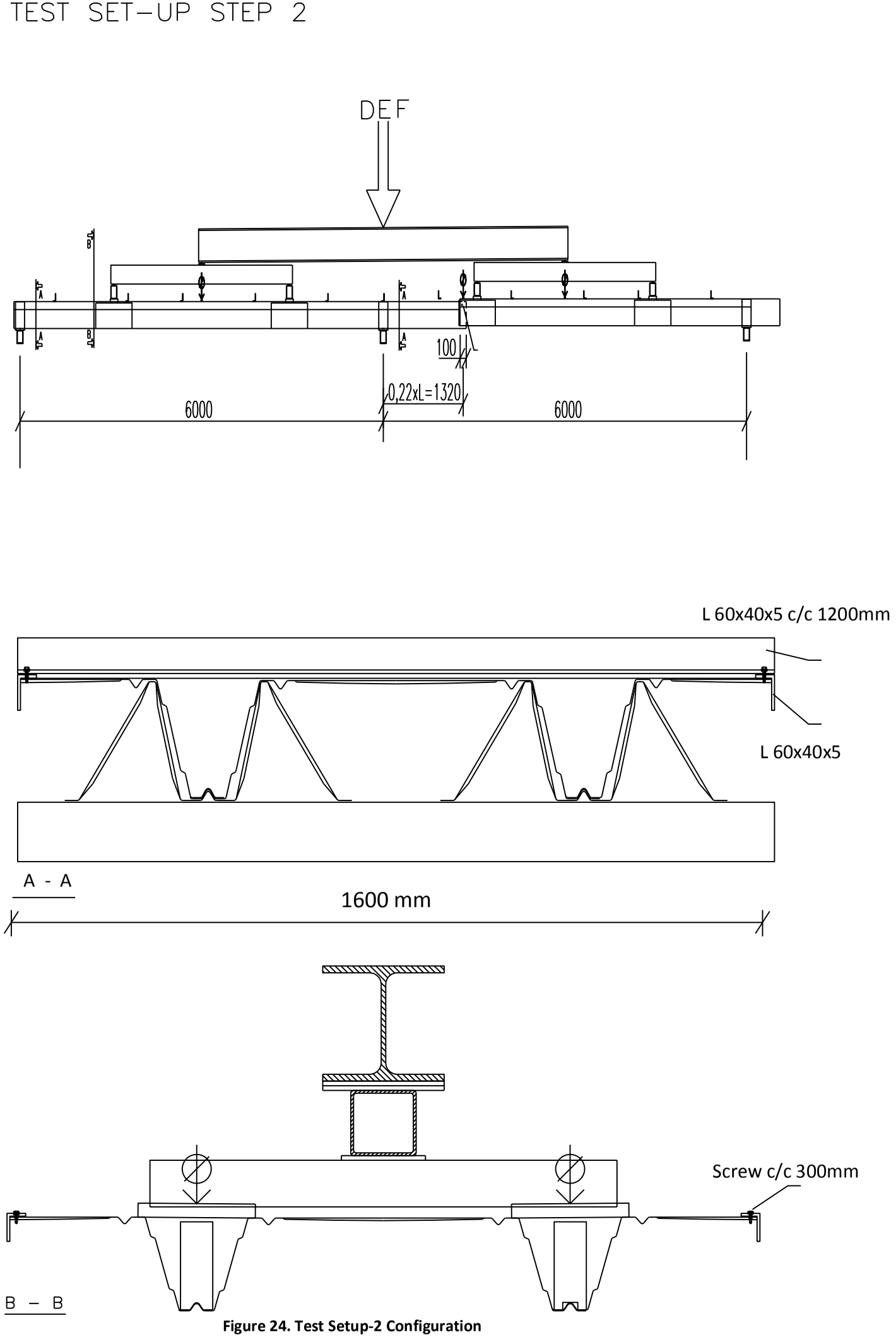

Figure 24. Test Setup-2 Configuration

These timber boards were then placed 6m apart from each other. The outer part of the top flange was then screwed to the support cleat. The distance of the screw from cleat edge is 20mm and the c/c distance is 110mm. A total of 2 screws in each cleat were used for this support connection.

Figure 25. Connection of support cleat with sheeting

3.1.3 Longitudinal and Transverse Ties

In order to prevent the section from distortion, EN 1993-1-3 Annex A.2.1 recommends using transverse ties and other test accessories. For this experimental test, two types of ties were provided which are: (i) Longitudinal Ties (ii) Transverse Ties. Both of these ties are made up of angle section L60x40x5. The longitudinal ties were provided throughout the longitudinal edge and were screwed with the sheet edges with the screw distance of 300mm c/c. Transverse ties were screwed and the distance between each tie is 1200mm.

3.1.3 Overlap

3.1.3.1 Side Overlap

Double Cross section was used for the experiment with one full section and one section cut into two halves. The half section was overlapped with a full section using a valley connection. The screws were drilled in the valley and this screw provided a clamping effect. The c/c distance between the screws is 500mm where the bottom flange is in tension and 250mm where bottom flange is in compression.

3.1.3.2 Hinge Overlap

The Gerber joint was provided by overlapping the two sheets and providing 3 screws at one end. This screw connection is at a distance of 1320mm from the internal support. As two tests were done on each thickness, the basic difference was the difference in the overlap length of these two sheets. In the first setup, the overlap length used was 500mm and in second setup it was 100mm.

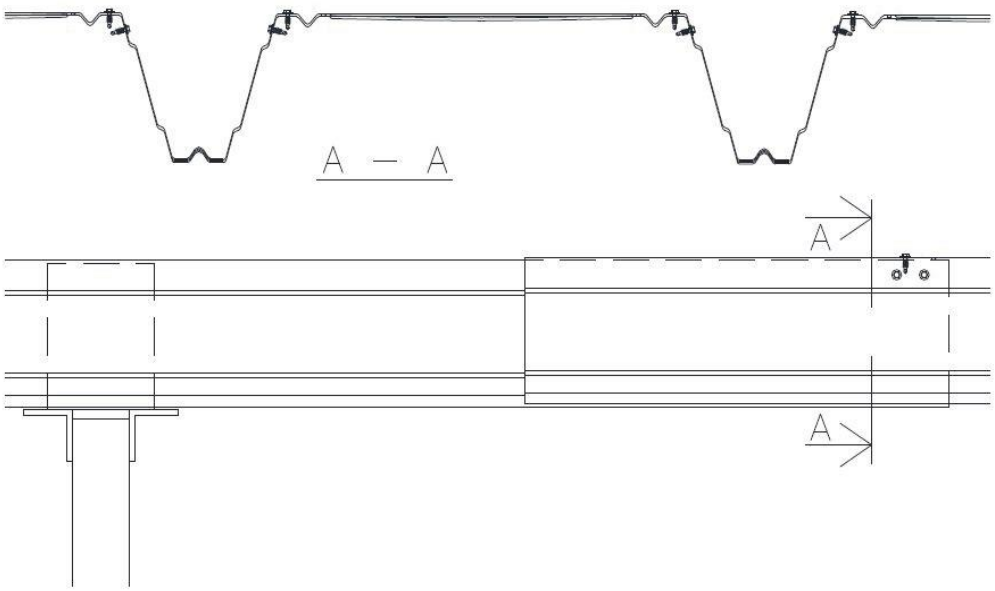

Figure 26. Location and Geometry of Hinge

3.1.4 Loading Mechanism

The loading was applied in the lab through a hydraulic jack to I section beam with a stroke of 2mm/min. The centre point of the load was in line with the centre of the middle support. This I-beam is supported on both sides to hollow sections which then turn transfer the loads through wooden blocks to the bottom flange of the sheet.

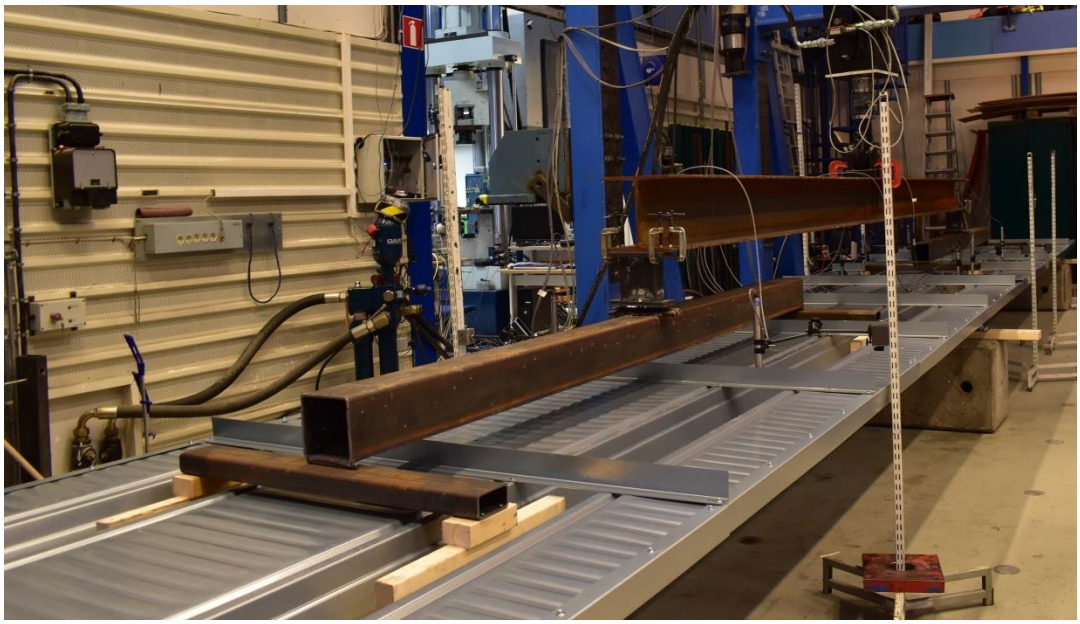

Figure 27. Loading Mechanism in Experimental Setup

3.1.5 Strain Gauges

The data of interest for this experiment was load-displacement curve. As explained in previous section, load was applied through hydraulic actuator. The displacements were

measured using the LVDTs at selected locations (Figure 29). The LVDT were placed at on a straight ruler placed on the top flange that will give average deflection of the section.

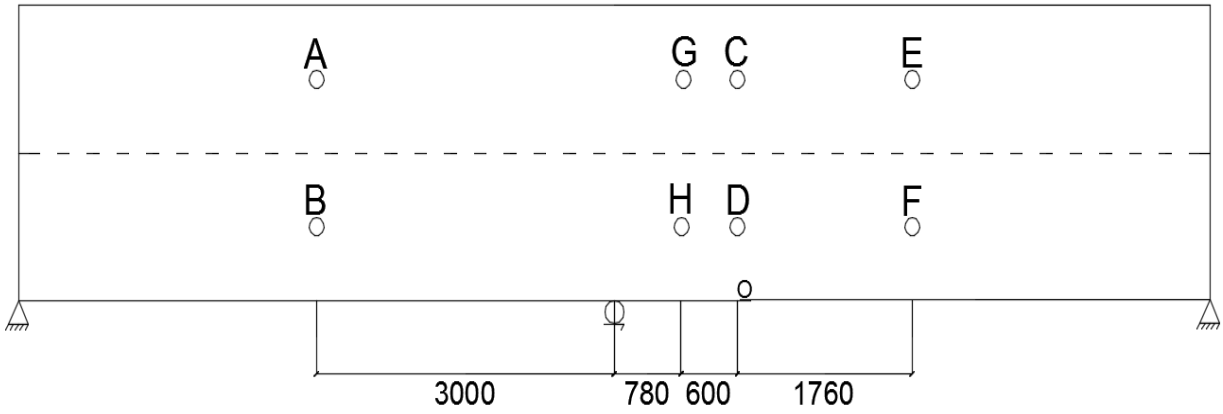

Figure 28. Location of LVDTs for Test Setup-1

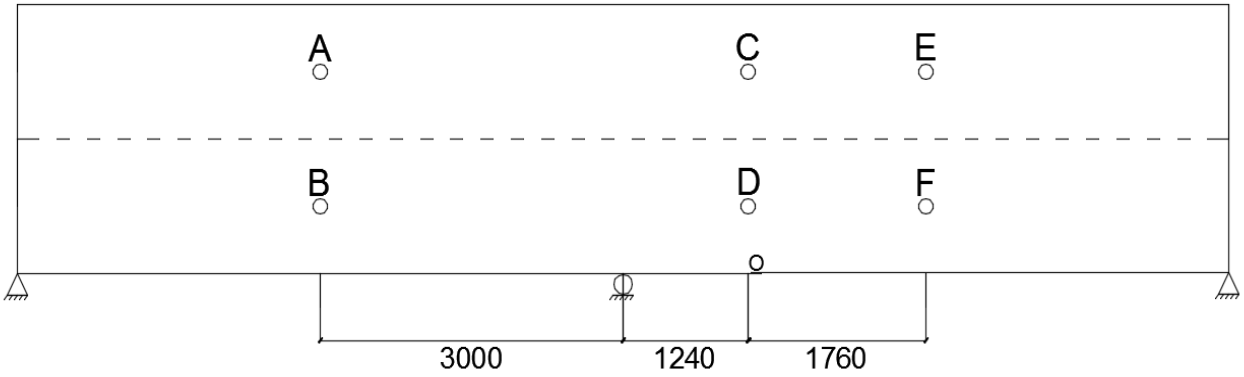

Figure 29 Location of LVDTs for deflection measurement

Table 2. Designation of LVDTs

Designation	LVDT No.	Deflection
A	1_2	Global
B	1_1	Global
C	1_4	Global
D	1_3	Global
E	2_4	Global
F	2_3	Global
G	2_2	Local
H	2_1	Local

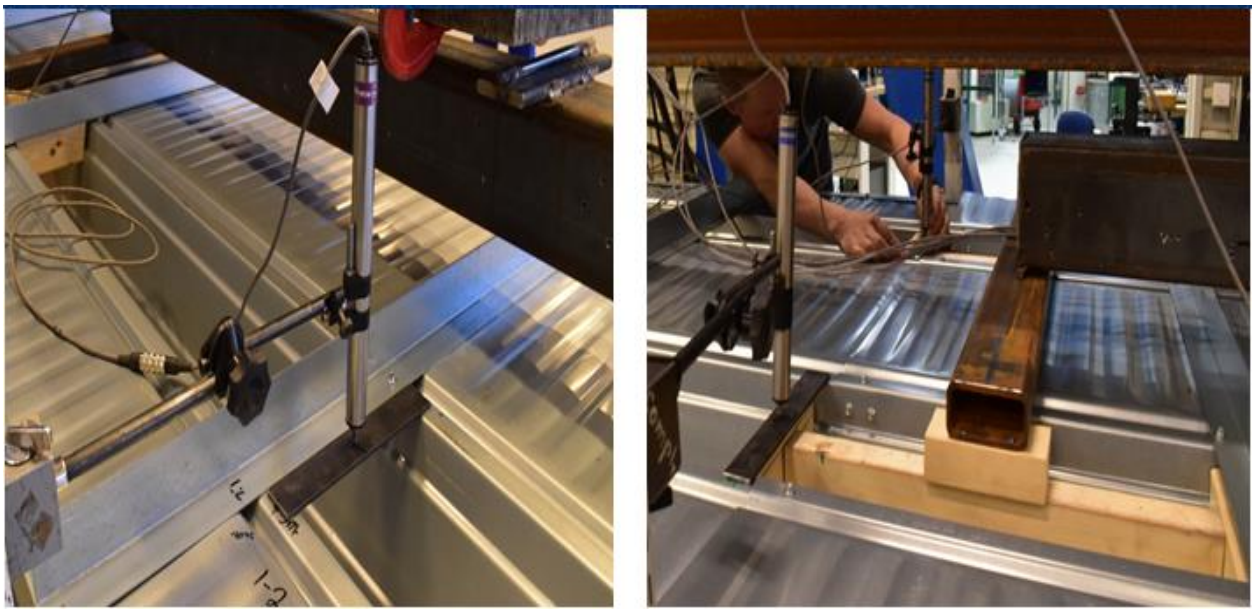

Figure 30. Placement of LVDTs in Laboratory

3.2 Test Results

This section deals with the discussion of results obtained for three thicknesses of the sheets tested (0.85, 1 and 1.5mm). These two types of hinge configuration behave same during the elastic range but differently after the elastic limit of section at interior support.

In the first test, the joint was made with 3 screws along-with sheets overlap of 500mm. During the elastic phase, this connection behaves as a perfect hinge as the gap between the two sheets opens up and the only interaction between the two sheets is through screws. But, as the section over the mid support fails, the gap between sheets closes and the contribution of the two sheets is achieved to resist further load. The system will now behave as continuous allowing large rotations to develop.

In the second setup, the joint was made with 3 screws but the overlap of sheets this time is just 100mm. No contribution of the sheets can assumed in this scenario and the joint will behave as a perfect hinge with two parts connected at this point which can rotate about it.

3.2.10.85mm Sheet

This sheet is the most slender section among all the sections testes. As mentioned before, the location of hinge is such that the failure will be initiated at the internal support. The load capacity against the elastic critical moment for the section with small flange located at internal support is 50.51kN.

3.2.1.1 Test Setup-1

For the First Setup with 500mm screws, the initial failure was observed at 58.30kN. After this elastic failure, the section at side (1_4) lost its strength and it kept deforming under the same load. Unloading was done till 54kN and again the section was reloaded. Right after the

reloading, the loads near the mid-span titled and damaged the section. The test was stopped at that load. Even till this load, the Gerber joint at hinge was still intact.

Figure 31. Tilting of loads and condition of internal support at collapse

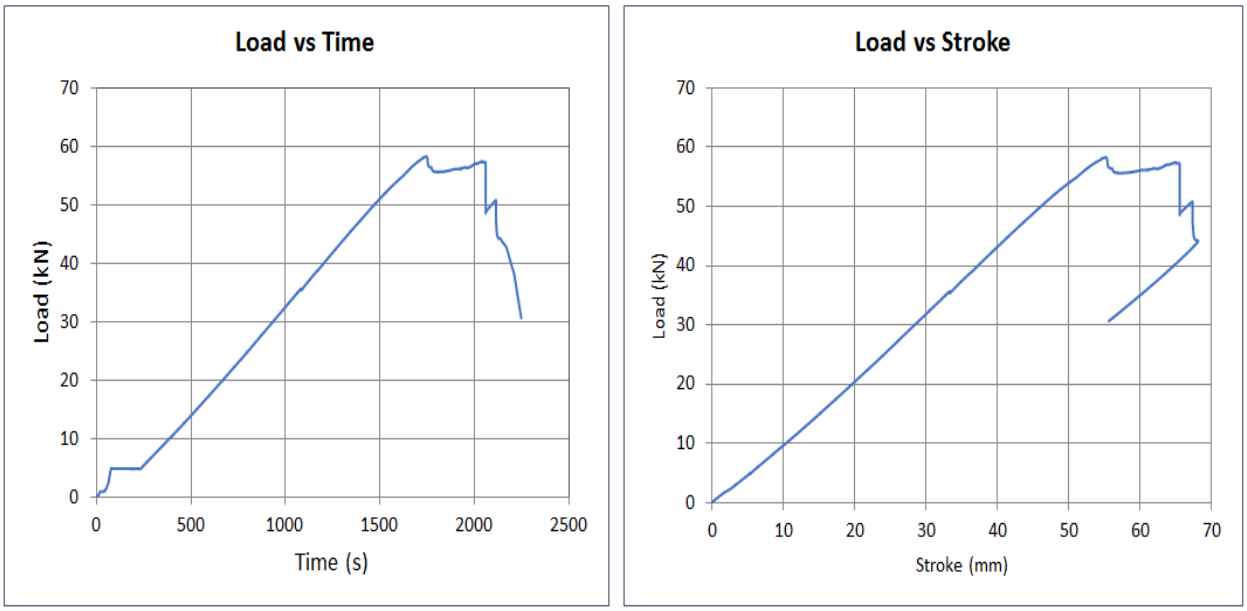

Figure 32. Variation of Load with time and stroke (0.85mm Setup-1)

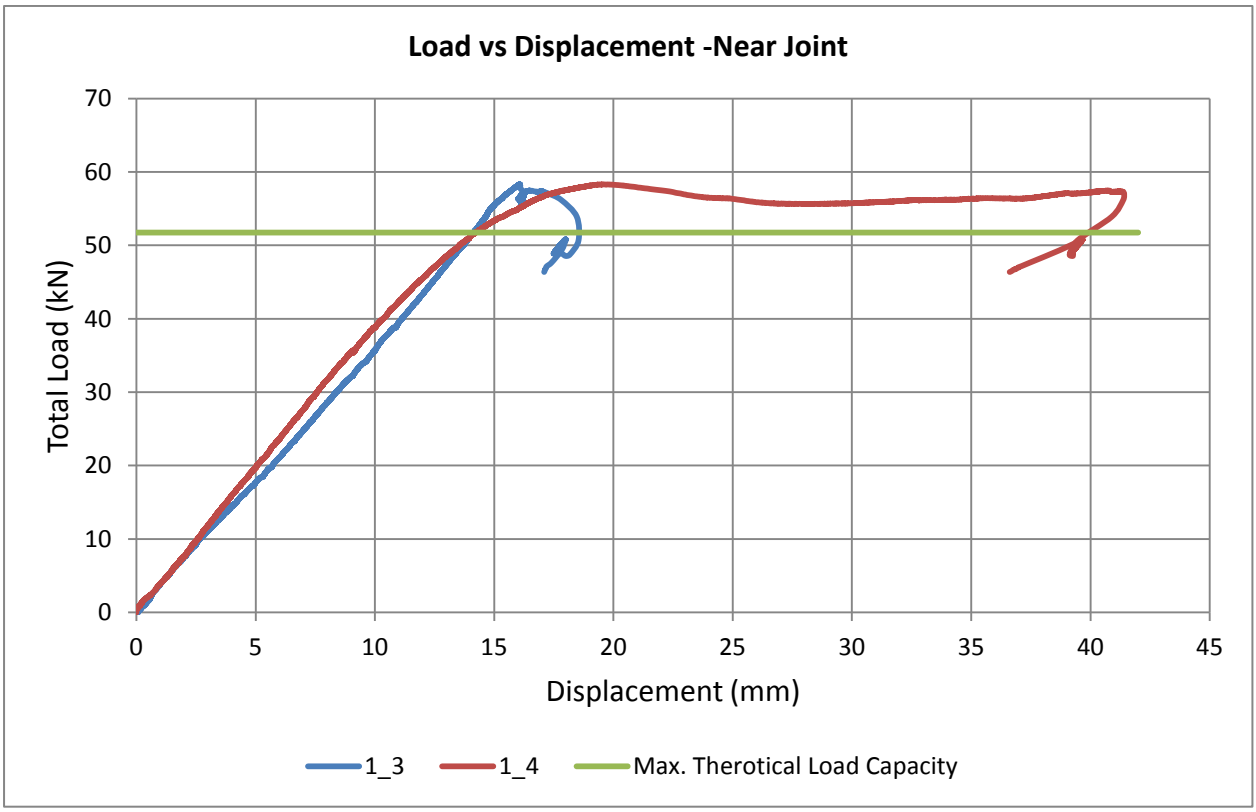

Figure 33. Load vs Displacement near the Gerber Hinge (085mm Setup-1)

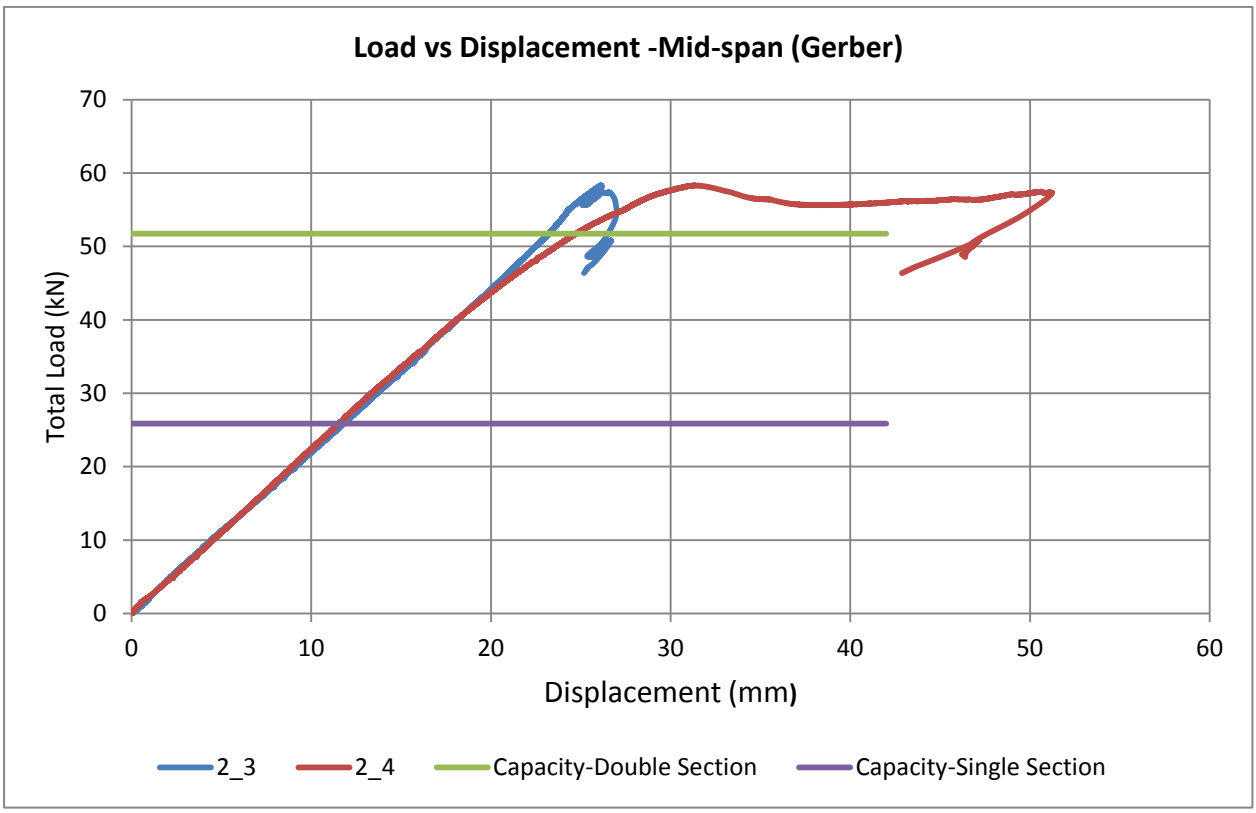

Figure 34. Load vs Displacement in mid-span (0.85mm Setup-1)

3.2.1.2 Test Setup-2

In this section, the results of the points near the hinge and at locations of both the mid-spans will be discussed. During the test, as the load increased, the beam deformed elastically under the applied loads. Around reaching the load of around 60.6229kN, the elastic failure was observed at the internal support. This value of load obtained through load is higher than the theoretically calculated load capacity by 17%.

After the breach of this yield load, the loading was relaxed. the load-deflection plot of one side (LVDT 1-3 & 2-3) indicates the formation of plastic hinge at the internal support section as the member keeps on deforming under the same load. However, the other section doesn't come back to its original position which indicates that this section has also reached its yield value and has now attained some residual deflection. From 30.69kN, the system was loaded again to check the inelastic reserve capacity of the section at the mid-support. During this loading phase, the system is now behaving as two different sections and one side is taking more load than the other. When applied load reached to a value of 38.38kN, the part of the sheet between internal support and hinge buckled.

Excessive buckling of the web and bottom flange can be seen. The side over-lap of the two sections failed because of this buckling and bearing of holes in the bottom sheet was observed but no screw failed itself.

As far as the hinge joint is concerned; the two sheets were not clamped any more. As it is a hinged joint and in this setup the overlap was just 100mm and thus it was not able to sustain large rotations it was subjected to. The screw failure itself was not observed but the connection failed due to bearing of holes in the bottom sheet.

Figure 35 Bearing around screw holes and detachment of sheets

Figure 36. Condition of 0.85mm Sheet at ultimate load (Setup-2)

Figure 37. Buckling of 0.85mm Sheet at ultimate load

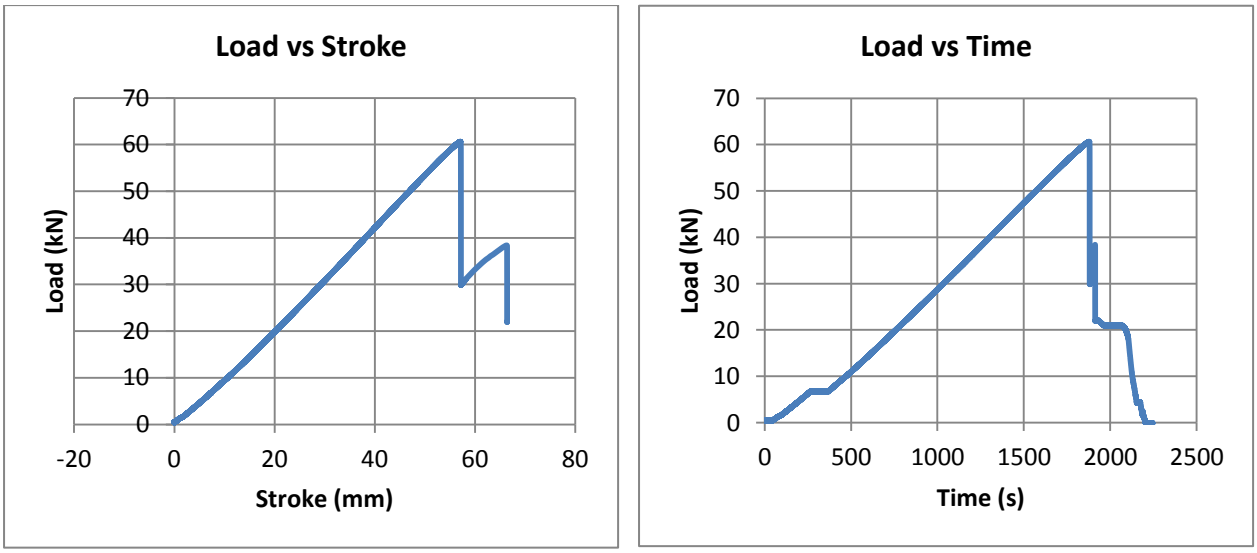

Figure 38. Variation of Load with time and stroke (0.85mm Setup-2)

At this point the test was stopped as the sheets as well as LVDTs were not in contact anymore. The load value of 38.38kN is taken as the ultimate load for the system.

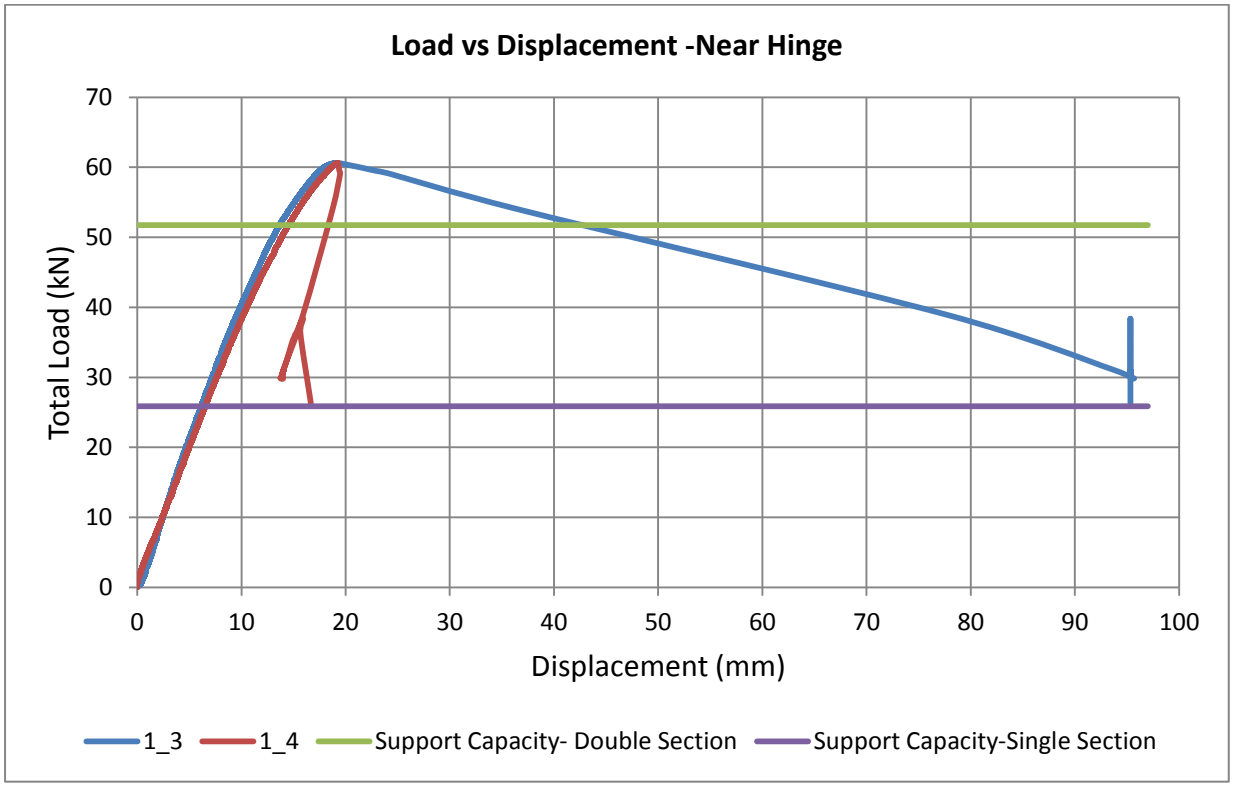

Figure 39 Load vs Displacement before the Hinge Point

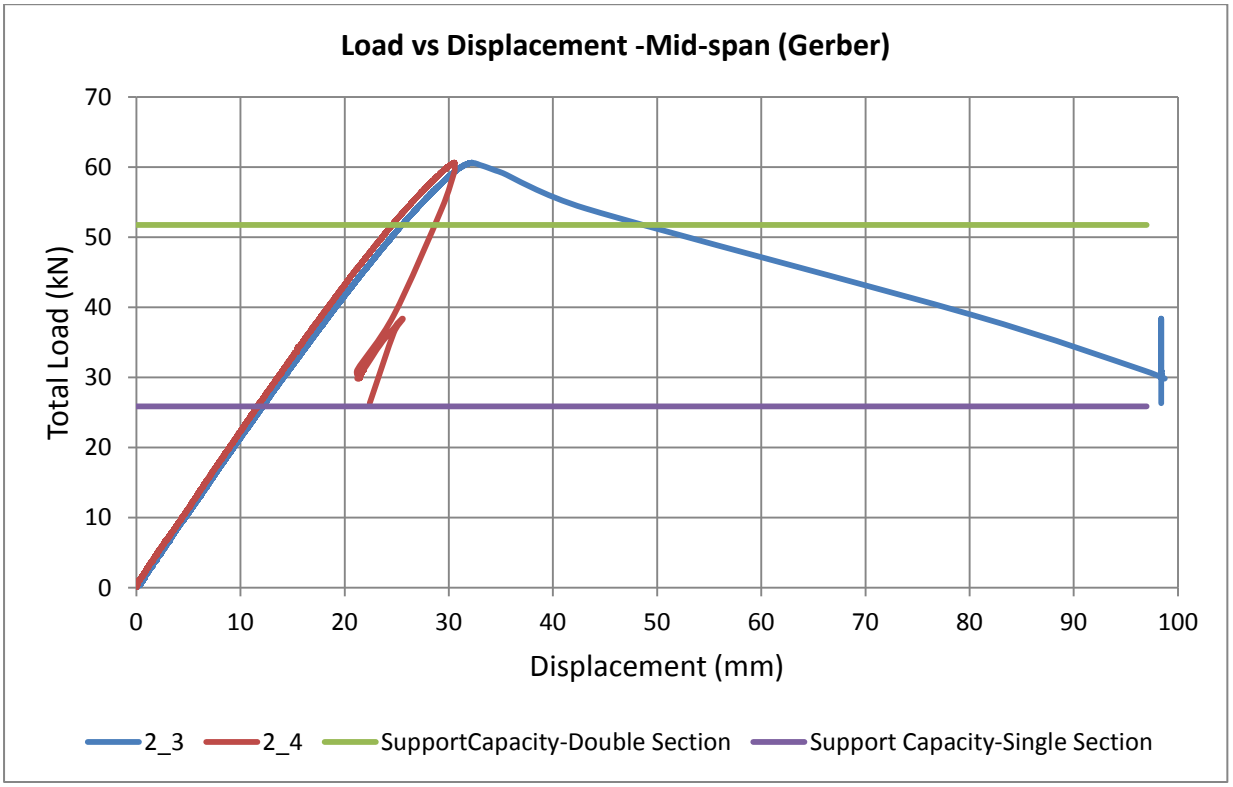

Figure 40. Load vs Displacement in Mid-span

3.2.2 1mm Sheet

3.2.2.1 Test Setup-1

For the First Setup with 500mm screws, the initial failure was observed at 83.53kN. After this elastic failure, both of the sections started deforming. Unloading was done till 75kN and after that, reloading was done. After reaching the load of 84kN, the section at mid-span failed. This experimental test exhibited the continuity of Gerber Joint after the elastic failure as the system deformed as a whole and both the field and span moment capacities were utilized.

Figure 41. Buckling of section over mid-support and mid-span (1mm Setup-1)

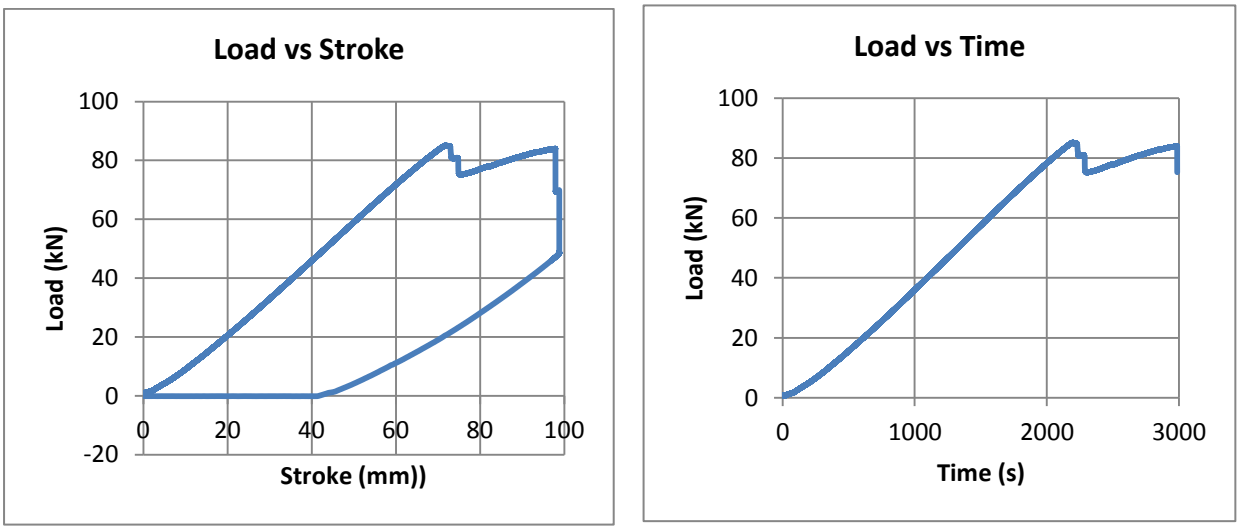

Figure 42. Variation of Load with stroke and time (1mm Setup-1)

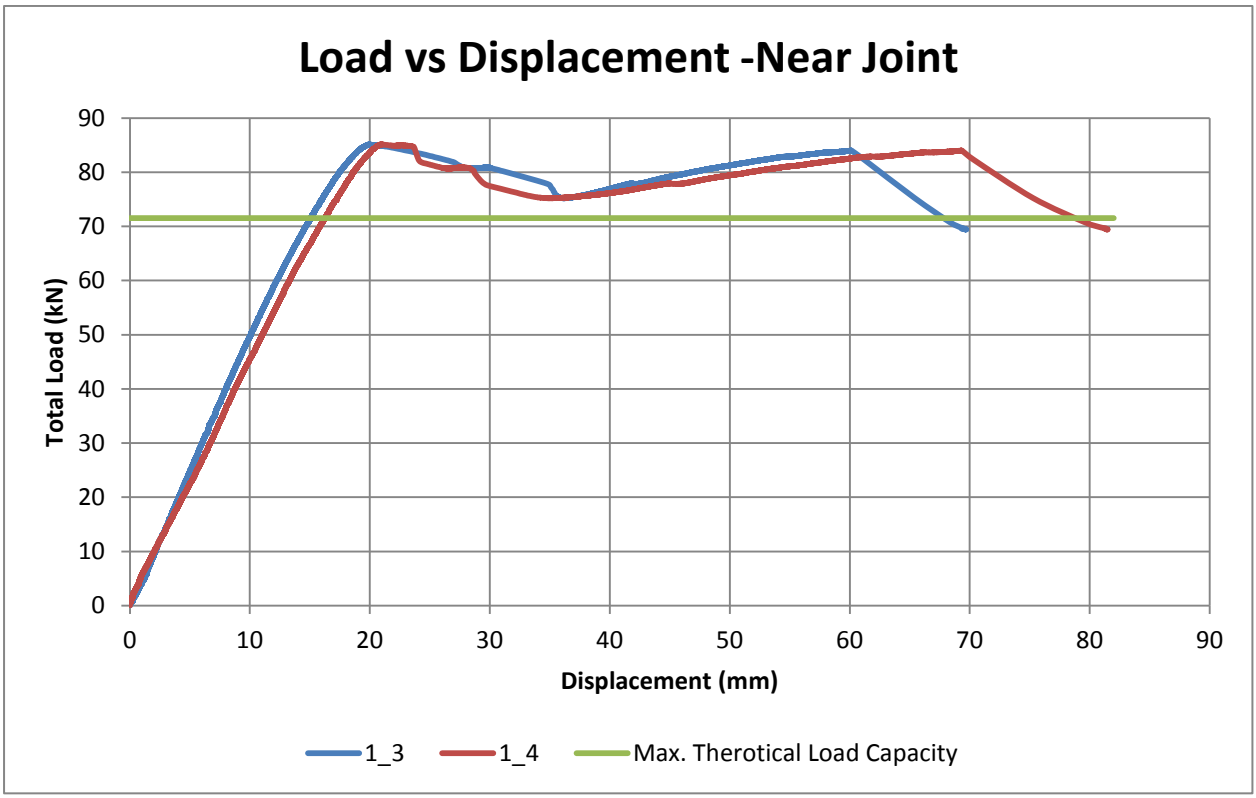

Figure 43. Load vs Displacement near joint (1mm Setup-1)

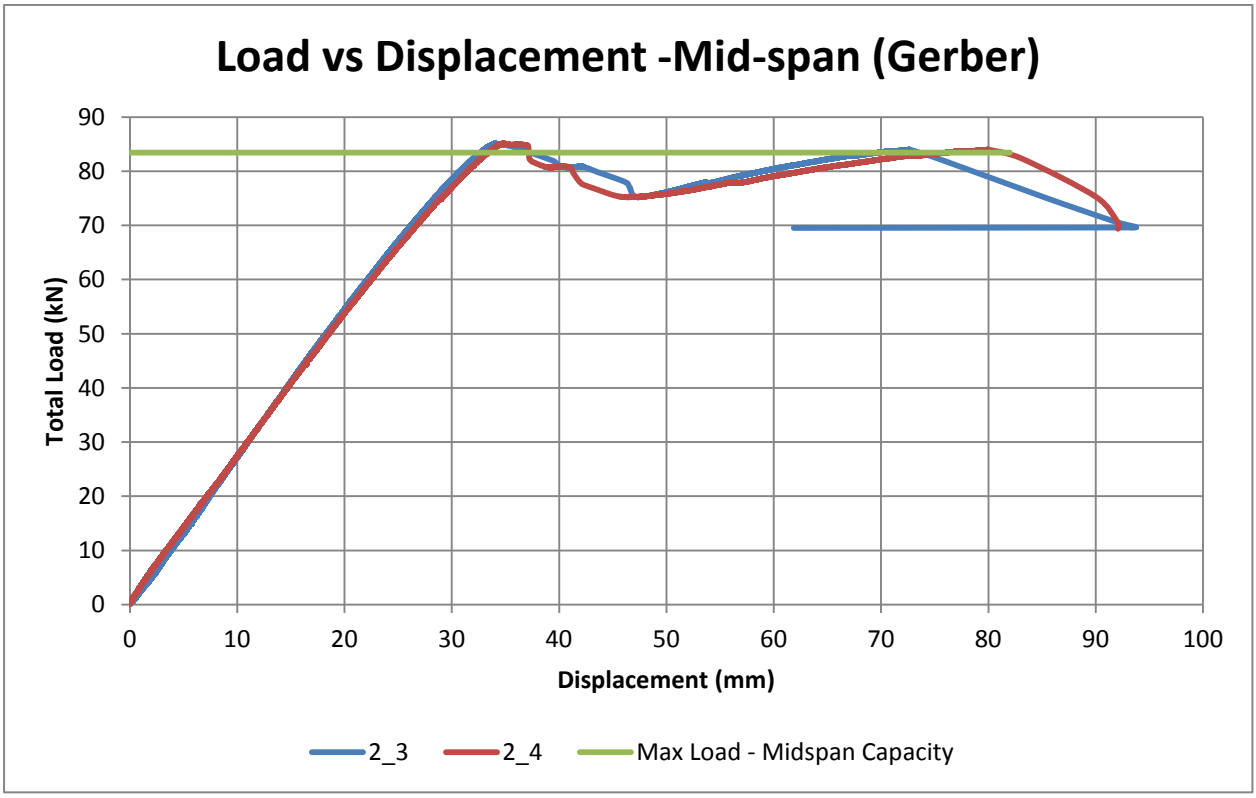

Figure 44. Load vs Displacement at mid-span (1mm Setup-1)

3.2.2.1 Test Setup-2

The second test was done on 1mm thick sheet. The theoretical maximum load capacity for this thickness is 71.53kN. As the system was loaded, elastic failure was first observed at the internal support on one side (1-3).The load corresponding to this failure is 73.25kN which shows that the section had 2.40% more capacity than the theoretically calculated one.

Figure 45. Buckling of section over mid-support (1mm Setup-2)

Figure 46. Condition at ultimate load (1mm Setup-2)

the unloading was done, this section did not come back to its original position rather it displayed a continuous displacement. On the other hand, the other side (LVDT 1-4) did not deform as this one but it shows a small amount of residual displacement which indicates that it has passed its elastic limit. The reloading started from 50.48kN and at reaching the load of 58.82kN, the section over the interior support on side (1-4) also buckled.

Large amount of rotations were observed in this scenario. However, the hinged joints were still intact and no failure was observed in the screws. A small amount of bearing was observed around the holes in the sheets due to which the clamping of the screws was not that much effective.

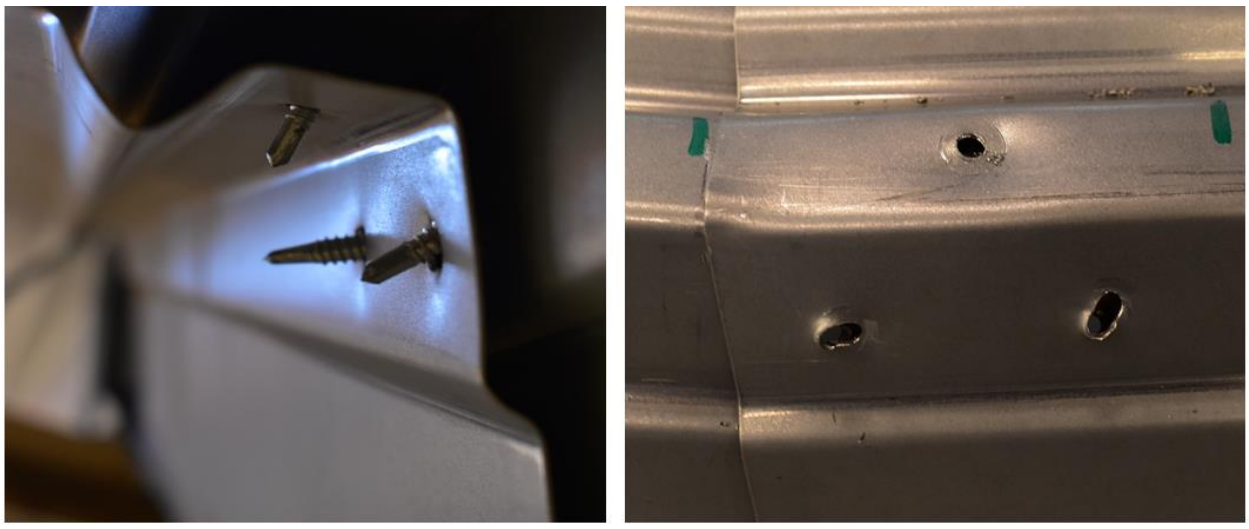

Figure 47. Condition of Hinge Connection at ultimate load (1mm Setup-2)

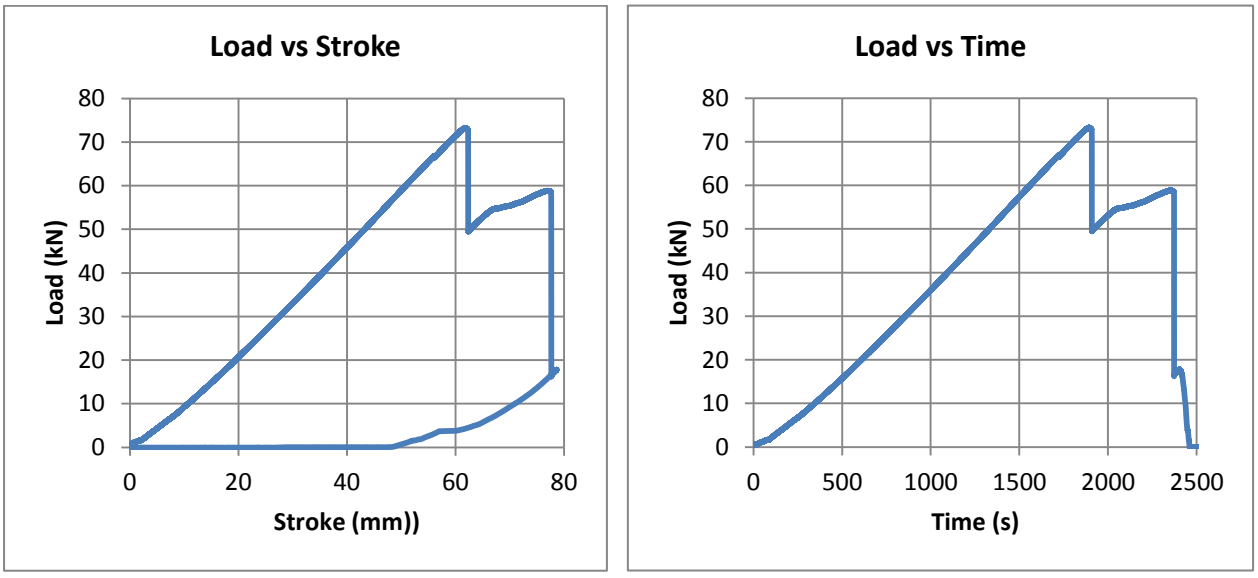

Figure 48. Load vs Stroke and Time (1mm Setup-2)

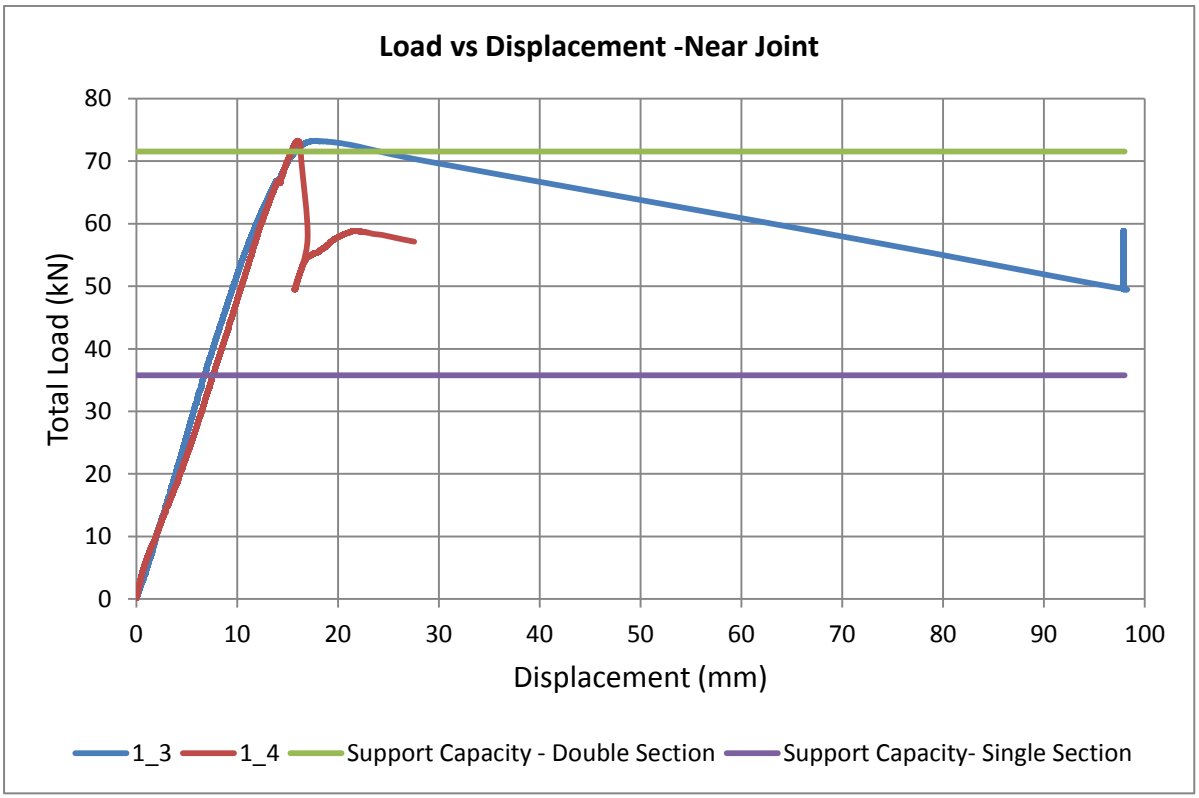

Figure 49. Load vs Displacement near hinge (1mm setup-2)

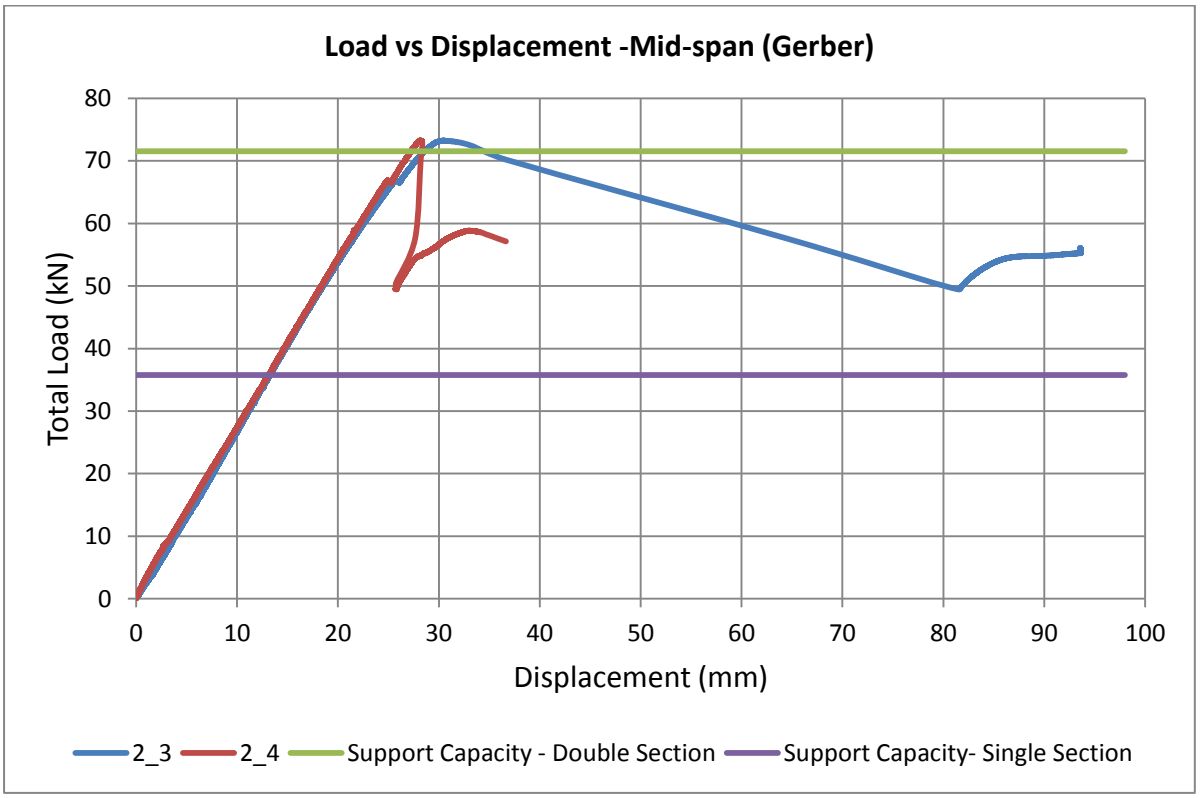

Figure 50. Load vs Displacement at mid-span (1mm Setup-2)

3.2.3 1.5mm Sheet

3.2.3.1 Test Setup-1

Third tests were done 1.5mm sheets and 1.25mm thickness was skipped. The maximum theoretical load capacity calculated for this sheeting is 121.05kN as per the capacity of the section over mid-support. After reaching the load of around 143kN, buckling started at the section over internal support. Upon reloading of the section, support cleats buckled and the test was stopped. Ultimate load for the system could not be achieved in this case.

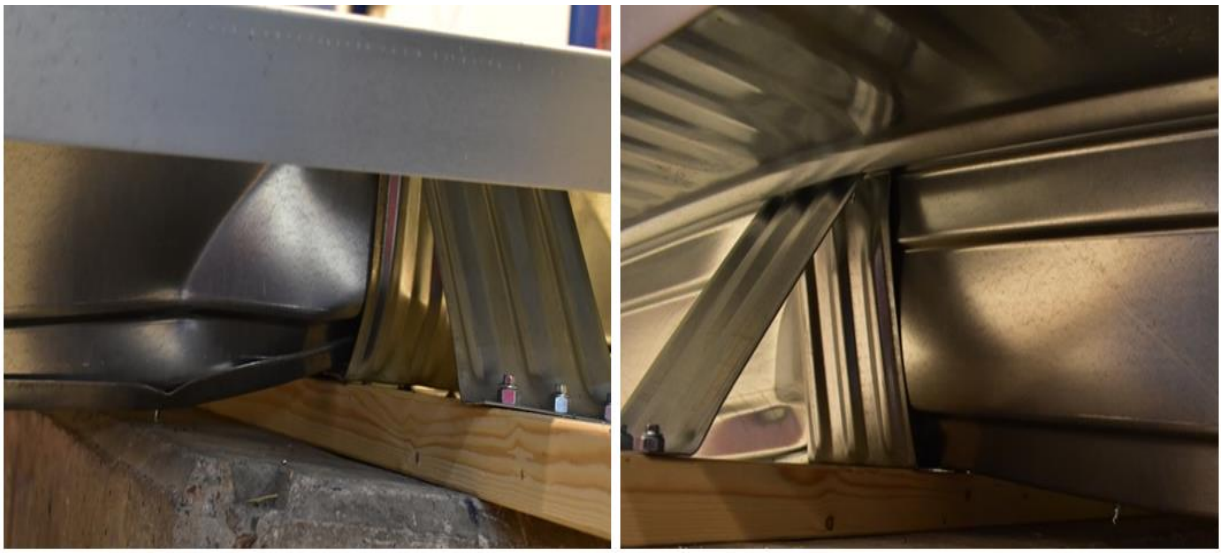

Figure 51. Buckling of section over mid-support and cleat (1.5mm Setup-1)

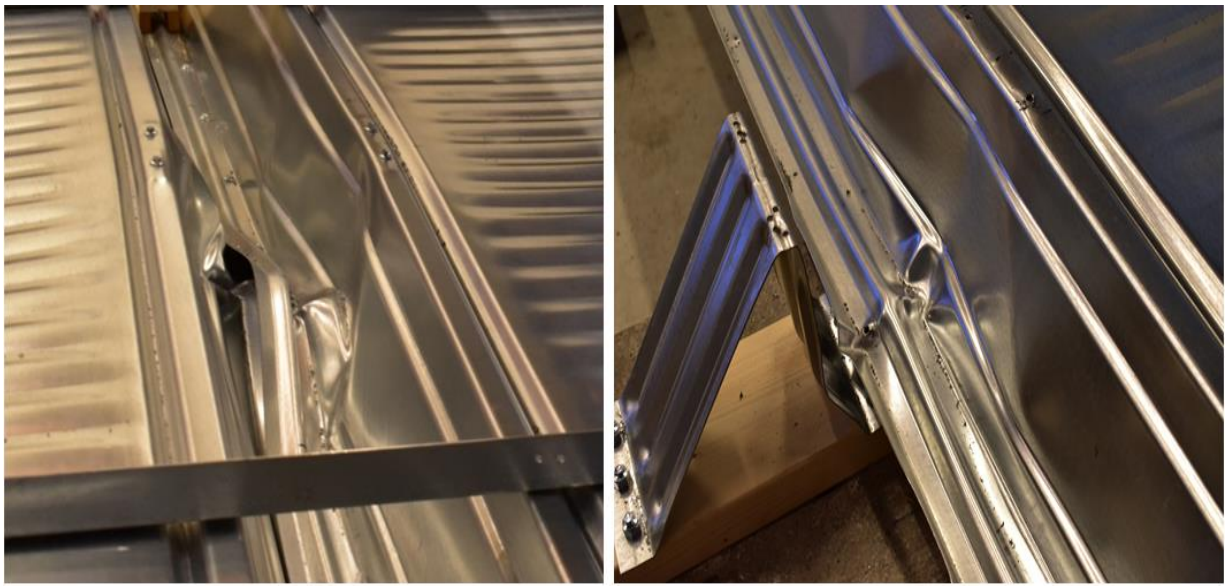

Figure 52. Condition of 1.5mm sheet at ultimate load (1.5mm Setup-1)

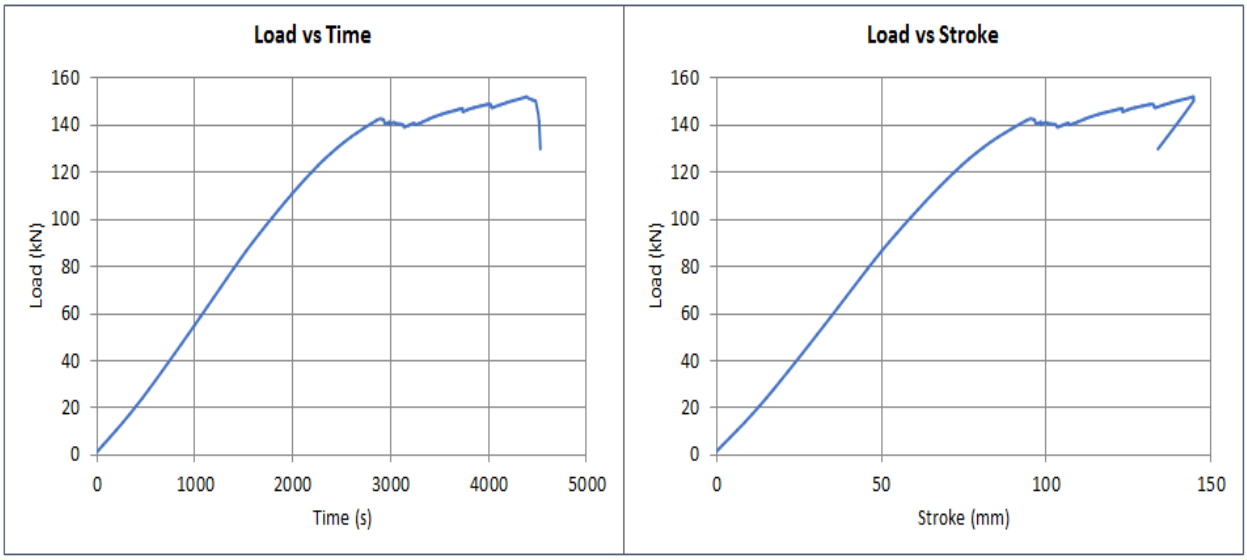

Figure 53. Load vs Time and Stroke for 1.5mm Setup-1

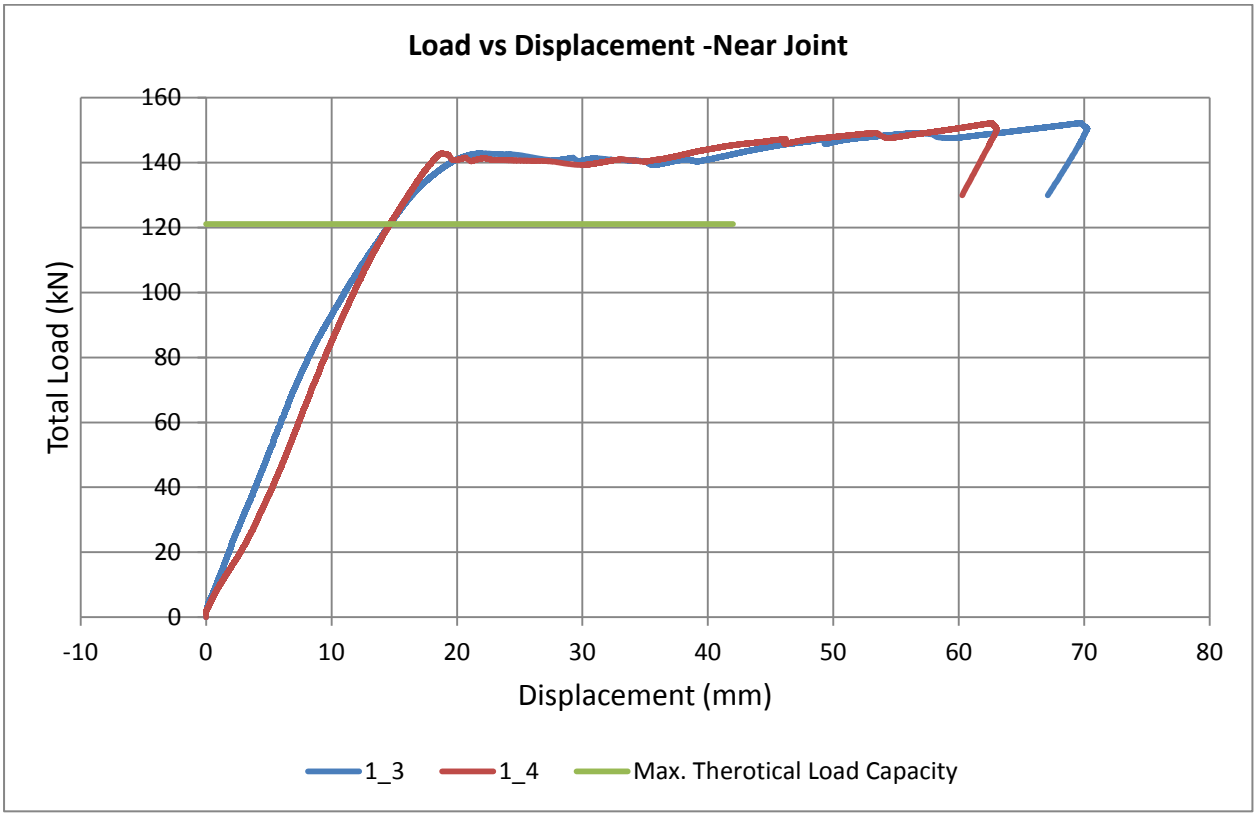

Figure 54. Load vs Displacement near hinge (1.5mm Setup-1)

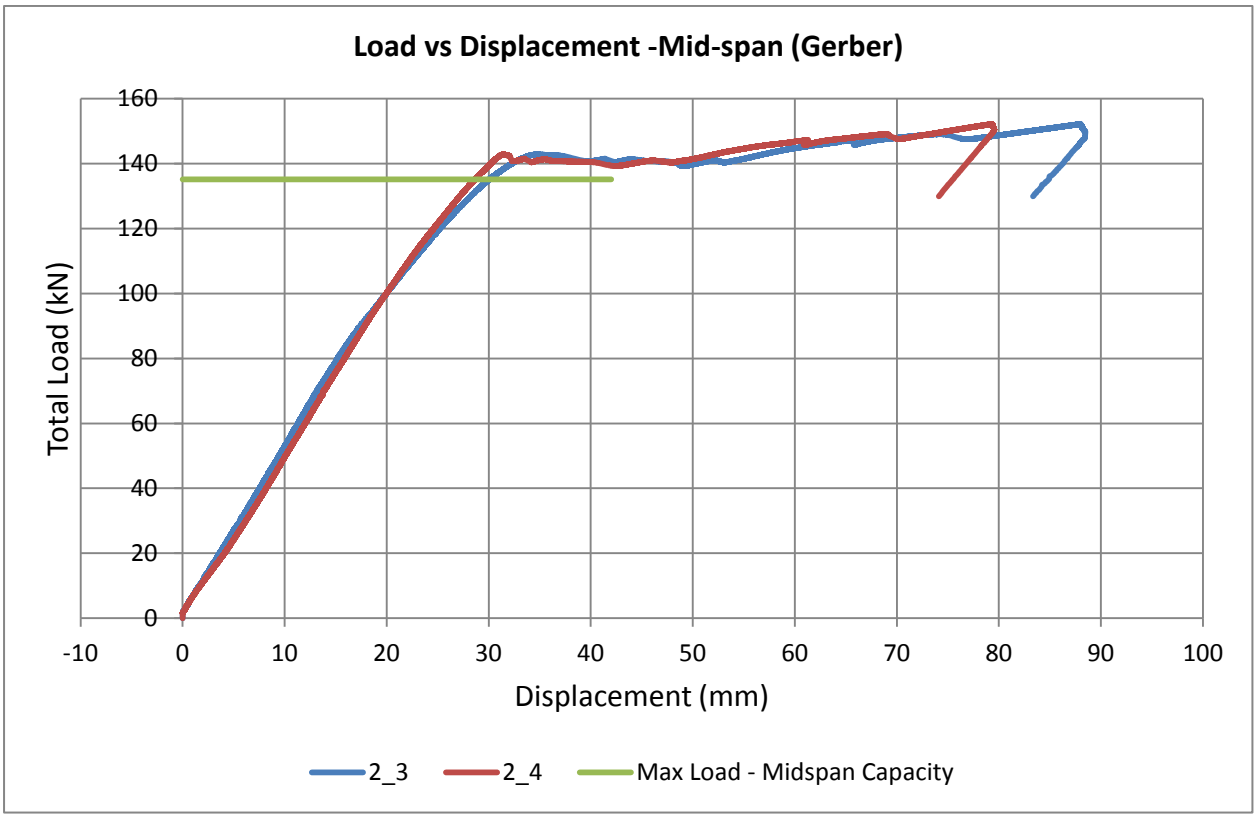

Figure 55. Load vs Displacement at mid-span (1.5mm Setup-1)

3.2.3.2 Test Setup-2

The maximum theoretical load capacity calculated for this sheeting is 121.05kN as well. As the load was increased till 142.46kN, the section on one side buckled. This buckling was accompanied with the buckling of the cleat itself. This particular failure was only observed for this sheet as the stiffness of the support cleat was not enough for such thick profile. Unloading was done from this point. During this unloading, this side started continued deforming on [LVDT (1_4 & 2_4). The other side was still stiff but did not come back to its initial position which shows a residual deformation.

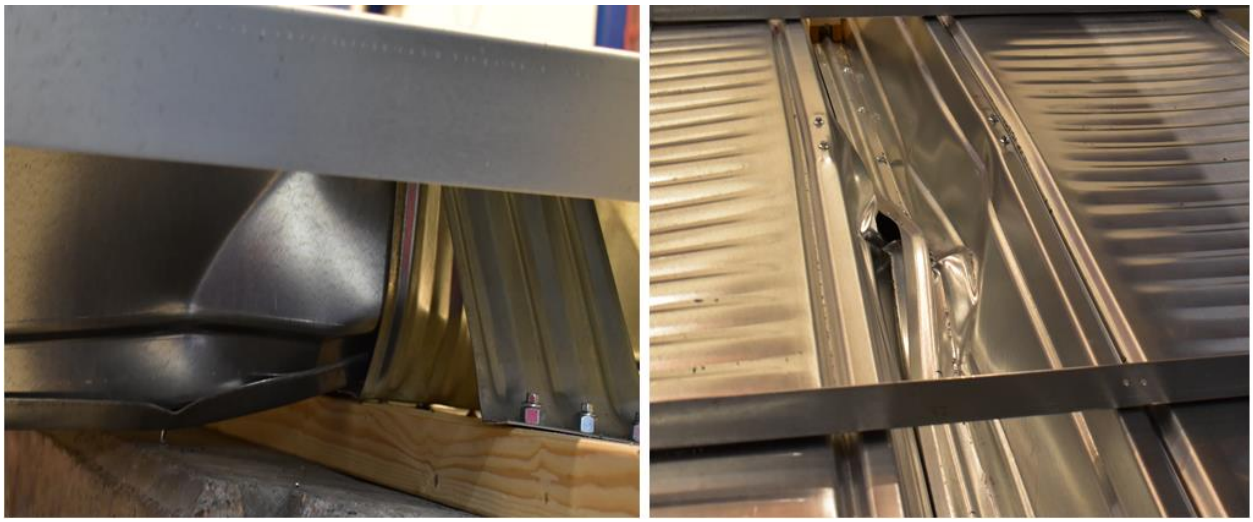

Figure 56. Buckling of section over mid-support and support cleat (1.5mm Setup-2)

The reloading was done from 105.74kN and after reaching the load of around 112.103kN, the other side also buckled. Large amount of deflection was observed at the hinge and the hinged joint was still able to sustain such high rotation. As the support cleat buckled, the test was stopped and the load corresponding to this buckling is termed as the ultimate load for this section.

Figure 57. Condition of Hinge at ultimate load (1.5mm Setup-2)

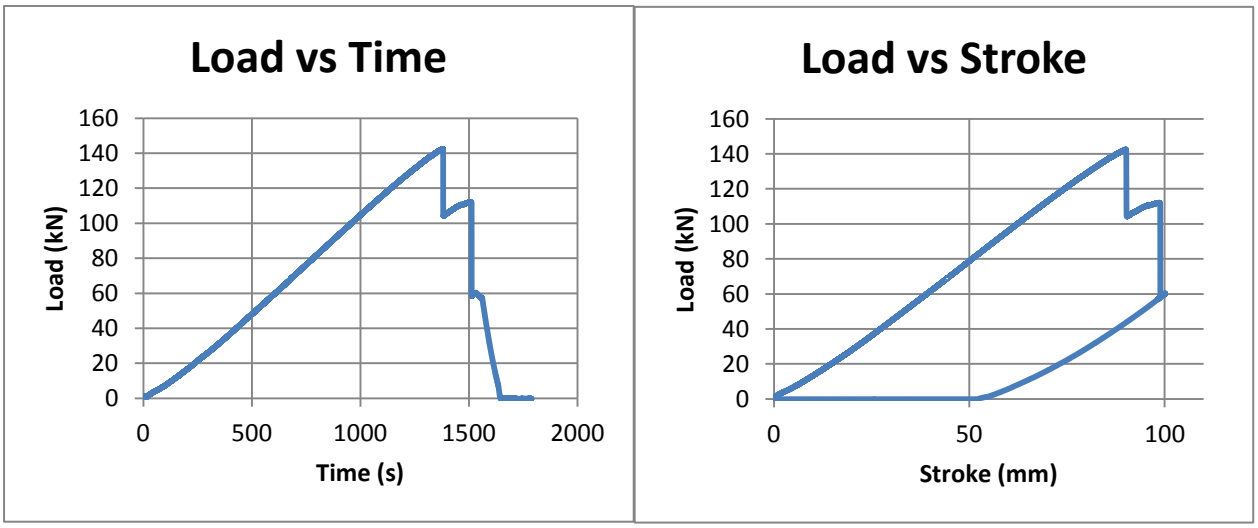

Figure 58. Load vs time and stroke for 1.5mm Setup-2

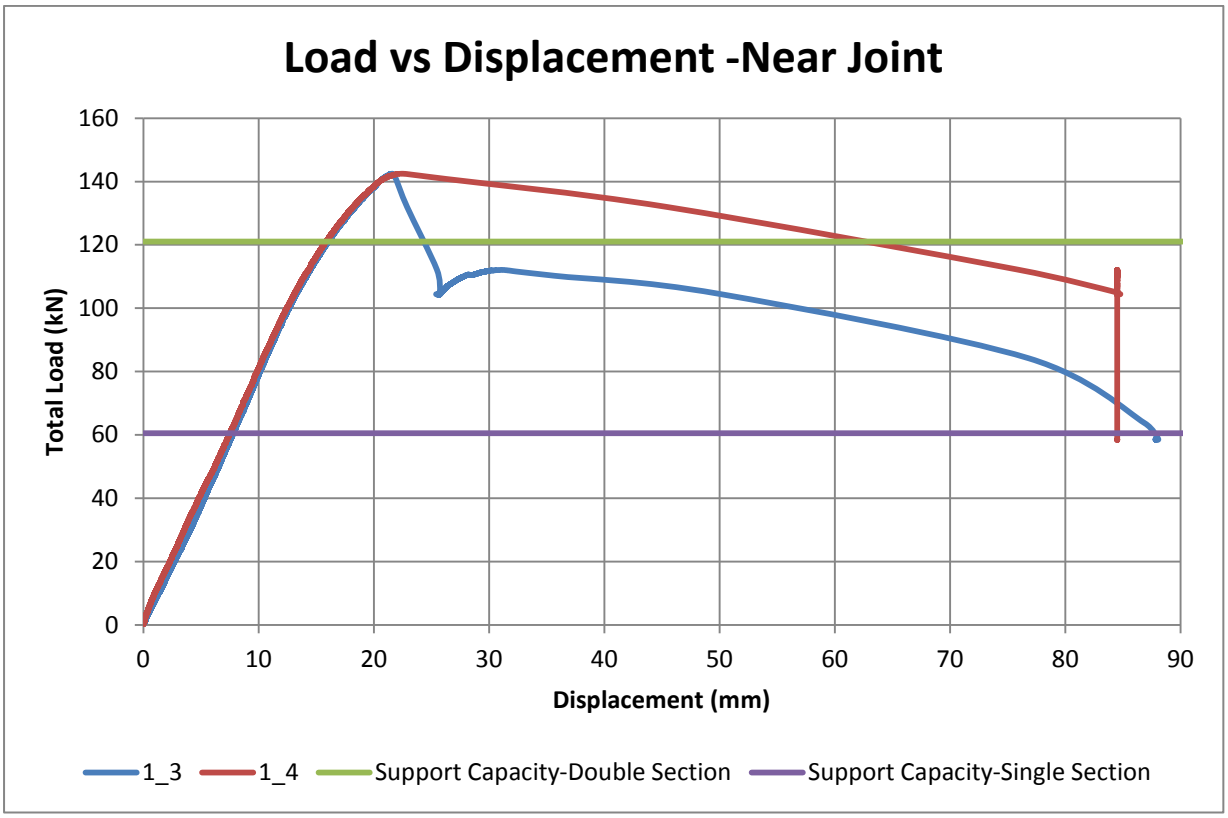

Figure 59. Load vs Displacement near joint (1.5mm Setup-2)

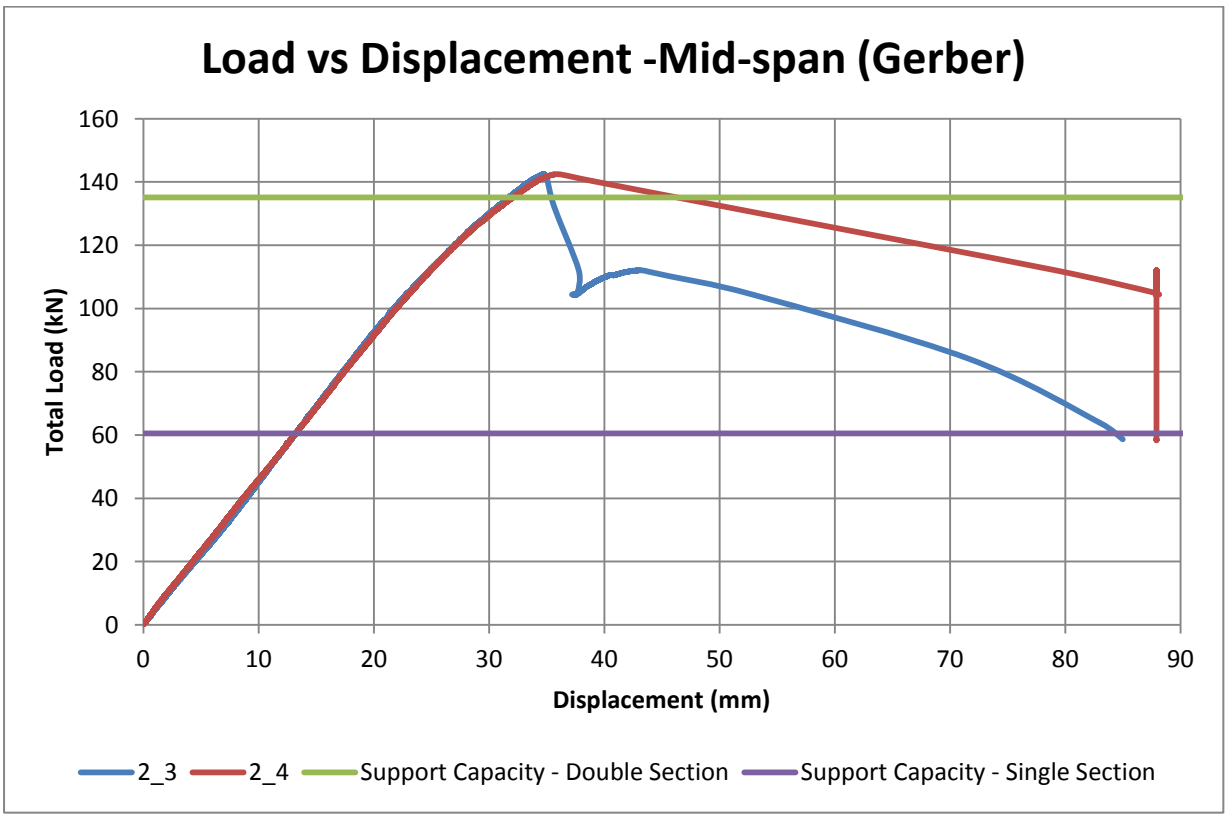

Figure 60. Load vs Displacement at mid-span (1.5mm Setup-2)

4 Numerical Modeling

For the numerical analysis of the sheeting, finite element analysis software ABAQUS 6.14 has been used. This software includes step by step logical modules for the modelling the desired system and at the end an input file is generated to proceed with the analysis. After the analysis, the visualization module is used to simulate the results of the analysis and generate output. This chapter will describe the assumptions and techniques used in different modules to model the assembly and the results that are generated from the software are presented and discussed at the end of this chapter.

4.1 Development of Model

To model the system in ABAQUS, some simplifications have to be made as per the requirements of the software. As the aim of finite element modelling is to study the desired behaviour and get the results which are necessary to draw conclusions, the system must be calibrated as accurately as possible and the results must be verified with analytical and experimental results. The longitudinal section and the loading arrangement is the same as used in experimental setup (Figure 61)

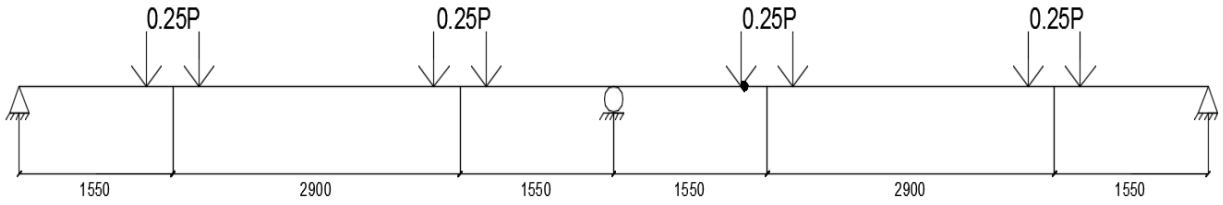

Figure 61. Beam Modelled in Abaqus

Since the system setup in ABQUS is unit-less, therefore, a consistent system of units has been used for the analysis in order to avoid errors and irregularities in results (Table 3).

Table 3. Units used for Abaqus Modelling

Dimensions	Force	Stress	Time
Mm	N	MPa	s

4.1.1 Part Module

The cross-section of the experimental assembly consists of two sections making a total width of 1600mm. For the computational efficiency, symmetry of the experimental setup has been taken into account and only one single section is used for Abaqus modelling. To replicate the test setup, this section is made by cutting one full section into two parts and then joining these two parts at the bottom flange (Figure 62). As the geometry of the section was provided by Lindab, so the sketch of the sheet was imported into Abaqus from the drawings provided. These sketches were made as deformable shell elements due to their thickness.

To replicate the support cleats, a shell part of 15mm width and 150mm length was made which will be connected to outer part of the top flange (Figure 63). This cleat will be connected to this top flange through point-based fasteners.

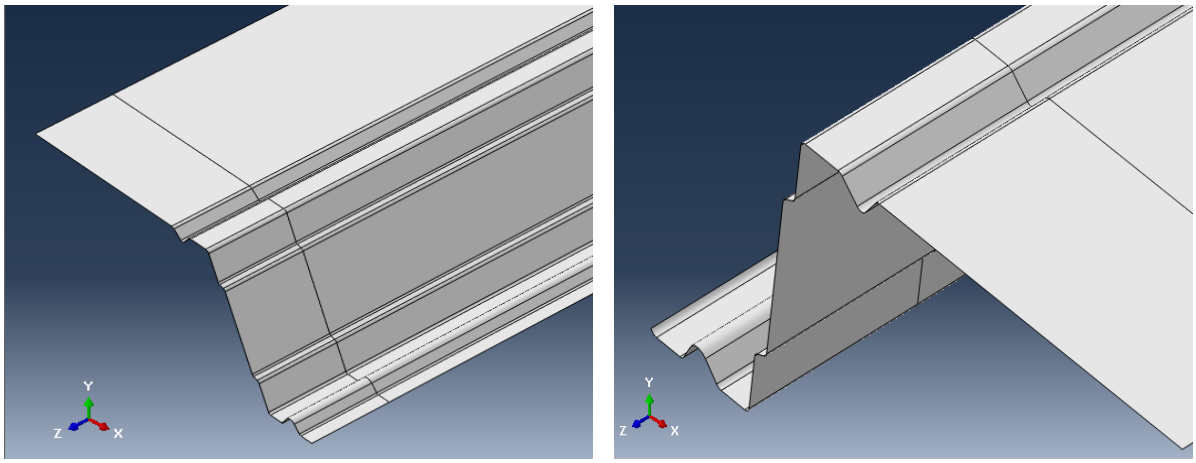

Figure 62. Parts of Trapezoidal Sheets modelled in Abaqus

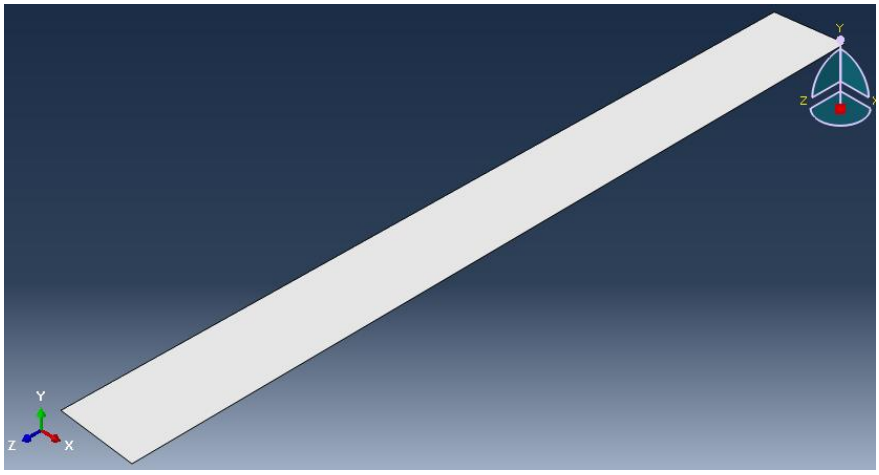

Figure 63. Plane shell replicating the support cleat

4.1.2 Property Module

This module is used to define the material properties and creating the sections that have these material properties. Two types of materials are defined in this analysis, one for the trapezoidal sheet and one for the plane shell part replicating the support cleat. For the trapezoidal sheets, non-linear material behaviour has been considered by defining the elastic as well as plastic properties. The material model that is used is taken from Annex C.6 of (EN 1993-1-5 - Plated structural elements, 2003).

- f_{yb} = 420MPa
- E = 210GPa
- Elastic Strain = $\varepsilon_e = \frac{f_{yb}}{E} = 2x10^{-3}$
- Plastic Strain = $\varepsilon_p = \frac{600 - f_{yb}}{E/100} = 0.086$

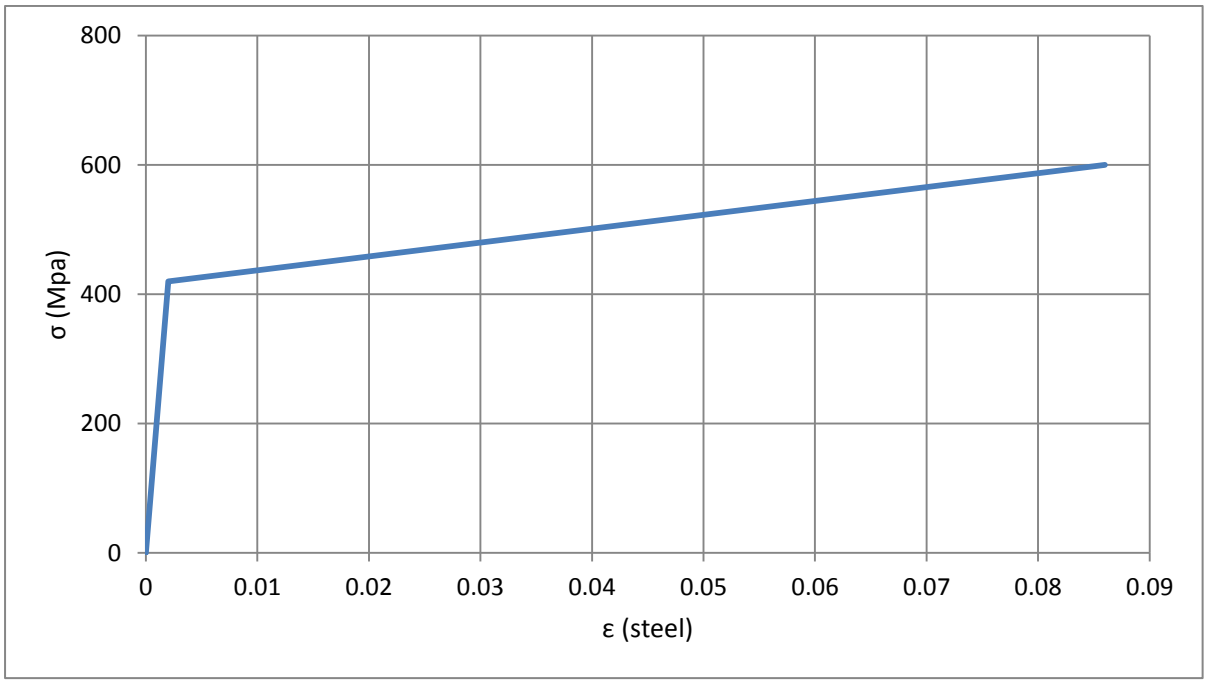

Figure 64. Bi-linear Material Curve used for Trapezoidal Sheet

For the section definitions, shell homogenous sections were used. For the trapezoidal sheet, both the elastic and plastic properties were used. Since the support cleat has to be rigid, only elastic section properties were used with modulus of elasticity 10 times higher than that of trapezoidal sheet (Table 4).

Table 4 Material Properties used for Abaqus Modelling

Part	Thickness	Elastic		Plastic	
		E (Mpa)	v	Yield Stress (Mpa)	Plastic Strain
Sheet	0.85 /1	210000	0.33	420	0
				600	0.086
Support Cleat	3	2100000	0.33	-	-

At the point of the section definition, Abaqus gives two options regarding the stiffness calculation of the section, wither during the analysis or before the analysis. For the stiffness calculated during the analysis, the thickness integration points defined to calculate the stresses and strains at those points (Abaqus Analysis User's Guide), thus allowing for the non-linear behaviour. However, for the stiffness calculated before the analysis, the material behaviour must be linear elastic.

For this non –linear analysis, the section integration during the analysis has been chosen with integration points as 5. The thickness of the section assigned is 0.85mm. Simpson's rule with 5 integration has been used which is the default method and suited for the results output at the shell surface (Abaqus Analysis User's Guide).

4.1.3 Assembly Module

In this module, the instances of the parts are created and they are arranged according to the real scenario and in this case, according to experimental setup. The instances that are

created here are dependent which means that they are meshed in the part module and any change in the part module will affect the instance as well. A total of 10 instances were created in the assembly, 4 instances for four sheets and 6 instances for plane shell replicating the support cleat. The instances were then arranged accordingly.

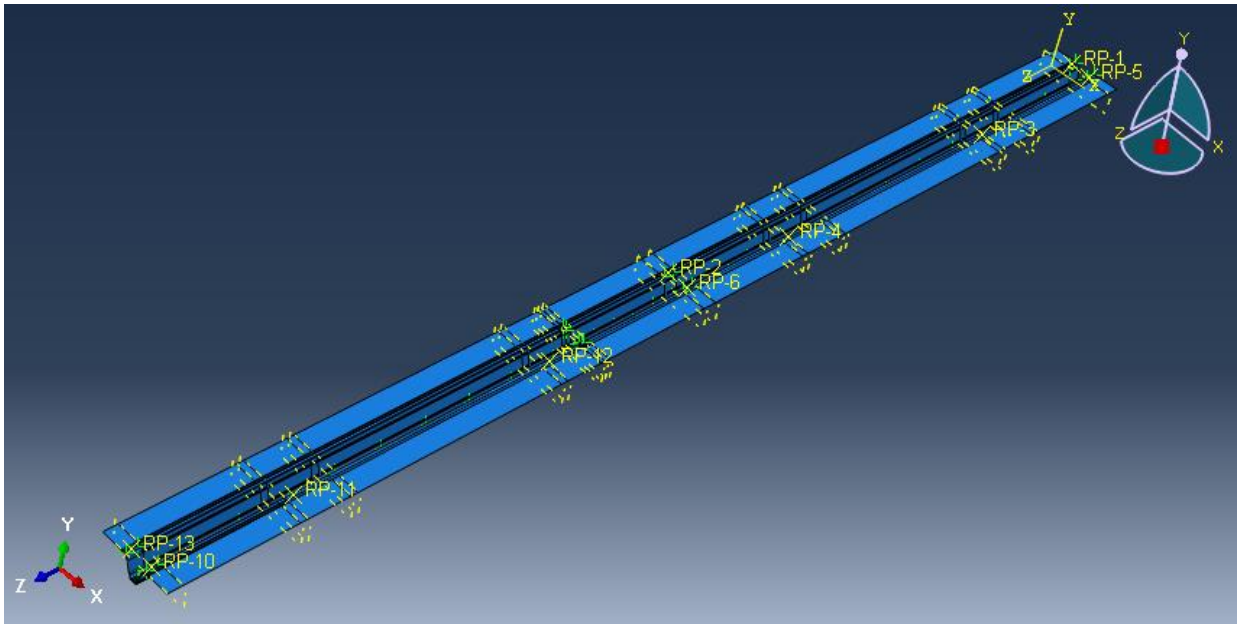

Figure 65. Assembly of sheets in Abaqus

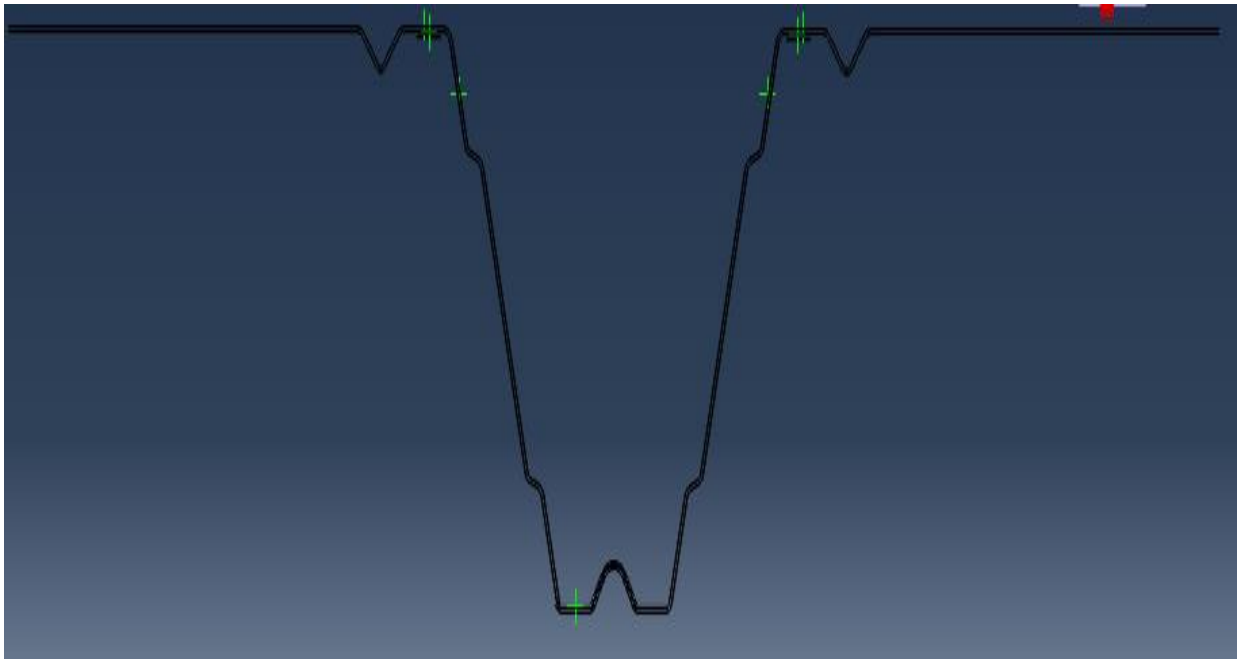

Figure 66. Cross Section in Abaqus Modelling

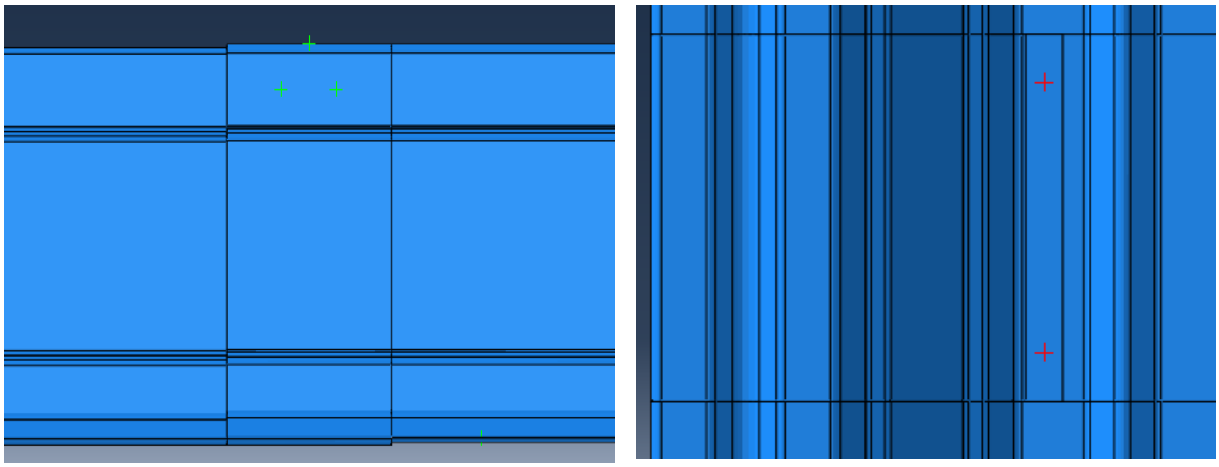

Figure 67. Hinge Joint and Side Overlap of Sheets

For the side overlap, the reference surfaces i.e. middle surfaces were stacked over each while keeping a distance according to shell thickness (Figure 67). The hinge joint was made by overlapping the sheets with a length of 100mm and 3 screws were placed as per the experimental setup. The support cleat was placed beneath the top flange and at a distance of 1.5mm from the web to avoid any penetrations at the start of analysis (Figure 68).

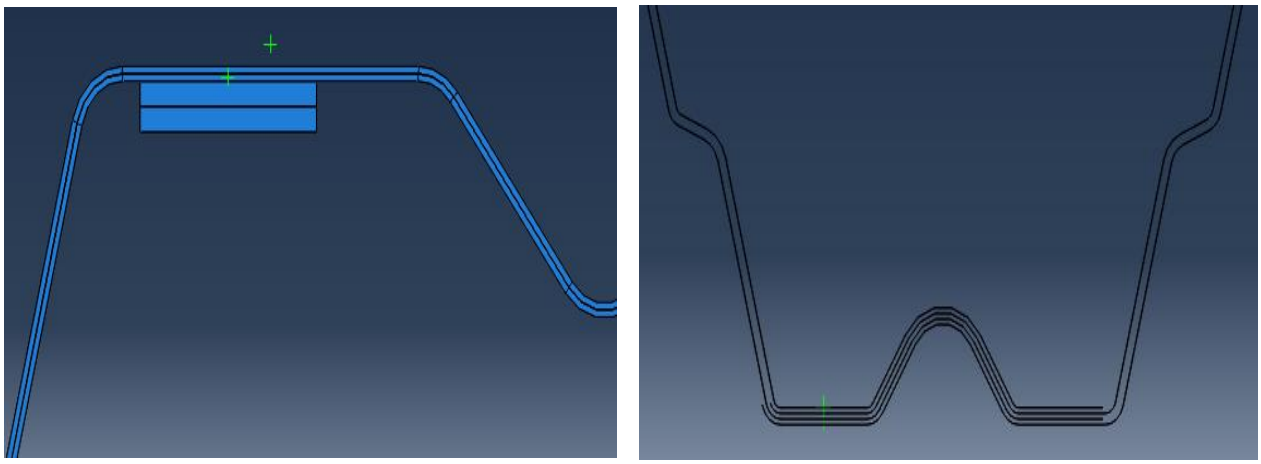

Figure 68. Position of support cleat and screw placement

After assembling the model, reference points were defined as per the geometry. These reference points are meant to constraint the partitions and then loads and boundary conditions are assigned to them. Total of 10 reference points were defined which can be categorized into types:

1. Category -1: These were defined so as to constraint the motion of plane parts Replicating the supports cleats.
2. Category -2: These reference points were defined to constraint the motion of sheet parts subjected to load. They were also defined at the centroid of these parts.

4.1.4 Step Module

The step module is used to define the sequence of one or more steps that will be followed during the analysis, specifying analysis controls and outputs requests. There is a default general analysis step named Initial which is used to specify the conditions at the very beginning of the analysis. In the steps module, further steps are defined which are used to model the changes in boundary condition, interactions or loading on the assembly.
For this analysis, static riks analysis step has been used. The static riks method is suitable for the problems which undergo buckling and the load-displacement relationship show a negative stiffness (Abaqus Analysis User's Guide). To capture the non-linearity of the geometry and the change of stiffness during the analysis, Nlgeom option was turned on for analysis step.

Table 5. Parameters used for Static Riks

Maximum Number of Increments	Arc Length Increment			Estimated Total Arc Length
	Initial	Minimum	Maximum	
1000	1.0E-04	1.0E-10	0.1	1

4.1.5 Interaction Module

This module is used to define the mechanical interaction between surfaces that are in contact with each other, the constraints on different part instances in the model, and the connectors to join different part instances along with connector section properties. Since these interactions are step-dependent, all of these interactions will be defined in the initial step so that they are active at the beginning of the analysis.

4.1.5.1 Interaction

The interaction property used for this modelling was General contact. As all the surfaces that interact in the model have the same properties, therefore, general interaction was used and a friction co-efficient of 0.3 was defined for its property. In order to avoid the convergence problem due to initial penetrations and over-closures in curved shells, contact initialization property was defined in which strain free adjustment of the surfaces was checked on. Turning on this option gradually removes the over-closures during the first analysis step.

4.1.5.2 Constraint

In this part of interaction module, the degree of freedom of a part instance or a region of a model is constrained to the motion of a point or a body. This is used to enforce boundary condition or load on a region or a part instance. In this analysis, two types of constraints have been used which serve the difference purpose.

- Coupling Constraint: This constraint is enforced between the parts of the sheet subjected to load and the reference point defined at the centroid of each loaded

part. In this constraint, kinematic coupling has been used constraining all the degrees of freedom of a surface to the constraint control point (Figure 69 a).

- Rigid Body Constraint: This constraint is enforced between the plane part replicating the support cleat and the reference point defined at the centroid of each cleat. This constraint will be used to define the boundary condition for the model (Figure 69 b).

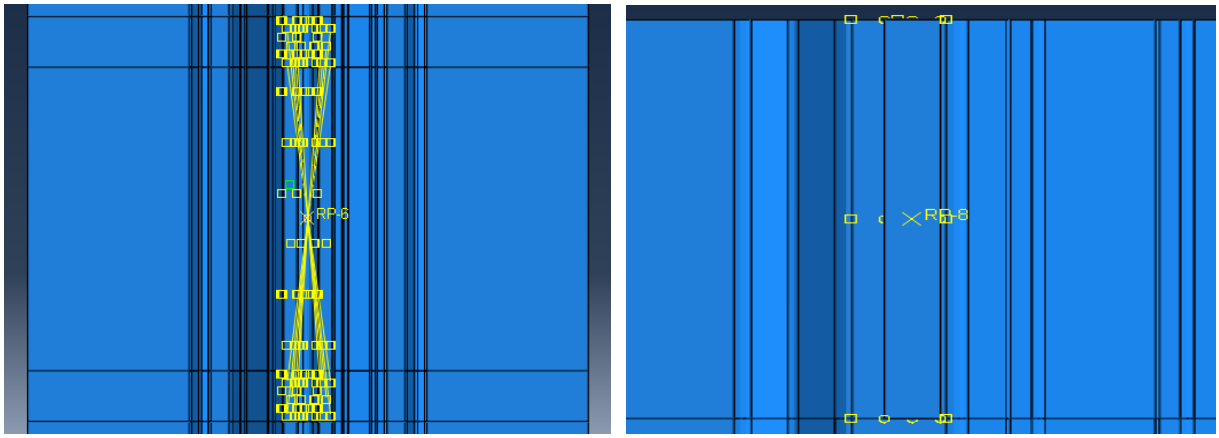

Figure 69. Kinematic Constraint (a) and Rigid Body Constraint (b)

4.1.5.3 Connectors

Connectors are used to model a connection between the part instances and are mesh-independent. The connector assignment between part instances consists of three steps. First of all, a connector section is defined which contains the desired properties of the section. Then attachment points are defined on the assembly where connectors are to be placed and finally the connector sections are assigned to these attachment points. In this analysis, two types of connections are used i.e. connection of side overlap of sheet, connection of support cleat with sheet flange.

For the connector section of support cleat and sheet flange, Hinge Connection category has been used which constraints all the degrees of freedom except the rotation about 1-axis i.e. X-axis. Thus the connection between the sheet and the cleat will behave as a pin connection. However, for connector sections of side overlap, beam type connections have been used which will constrain all degrees of freedom.

4.1.6 Load Module

This load module is used to define the boundary conditions and loads on the model. The load that is applied in this module will be used to calculate the load proportionality factor for static riks analysis step. The load is applied on 4 reference points which transfer them onto the surfaces they are constrained through coupling. The load value at each reference point is 500N which makes a total load of 2kN which will be applied as per the proportionality factors defined in step module.

There are six boundary conditions for the setup, one for each cleat. The boundary condition that is applied is to each reference point constraints all the degrees of freedom. As the cleat

is joined to outer part of the top flange through hinge connection, thus it will replicate the pin boundary condition.

4.1.7 Mesh Module

As the model contains two types of parts; sheet and plane part replicating the support cleat, different mesh size was used for both. For sheets, a mesh size of 40mm was used and S4R elements were assigned to them as they are meant for doubly curved thin or thick shells. However, for the support cleats, a bigger mesh size of 75 was used as they were not intended to get any result and also they were assigned as rigid bodies.

4.2 Results

A good correlation was observed between the results from Abaqus and experimental tests. As predicted, the section over the internal support was the most stressed zone in the model.

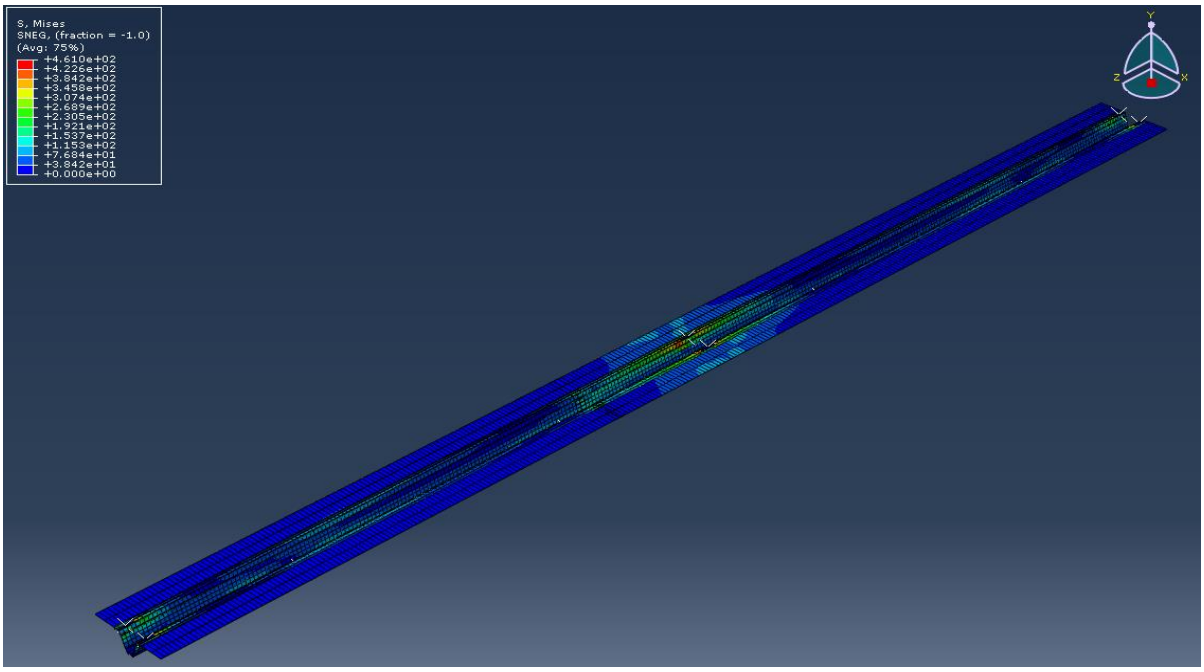

Figure 70. Stress result from Abaqus Model

The maximum stress that in the Abaqus model is 463MPa and this stress is around the screws in the support cleat. Tension yielding is observed around the screws in top flange of the sheet and the maximum stress path then travels into the webs. These webs then buckle causing the failure of the section.

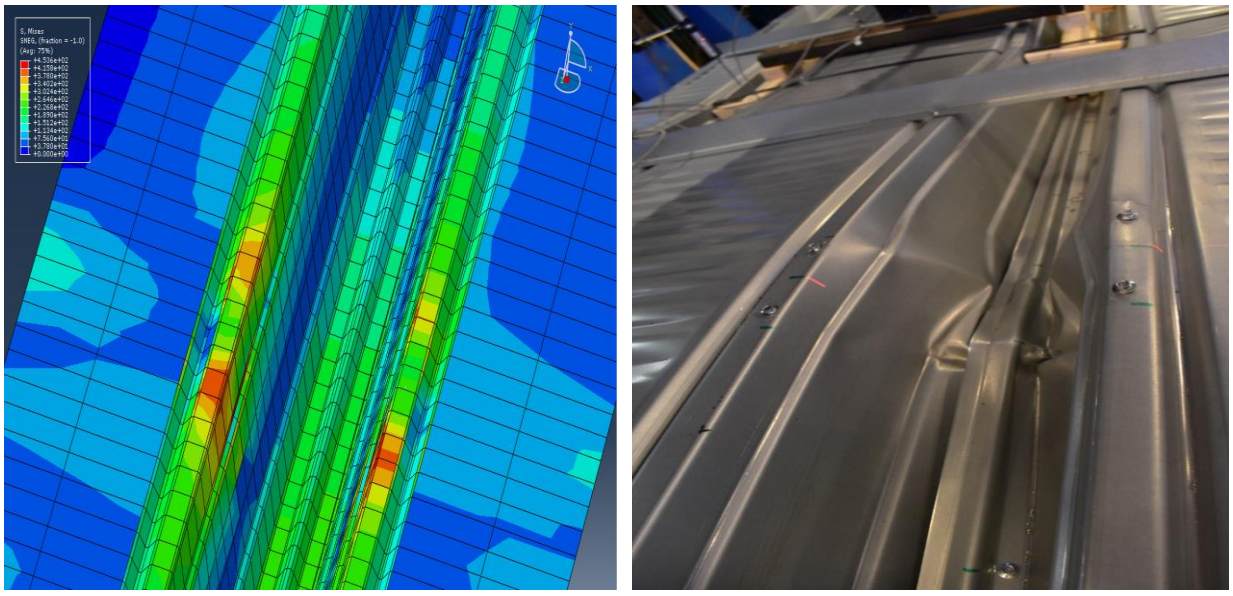

Figure 71. Stress at support (Abaqus vs Experiment)

The deformation scale factor in the visualization mode was enhanced to see the buckled shape of the member in Abaqus which had the similar pattern as observed in the experimental test.

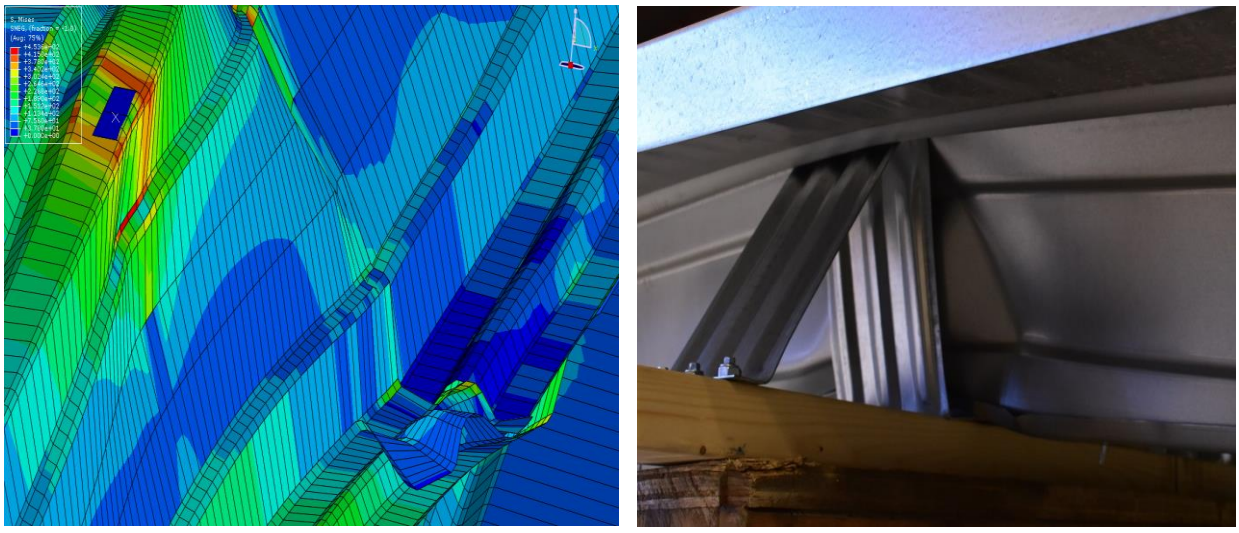

Figure 72. Buckling of section over mid-support (Abaqus vs Experiment)

Load-displacement curve was obtained for the points near the hinge and the mid-span having the Gerber joint. These load-displacement curves were compared with the ones obtained from the experimental setup and the results from both the scenarios were quite close. The load-displacement for the mid-span lies exactly on the curve of experimental test while for the location near the hinge, the two curves was quite close.

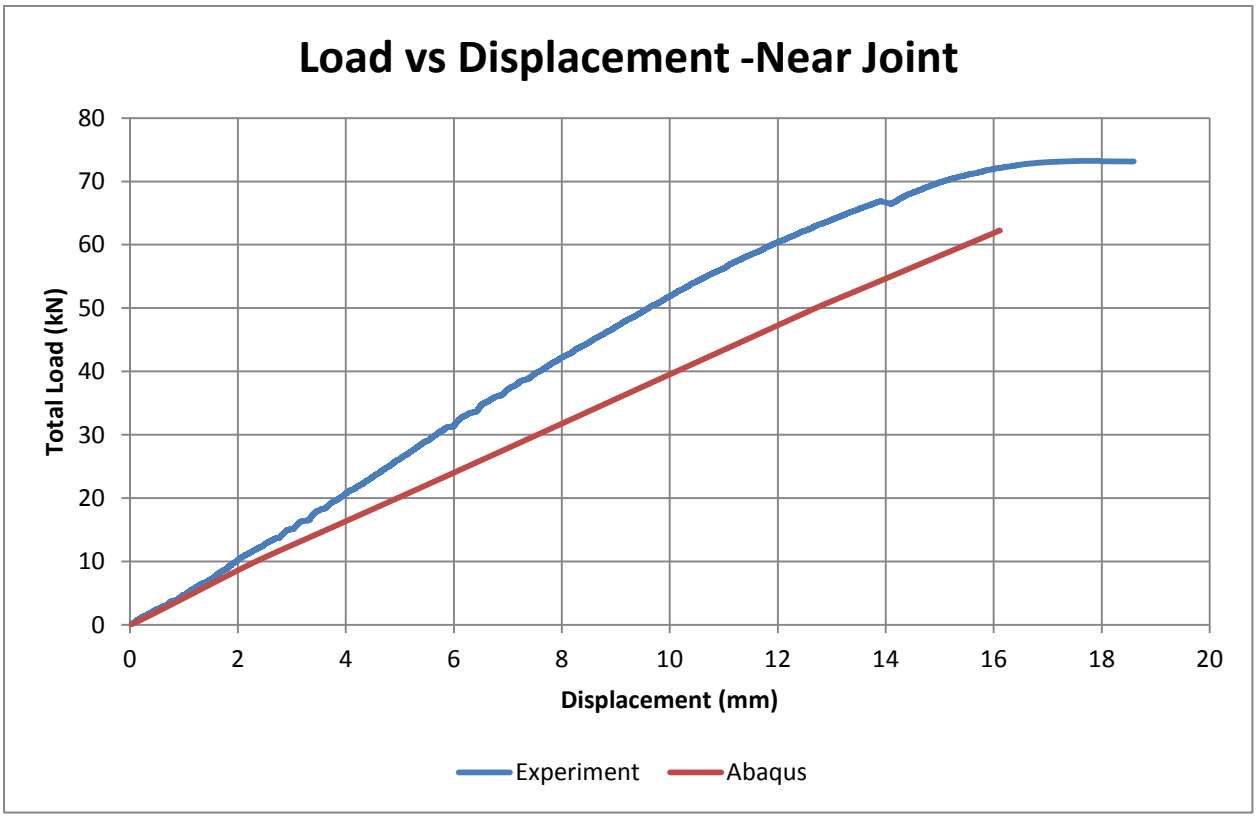

Figure 73. Load vs Displacement near Joint (Abaqus vs Experiment)

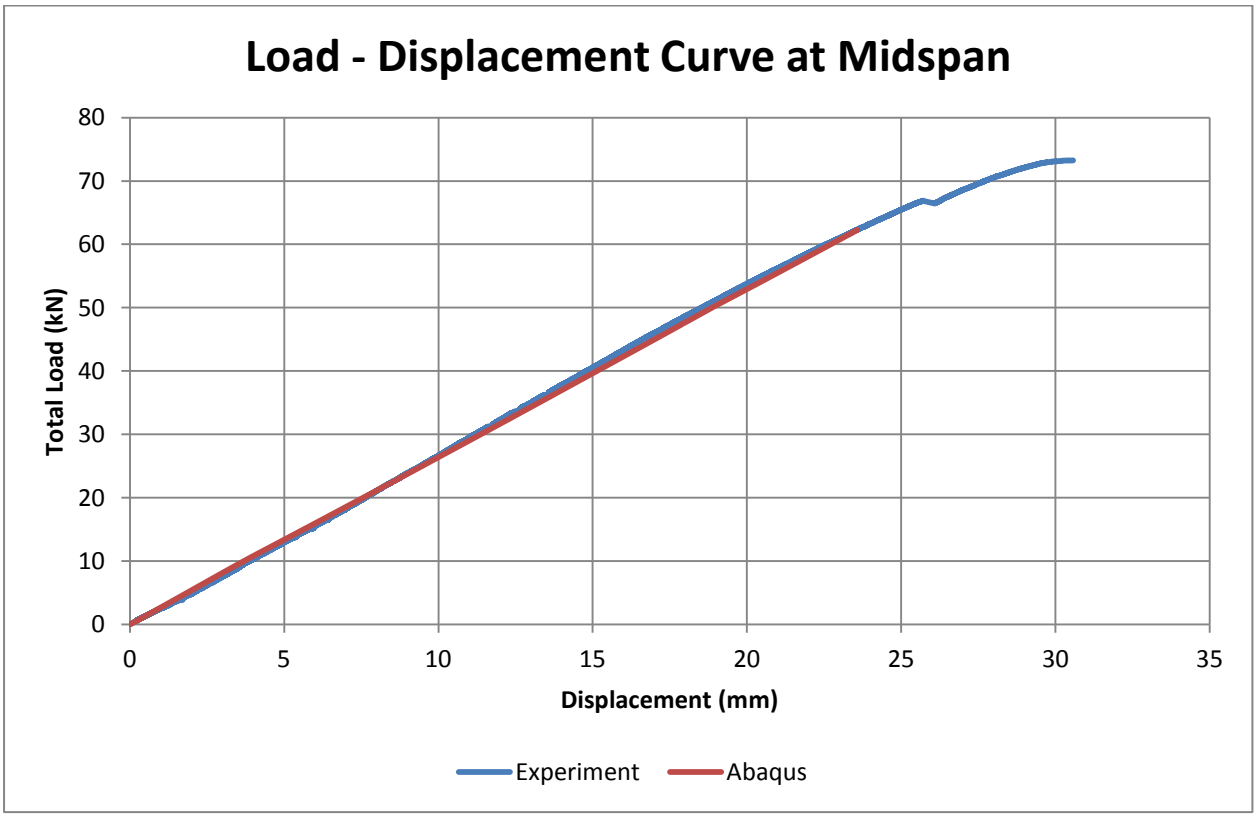

Figure 74. Load vs Displacement in mid-span (Abaqus vs Experiment)

However, the modelling was not successful to capture the behaviour of the section after its elastic failure. As soon as some parts of the model reach their yield stress, Abaqus gave convergence problems due to which it was not possible to achieve the complete ultimate collapse of the system. It would be interesting to model the system with initial imperfections without the plastic material properties for future studies to get the behaviour of the system at the ultimate load.

5. Computation of Reserve Moment Capacity & Moment Redistribution

Cold Formed Steel members possess some inelastic reserve capacity which can be assessed through experimental tests. This inelastic reserve capacity is a dictating factor for moment that a joint is subjected to after the section at the internal support has buckled. As the experimental tests were performed on two types of joint configuration as discussed in previous sections, this inelastic reserve capacity can be calculated from both tests and ultimately the redistributed moment diagram can be developed. This chapter discusses the calculations made for the computation of this inelastic capacity and in the end; the redistributed moment diagram is presented.

5.1 Methodology

For the calculation of reserve moment capacity, different approaches have been used for both test scenarios as per the post elastic behaviour of joint.

5.1.1 Test Setup-1

For the first test-setup i.e. joint with 3 screws and 500mm overlap, three scenarios concerned with the integrity of section of interior support are considered:

i) Scenario 1: The distribution of bending moments in elastic range. (Figure 75)
ii) Scenario 2: Zero stiffness of the section over internal support and the two spans behaving as simply supported. (Figure 76)
iii) Scenario 3: Comparison of the mid-span capacity obtained from scenario 2 with ultimate load from the lab test and back calculating the moment carried by internal support.

The moment value obtained from Scenario 3 gives the reserve capacity of the section over mid-support as the further load leads to collapse of the system.

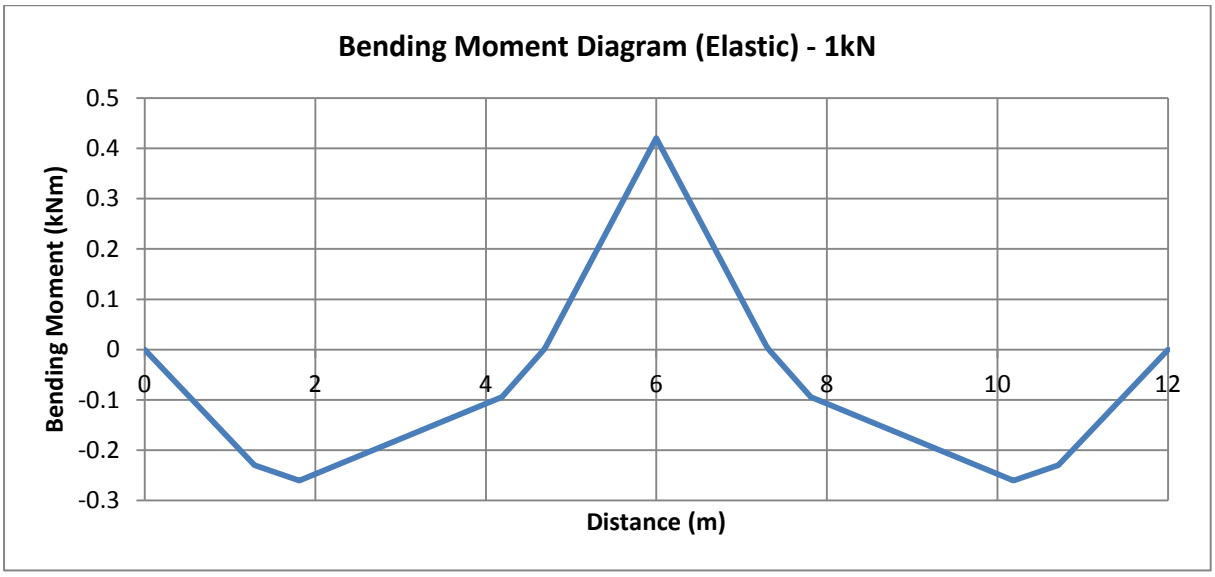

Figure 75. Bending Moment Diagram for 1kN load in Elastic Range

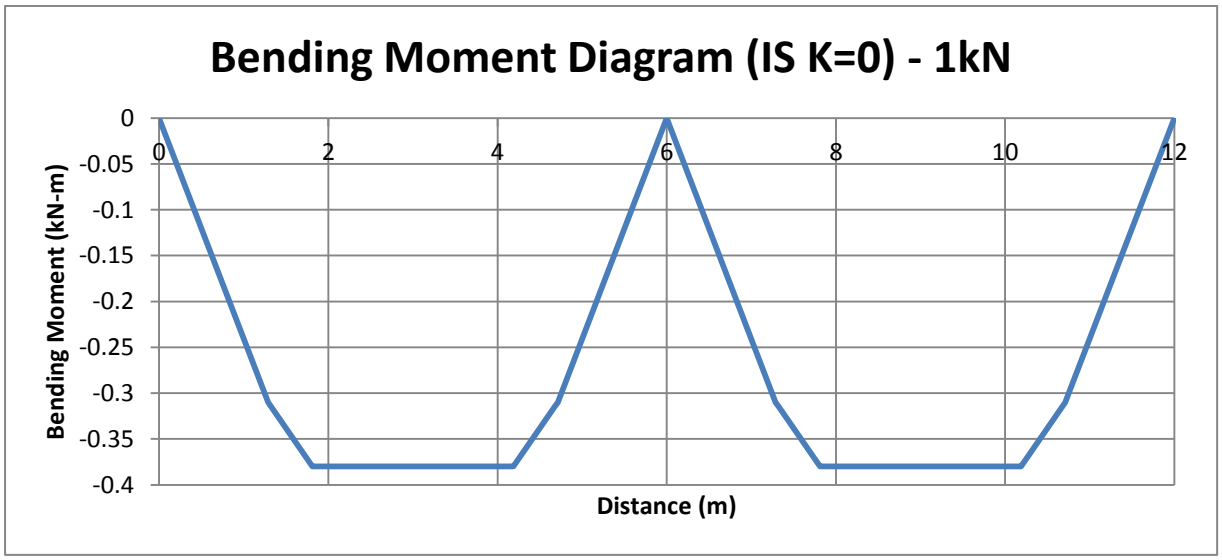

Figure 76. Bending Moment Diagram for 1kN with 0 internal support stiffness

5.1.2 Test Setup-2

For the first test-setup i.e. joint with 3 screws and 100mm overlap, the joint does not provide continuity as in setup-1. For this scenario, the deflection was measured near the joint. From this deflection, the moment-rotation relationship was derived and this relationship was used to calculate the variation in bending stiffness of the section over mid-support. Within the elastic limit, this bending stiffness is constant and the section takes the full moment as per the elastic distribution. As it reached its elastic limit, there is a dramatic drop in its stiffness as seen from the load-displacement curve. Upon reloading, the section still has some bending stiffness but it is very small as compared to the initial one. This variation in bending stiffness was calculated through experimental setup and a simply supported beam with a rotational spring was model in Abaqus. This stiffness of this spring was varied and the resulting impact on the bending moment was observed. The final moment redistribution diagram was obtained for the bending stiffness at the reloading phase in each setup.

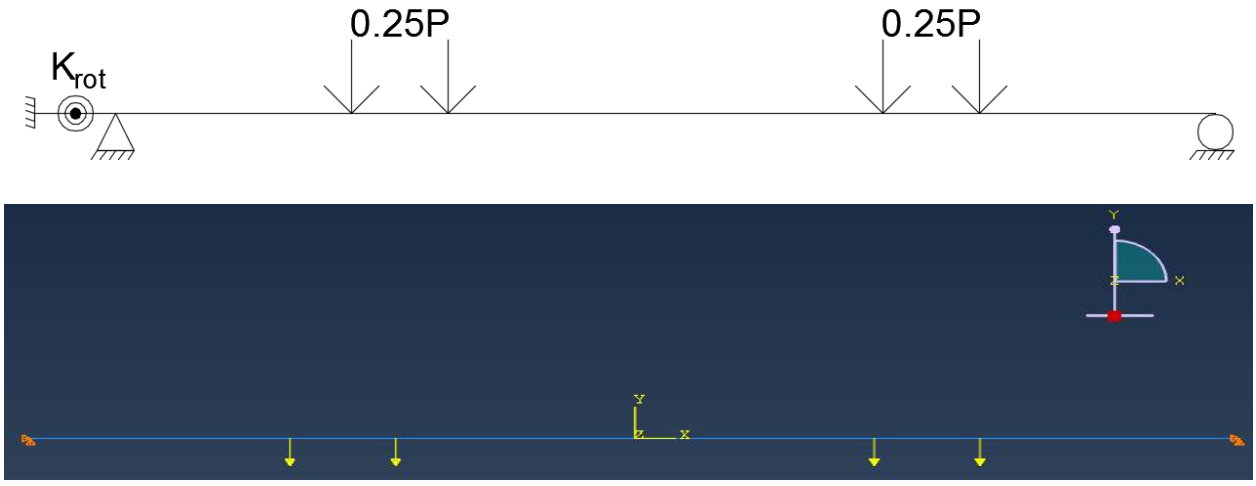

Figure 77. Simply supported beam with a rotational spring

5.2 Reserve Capacity Computation

5.2.1 0.85mm Sheet

5.2.1.1 Test Setup-1

The Limiting loads as per the capacities in both scenarios are summarized in the Table below:

Table 6. Capacities and Limiting Loads for 0.85mm Sheet

Disc.	Capacity - Elastic Limit		Capacity- IS (K=0)	
	Moment kN-m	Load kN	Moment kN-m	Load kN
Internal Support	21.22	50.51	-	-
Mid-span	15.47	59.5	15.47	40.71

Loads that were applied in Lab for the elastic and ultimate limit are,

- Elastic Limit: 60.63kN
- Ultimate Load: 57.32kN

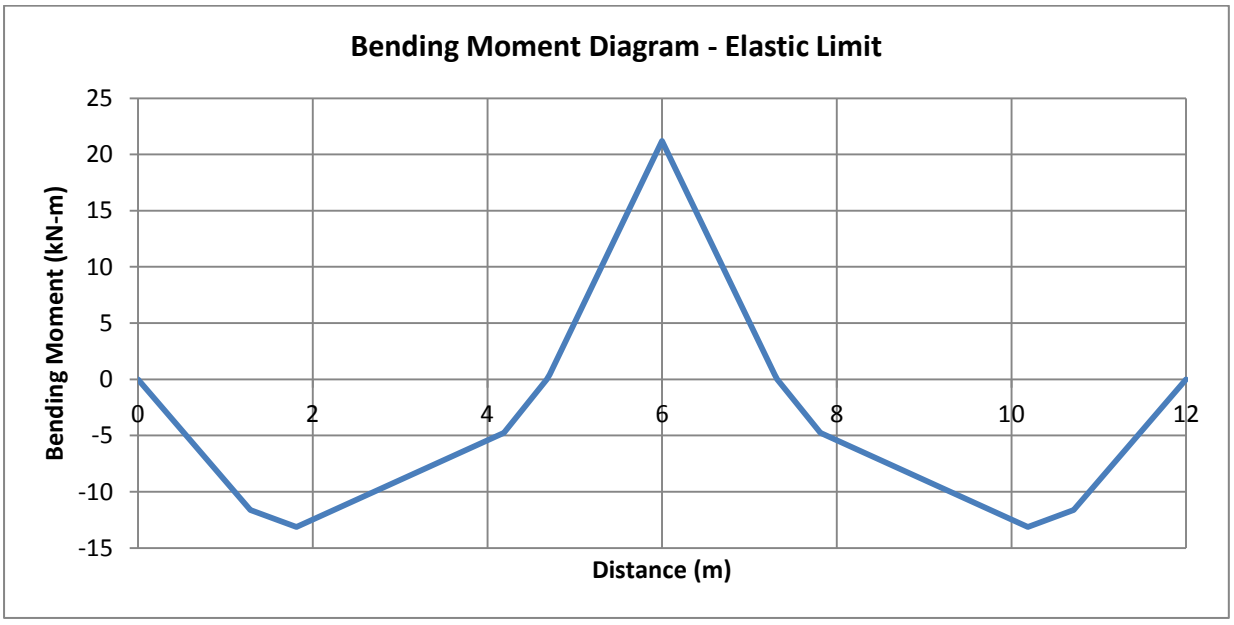

Figure 78. Bending Moment Diagram for 0.85mm Sheet at elastic limit

For the scenario 2 i.e. Internal Support with zero stiffness, the two spans behave as simply supported. The bending moment distribution for this scenario is:

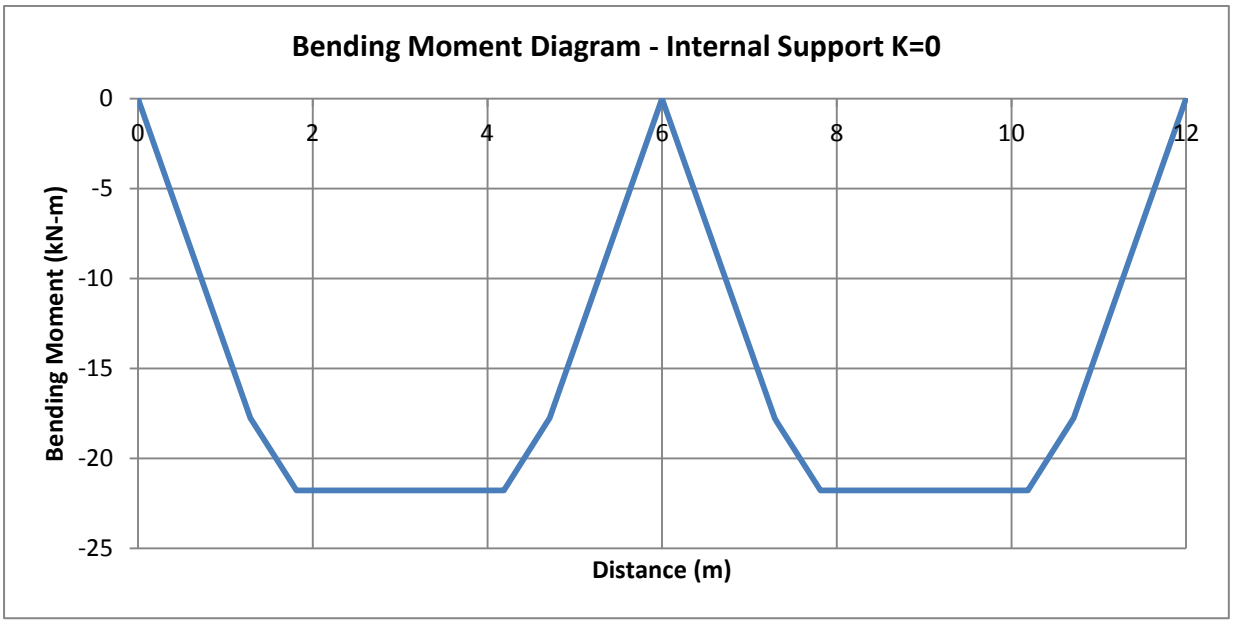

Figure 79. Bending Moment Diagram for 0.85mm Sheet with 0 internal support stiffness

As per the ultimate load applied in the lab, the moment that should act on the mid-span is 21.78kNm. Since the capacity of this section is 15.47kNm and through comparison it is evident that the mid-span capacity has been breached but it was not the scenario, it shows that the internal support is still carrying bending moments with and amount which balances the moments at mid-span (Figure 80). The difference of mid-span capacity and applied moments in scenario 2 is 6.4kNm, which is half of the moment at internal support. From this value, we can calculate the moment which the section at internal support is carrying.

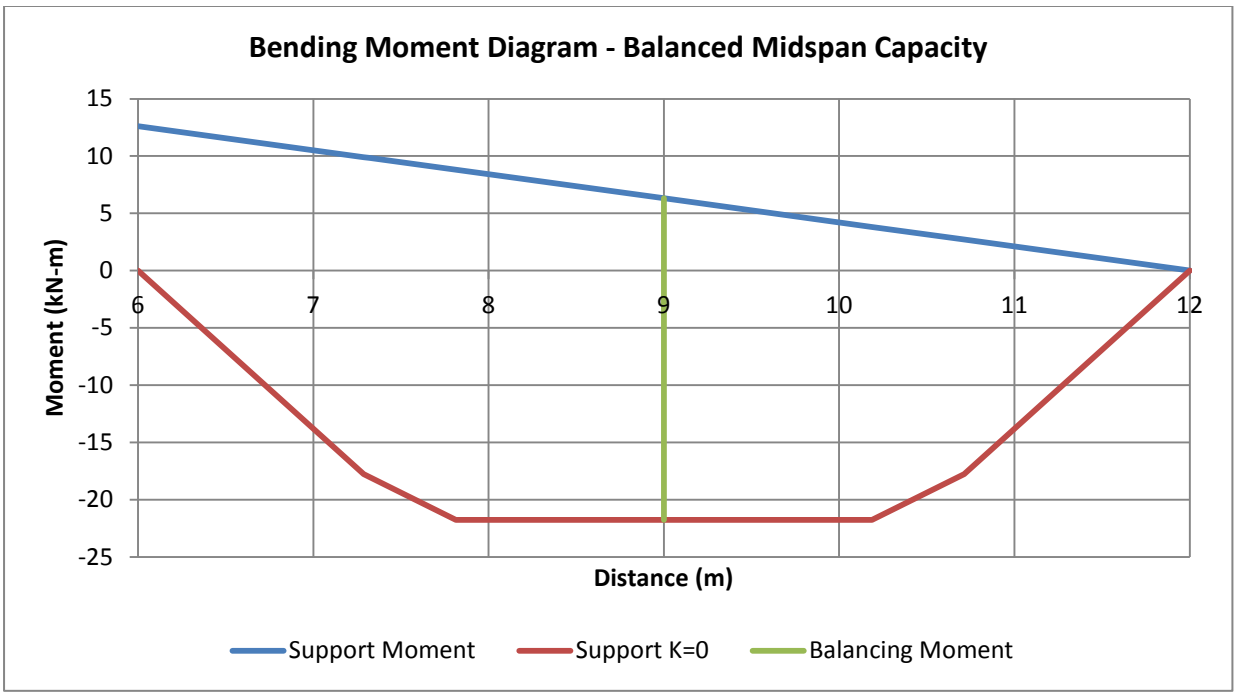

Figure 80. Balancing Bending Moment

The moment obtained at this ultimate load is the reserve capacity of the section. The reserve capacity of the section at the internal support is given by the alpha factor.

$$\alpha = \frac{M_{collapse}}{M_{elastic}} * 100$$

$$\alpha = \frac{12.62}{21.22} * 100$$

$$\alpha = 59\%$$

The amount of moment joint is subjected to for 1mm sheet is 8.17kN-m.

5.2.1.2 Test Setup-2

For this setup, the joint in the mid-span behaves as a perfect hinge and thus does not provide continuity effect after elastic failure over mid-support as in setup 1. The distribution of moments can be calculated by the variation of bending stiffness over the mid-support. The bending stiffness depends on the moment it is subjected to and the rotation it undergoes. Within the elastic limit, the bending stiffness is almost constant but as we cross the yield load, the stiffness drops dramatically (**Error! Reference source not found.**). Upon reloading, the section still carries moments but since the stiffness has dropped, so the capacity will be less.
The deflection was measured near the hinge and rotation angle was calculated through it. This rotation angle can be used to calculate the bending stiffness and ultimately the distribution factor.
Average Bending Stiffness in Elastic Limit = 1262.08kNm/rad

Bending Stiffness at the Ultimate Load (1_4) = 439.61kNm/rad

Percentage of Bending Stiffness at Ultimate Load = $\frac{439.61}{1262.08} = 35\%$

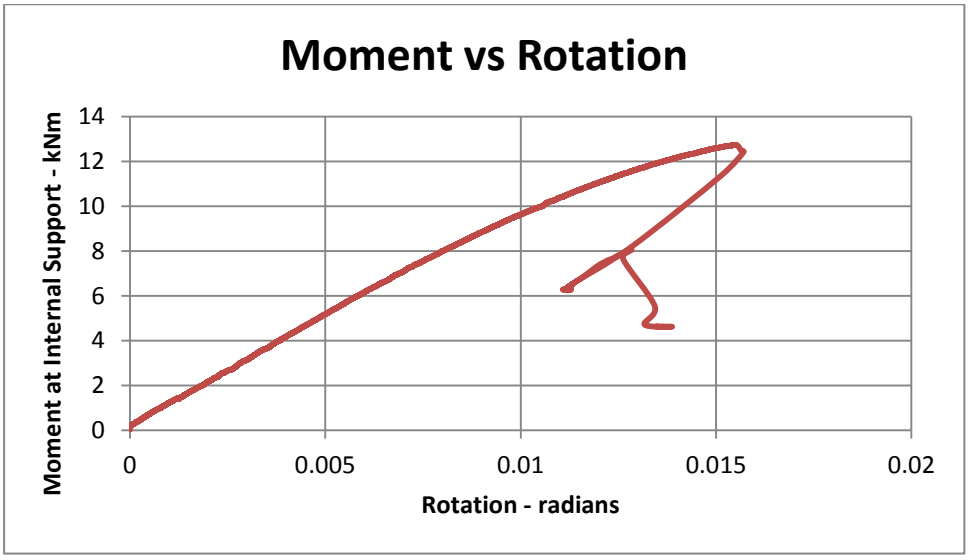

Figure 81. Moment Rotation Relationship between mid-support and hinge point (0.85mm Setup-1)

A simply supported beam depicting the right hand side of the system was modelled in Abaqus. As the ultimate goal is to achieve the bending moment diagram for the setup-2 i.e. connection with 500mm overlap, which behaves as a continuous beam in post elastic range, this simply supported beam has been modelled without hinge. The calculation at this stage is for the ultimate load of test setup-2 but the redistributed bending moment diagrams at the end will be presented for ultimate load in test setup-1.

Table 7. Variation of Bending Moment with Stiffness (0.85mm Profile)

Bending Stiffness		Bending Moments at X (kN-m)							
%	kNm/radians	0	1.2875	1.32	1.8125	3	4.1875	4.7125	6
100	1262.0768	8.17	0.26	0.1	-1.71	-3.33	-4.95	-4.41	0
75	946.5576	5.88	-1.55	-1.65	-3.32	-4.48	-5.65	-4.9	0
50	631.0384	5.15	-2.12	-2.22	-3.83	-4.85	-5.86	-5.06	0
35	439.6128	4.44	-2.68	-2.78	-4.32	-5.2	-6.08	-5.21	0
0	0	0	-6.16	-6.24	-7.42	-7.42	-7.42	-6.16	0

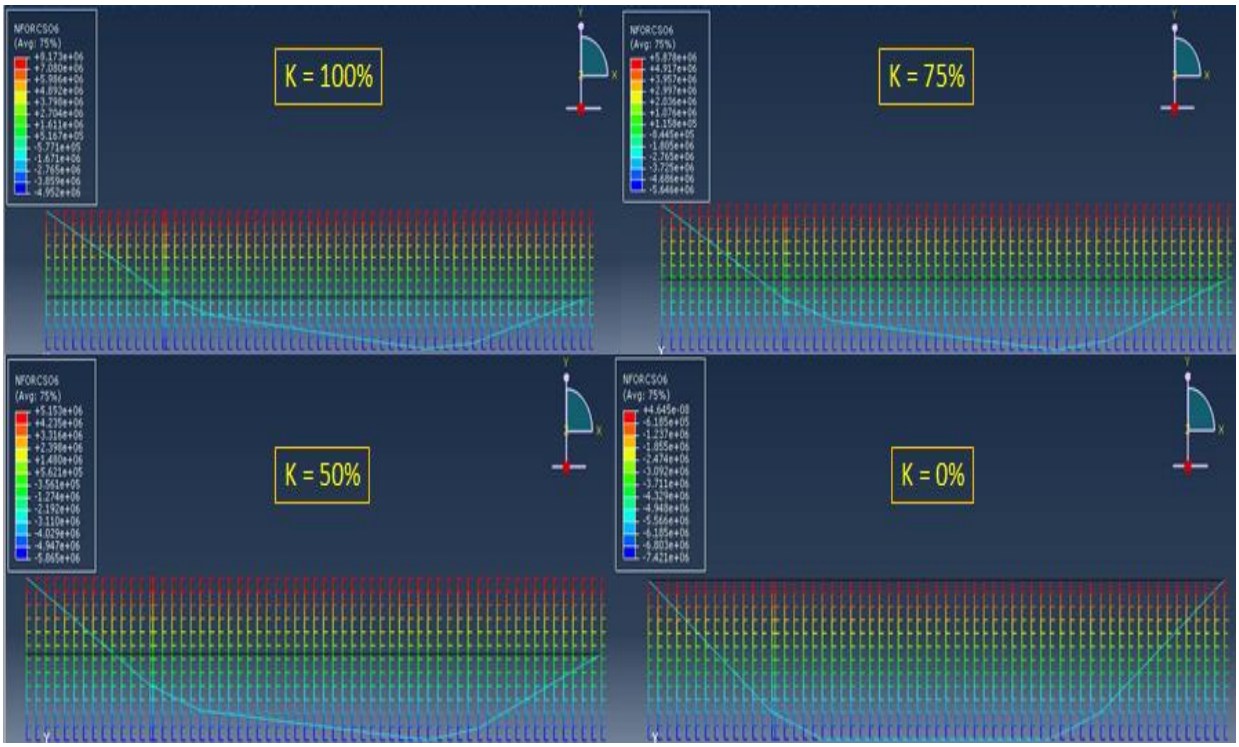

Figure 82. Variation of Bending Moment with changing stiffness (0.85mm Profile)

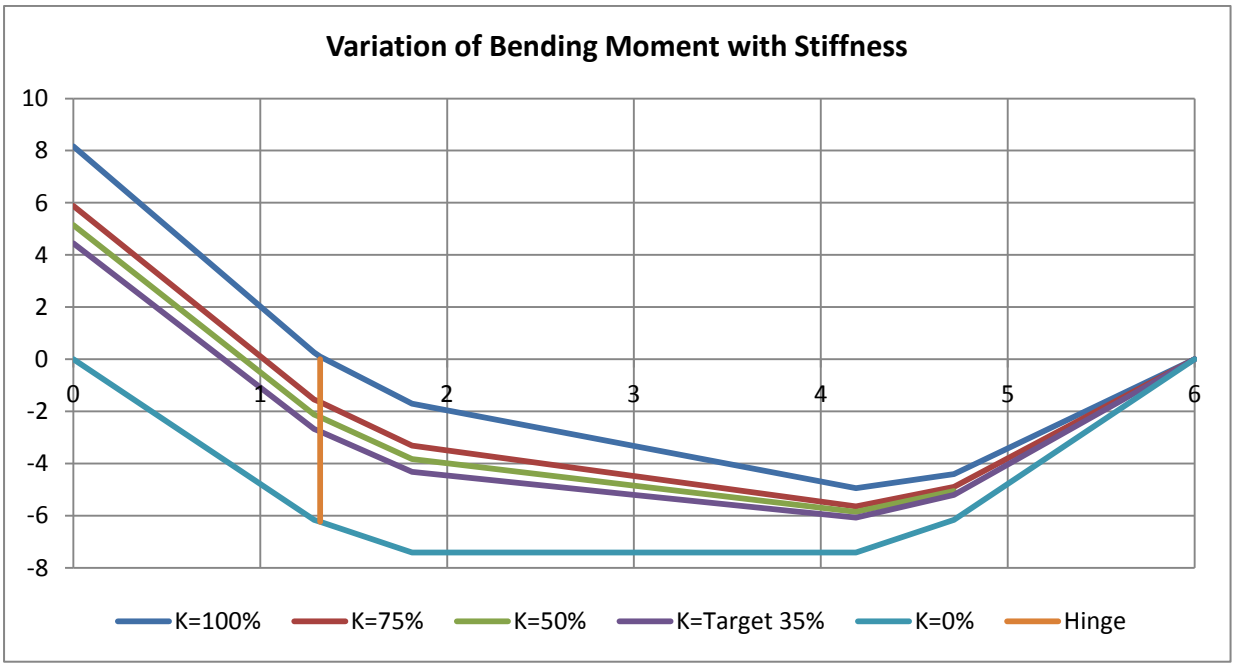

Figure 83. Bending Moment Diagram of right span with different stiffness (0.85mm Profile)

The bending stiffness calculated from the experiment is 35% and the moment at the support against this bending stiffness is 4.44kN/m and at the hinge is -2.78kNm.

5.2.2 1mm Sheet

5.2.2.1 Test Setup-1

The Limiting loads as per the capacities in both scenarios are summarized in the Table below:

Table 8. Capacities and Limiting Loads for 1mm Sheet

Disc.	Capacity - Elastic Limit		Capacity- IS (K=0)	
	Moment kN-m	Load kN	Moment kN-m	Load kN
Internal Support	29.33	69.83	-	-
Mid-span	21.76	83.75	21.76	57.31

Loads that were applied in Lab for the elastic and ultimate limit are,

- Elastic Limit: 73.25kN
- Ultimate Load: 58.82kN

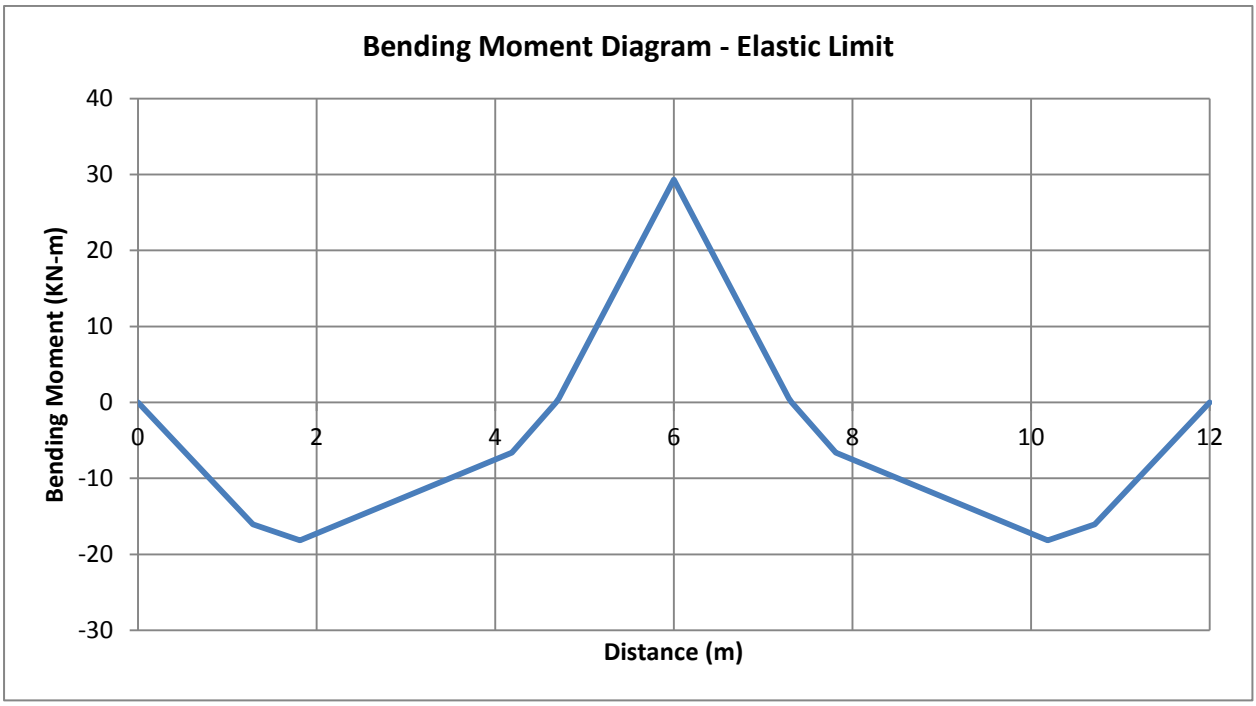

Figure 84. Bending Moment Diagram of 1mm sheet at Elastic Limit

For the scenario 2 i.e. Internal Support with zero stiffness, the two spans behave as simply supported. The bending moment distribution for this scenario is:

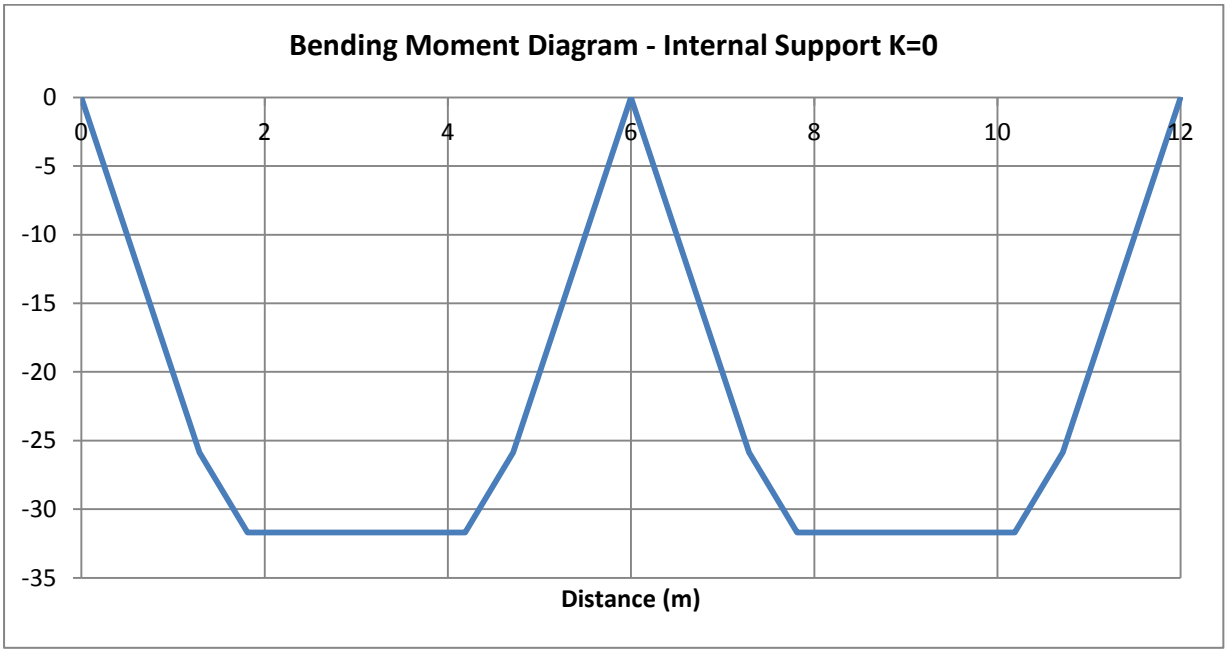

Figure 85. Bending Moment Diagram for 1mm Sheet with 0 internal support stiffness

As per the ultimate load applied in the lab, the moment that should act on the mid-span is 31.70kNm. Since the capacity of this section is 21.76kNm and through comparison it is evident that the mid-span capacity has been breached but it was not the scenario, it shows that the internal support is still carrying bending moments with and amount which balances the moments at mid-span (Figure 86). The difference of mid-span capacity and applied

moments in scenario 2 is 9.93kNm, which is half of the moment at internal support. From this value, we can calculate the moment which the section at internal support is carrying.

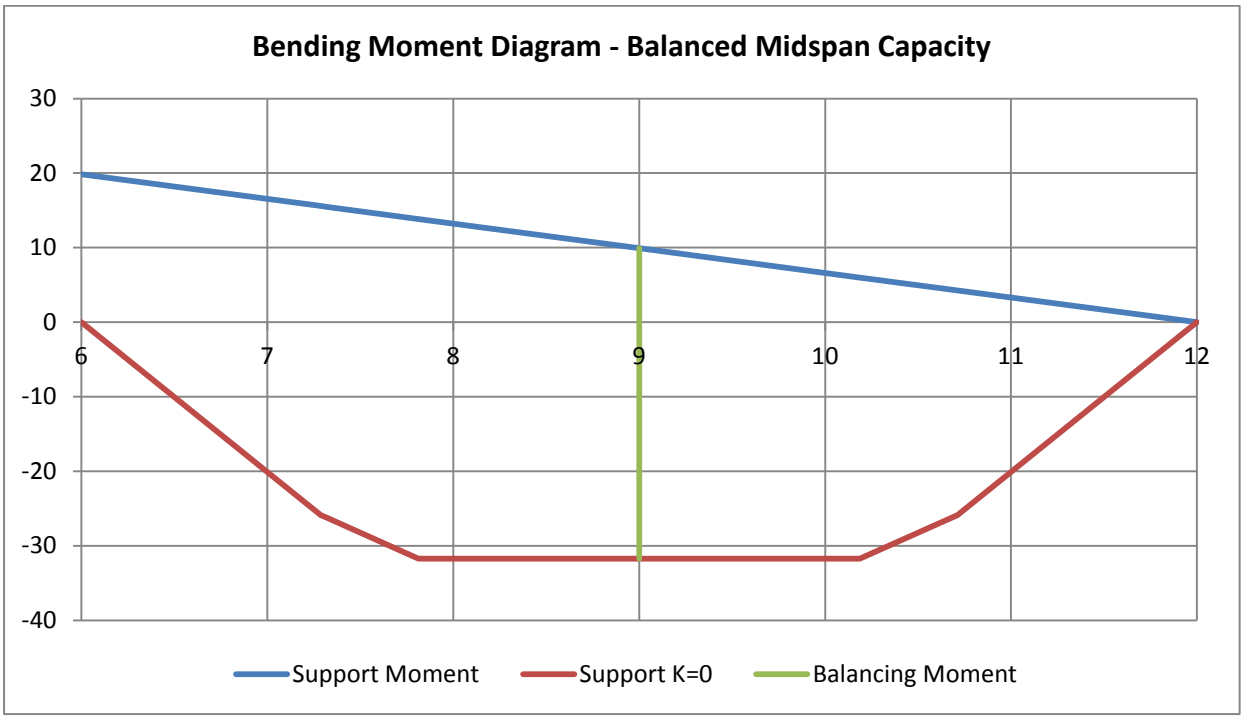

Figure 86. Balancing Bending Moment

The moment obtained at this ultimate load is the reserve capacity of the section. The reserve capacity of the section at the internal support is given by the alpha factor.

$$\alpha = \frac{M_{collapse}}{M_{elastic}} * 100$$

$$\alpha = \frac{19.85}{29.33} * 100$$

$$\alpha = 68\%$$

The amount of moment joint is subjected to for 1mm sheet is 10.74kN-m.

5.2.2.2 Test Setup-2

The same methodology was applied as in section 5.2.2.1. The variation of rotational stiffness with applied load is presented in the graph below.

Average Bending Stiffness in Elastic Limit = 1379.65kNm/radians

Bending Stiffness at the Ultimate Load (1_4) = 653.49kNm/radians

Percentage of Bending Stiffness at Ultimate Load = $\frac{653.49}{1379.65}$ = 47%

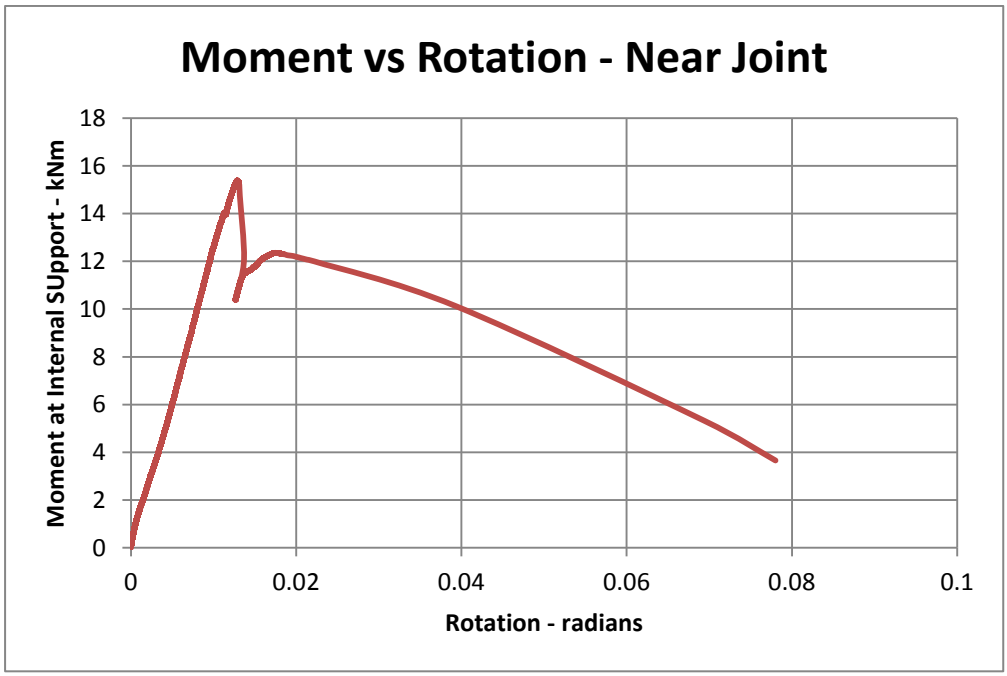

Figure 87. Moment Rotation Relationship between support and hinge point (1mm Profile)

Table 9. Variation of Bending Moment with Stiffness (1mm Profile)

Bending Stiffness		Bending Moments at X (kN-m)							
%	kNm/radians	0	1.2875	1.32	1.8125	3	4.1875	4.7125	6
100	1379.6544	12.55	0.39	0.2	-2.6	-5.12	-7.6	-6.77	0
75	1034.7408	8.75	-2.59	-2.76	-5.29	-7.02	-8.75	-7.59	0
50	689.8272	7.6	-3.5	-3.66	-6.09	-7.6	-9.09	-7.83	0
47	653.49	7.437	-3.62	-3.78	-6.2	-7.68	-9.15	-7.87	0
0	0	0	-9.47	-9.68	-11.4	-11.4	-11.4	-9.47	0

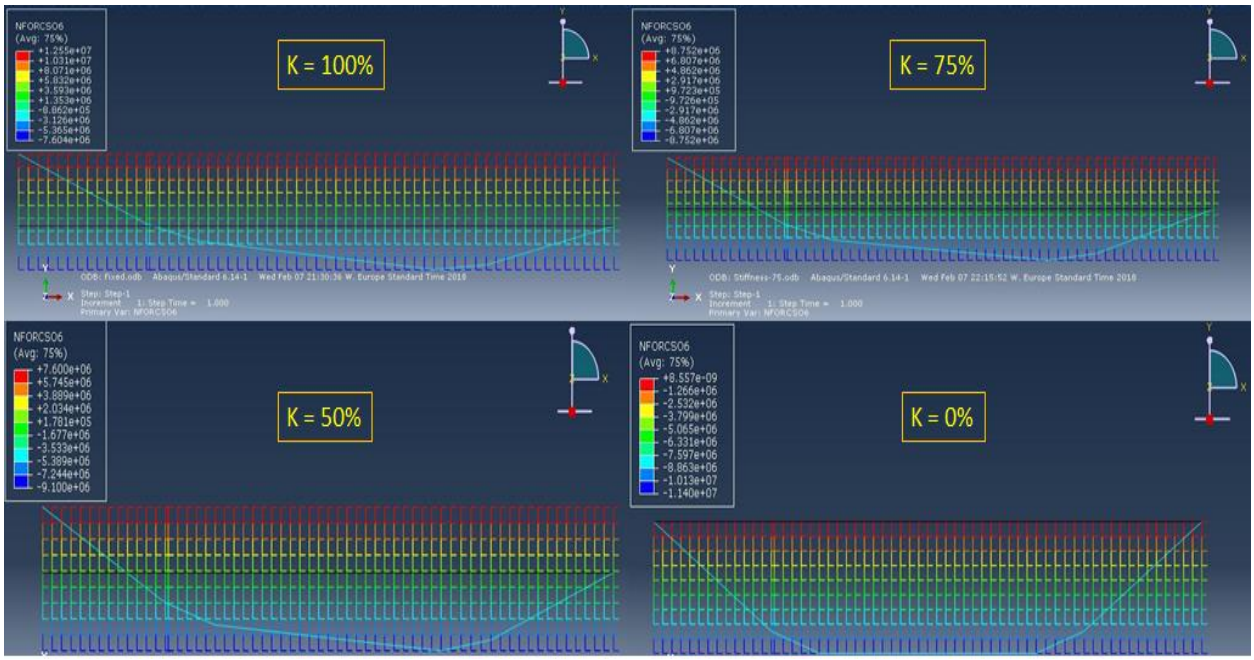

Figure 88. Variation of Bending Moment with changing stiffness (1mm Profile)

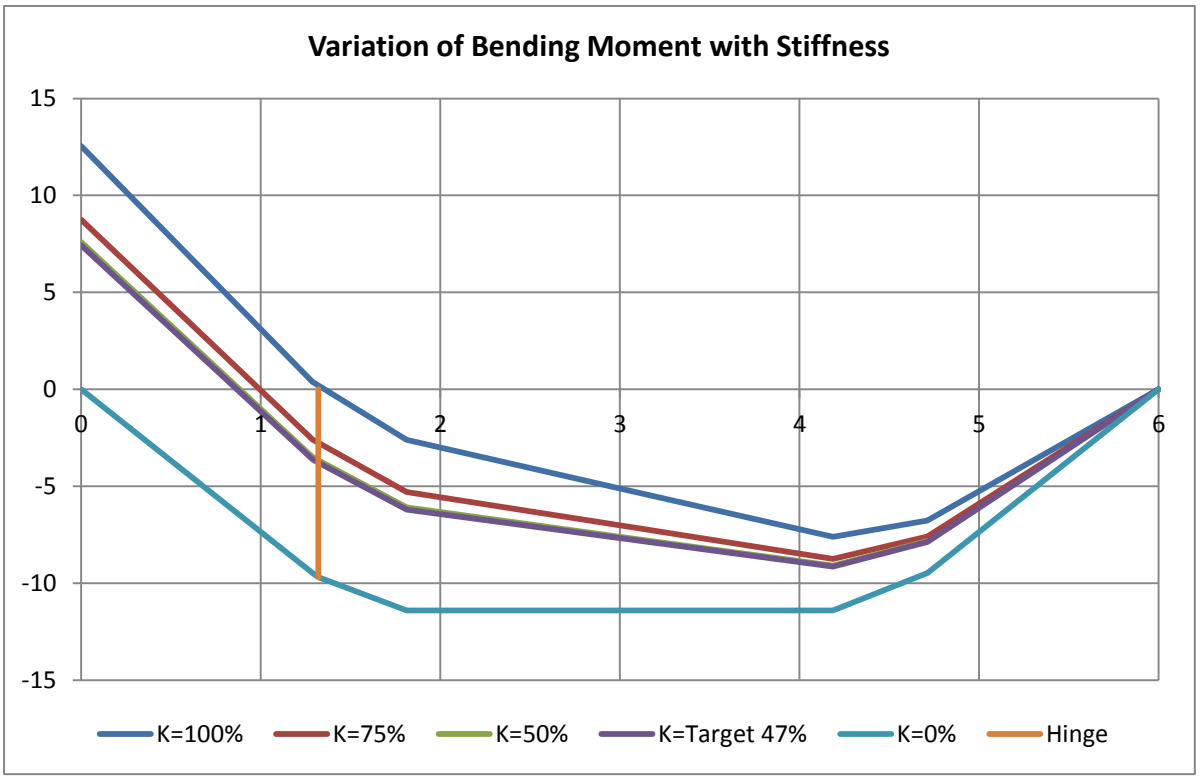

Figure 89. Bending Moment Diagram of right span with different stiffness (1mm Profile)

The bending stiffness calculated from the experiment is 47% and the moment at the support against this bending stiffness is 7.437kN/m and at the hinge is -3.78kNm.

5.2.2 1.5mm Sheet

5.2.2.1 Test Setup-1

The Limiting loads as per the capacities in both scenarios are summarized in the Table below:

Table 10. Capacities and Limiting Loads for 1.5mm Sheet

Disc.	Capacity - Elastic Limit		Capacity- IS (K=0)	
	Moment kN-m	Load kN	Moment kN-m	Load kN
Internal Support	49.26	118.17	-	-
Mid-span	35.26	135.62	35.26	92.79

Loads that were applied in Lab for the elastic and ultimate limit are,

- Elastic Limit: 142.46kN
- Ultimate Load: 112.103kN

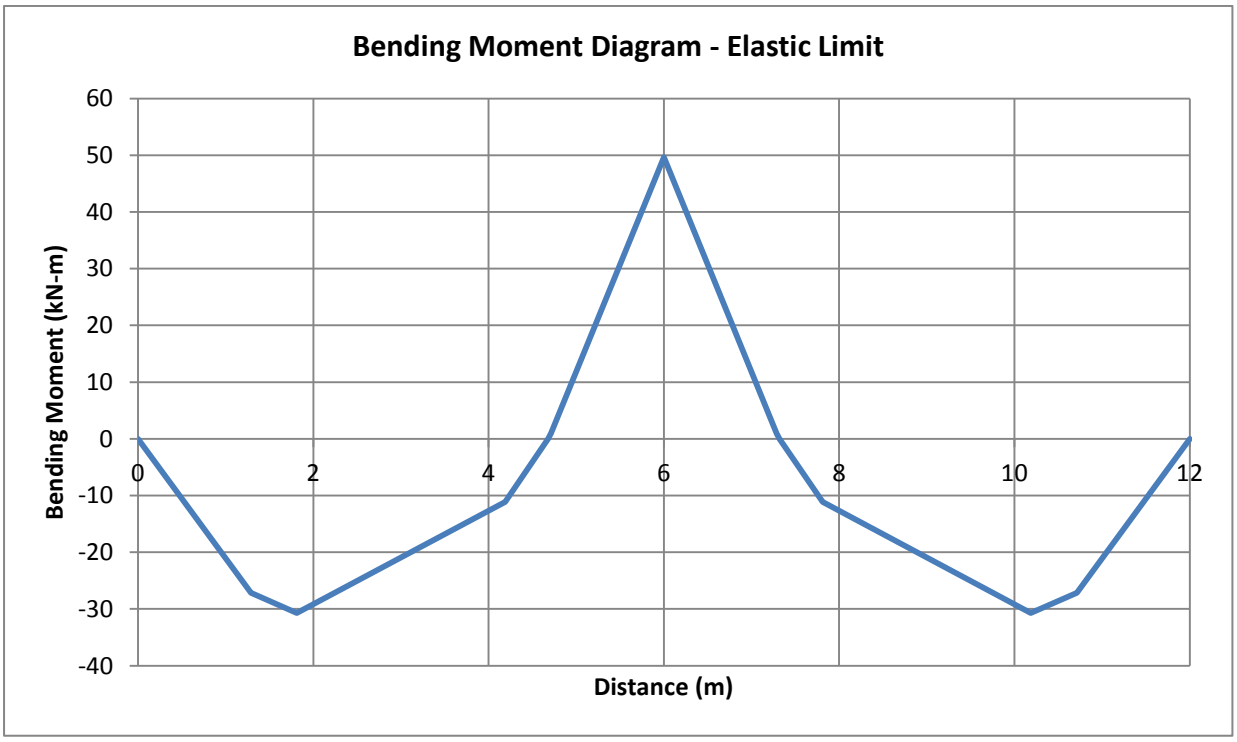

Figure 90. Bending Moment Diagram of 1.5mm sheet at Elastic Limit

For the scenario 2 i.e. Internal Support with zero stiffness, the two spans behave as simply supported. The bending moment distribution for this scenario is:

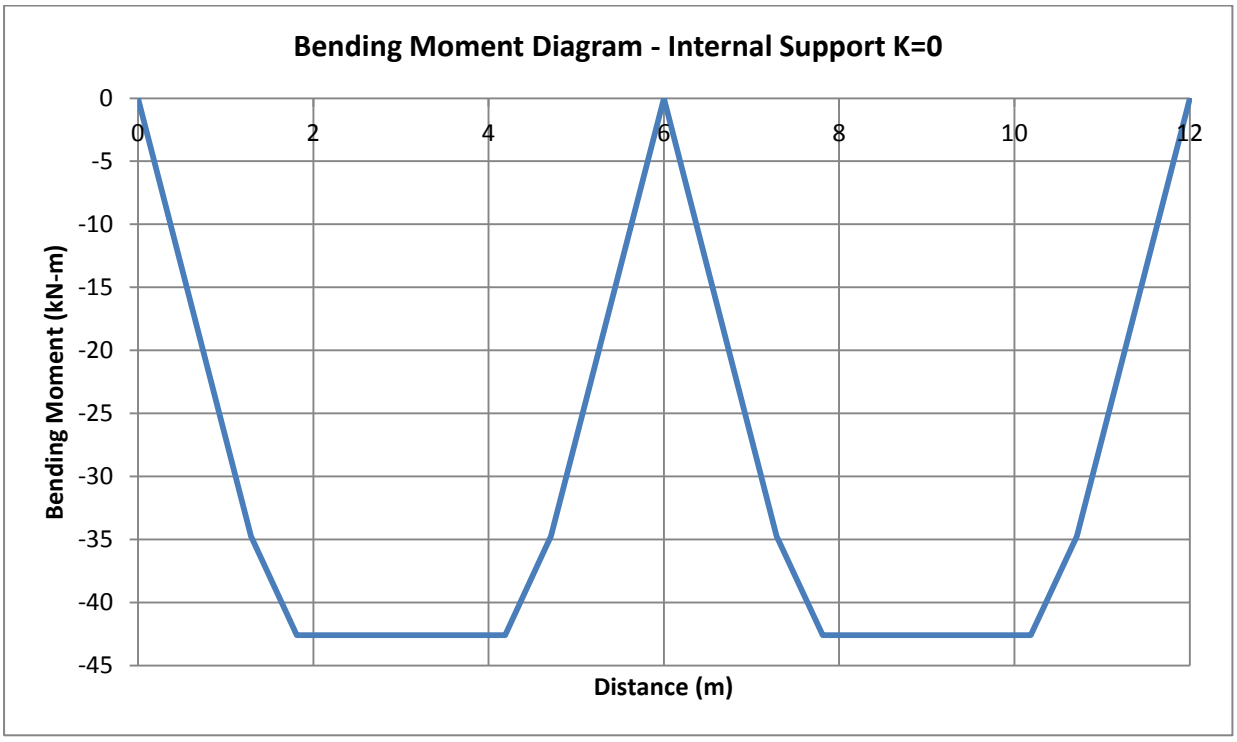

Figure 91. Bending Moment Diagram for 1.5mm Sheet with 0 internal support stiffness

The ultimate load applied in the lab was 112.10kN which would impose a bending moment of 42.60kNm in the mid-span in case if internal support has no stiffness. But in the case of

1.5mm sheet, the capacity of mid-span as well as the inelastic reserve capacity of the small flange section was not completely utilized as the support cleats buckled as well. While applying the same procedure as in case of 0.85mm and 1mm sheet, the inelastic reserve capacity will be very conservative. If the support cleats had not buckled, it can be expected that more load could be applied in the system and the ultimate behaviour of the system could be captured and close to reality reserve capacity cold be calculated.

5.3 Redistribution of Bending Moments

The reserve moment capacity and ultimately the redistribution of bending moment diagram was obtained for both the scenarios as discussed in the previous section. In this section, results and outcome of this thesis is presented.

Table 11. Summarized Table for 0.85 and 1mm Profile

Desc.	$M_{support}$ (kNm)		M_{Hinge} (kNm)		Reserve Capacity %	
	Setup-1	Setup-2	Setup-1	Setup-2	Setup-1	Setup-2
0.85mm	6.32	6.64	-4.08	-4.16	59	62
1.0mm	9.92	10.62	-5.37	-5.4	67	72

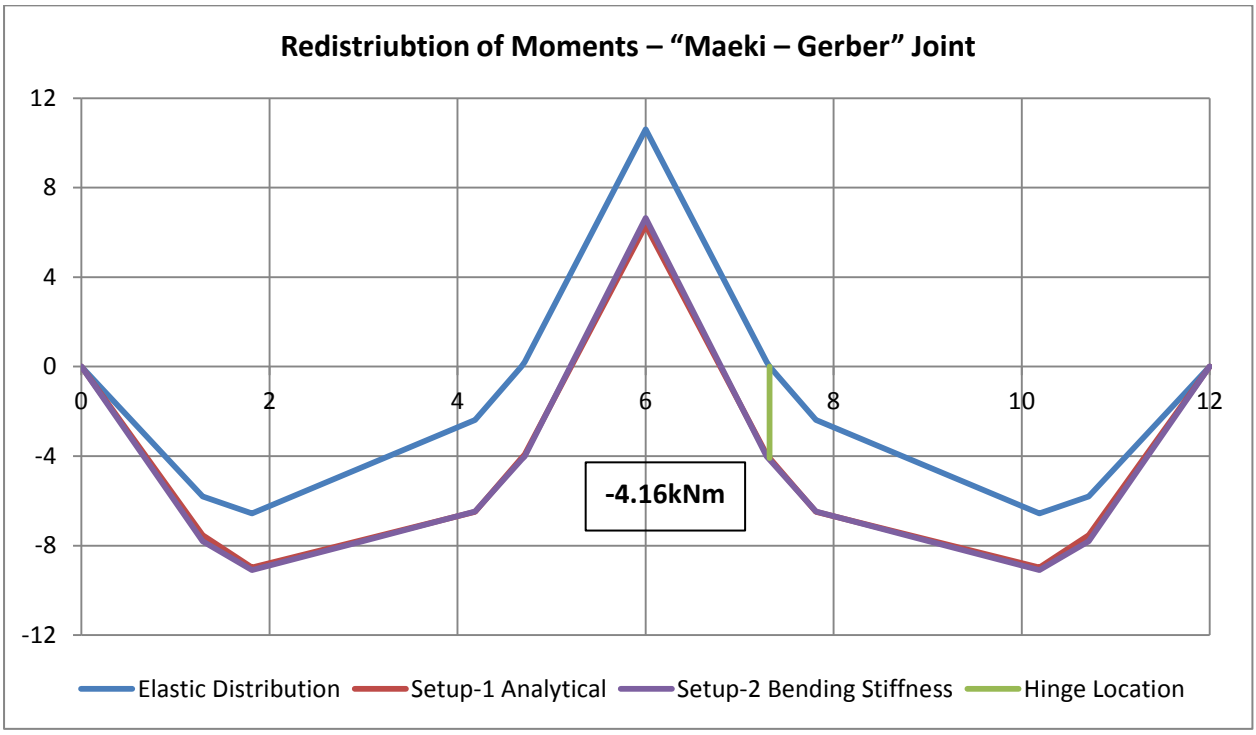

Figure 92. Redistribution of Bending Moments in 0.85mm Profile

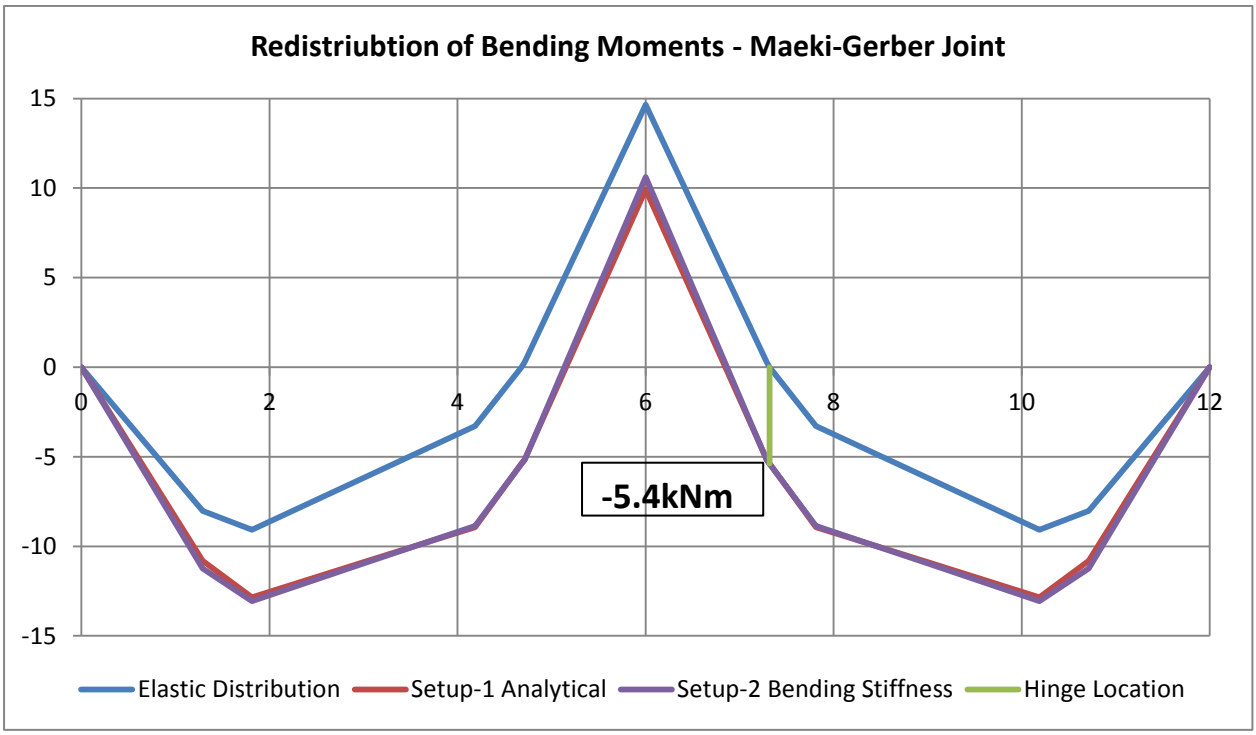

Figure 93. Redistribution of Bending Moments in 1mm Profile

6. Conclusions

The basic objective of this dissertation was to calculate the inelastic reserve capacity of the section over mid-support for a double span system. Results obtained from both the setups were used for analytical calculations and the reserve capacity was calculated. From this reserve capacity, the redistribution of bending moments was drawn and the moments applied to join corresponding to this distribution were highlighted. There are some peculiar observations that can be pinned down as conclusions.

- As the thickness of the sheets increase, the reserve capacity of the section increase and so does the moment on the joint.
- Since the tests were performed on the setup with designed joint configuration, it was observed that the joint does exhibit the properties of continuous beam in the post elastic range and distributes the bending moments as seen from the load-deflection curves of both experiments.
- The system showed more capacity against the ultimate loads in case of test setup-1, which also exhibits the contribution of sheets in the post-elastic range.
- In all the cases with 500mm overlap, the joint was intact in the post elastic range. Particularly in case of 1mm sheet, ideal redistribution of bending moments was observed as both the span and field moment capacities were utilized.
- For the sheet with 1.5mm thickness, the support cleats were not able to resist the loads till the collapse of the system, therefore, it is recommended to use cleats with higher stiffness.
- For further study on the system, it will interesting to perform the buckling analysis of the sheeting first and then introduction of some initial imperfection with elastic material properties so as to see the behaviour till collapse in Abaqus.
- It will also be interesting if a full beam element model is made in Abaqus and redistribution of moments calculated using its results.

References

[1] EN 1993-1-5 - Plated structural elements. (2003).

[2] Eurocode 3 - Design of steel structures - Part 1-3: General rules. (2009). Brussels.

[3] Abaqus Analysis User's Guide. (6.14)

[4] Bernuzzi, C., & Cordova, B. (2016). "*Structural Steel Design to Eurocode 3.* John Wiley & Sons, Lt".

[5] Dubina, D., Ungureanu, V., & Landolfo, R. (2012). "*Design of Cold Formed Steel Structures.* ECCS – European Convention for Constructional Steelwork".

[6] Hui, C., Gardner, L., & Nethercot, D. A. (2015). "Moment Redistribution in Cold-Formed Steel Continuous Beams". *Elsevir*.

[7] SJÖLANDER, J., & TIDERMAN, E. (2016). "*Gerber Splicing in Thin Steel Sheeting of.* Gothenburg".

[8] https://www.steelconstruction.info/Building_envelopes.

Annex-A

Analytical calculations were made for the steel trapezoidal sheet. For analytical computations, single sheet of 0.85mm thickness and 800mm width have been taken.

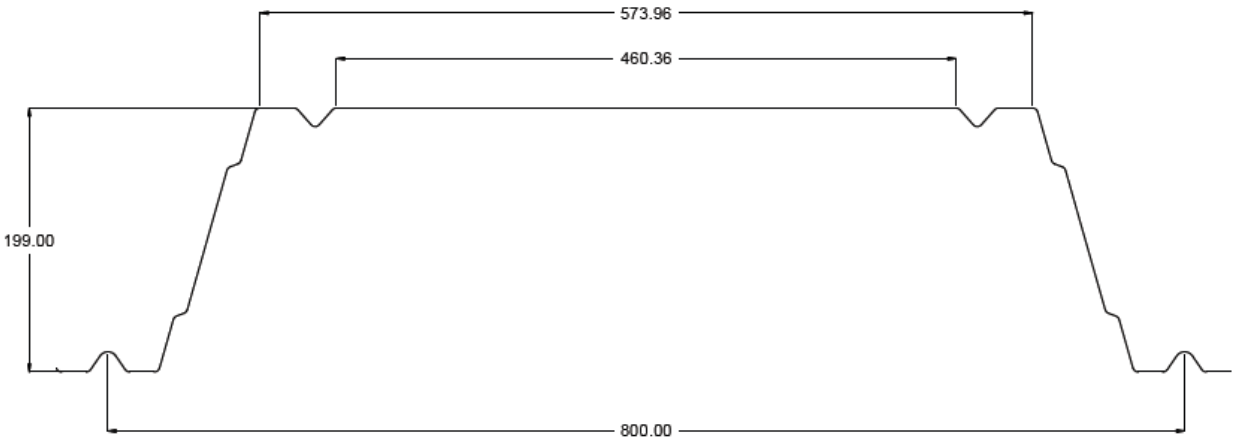

First of all, the section was converted into an equivalent section with sharp corners as per Eurocode EN 1993-1-3 section 5.1. For the ease of computation and display, half of the section has been taken i.e. 400mm.

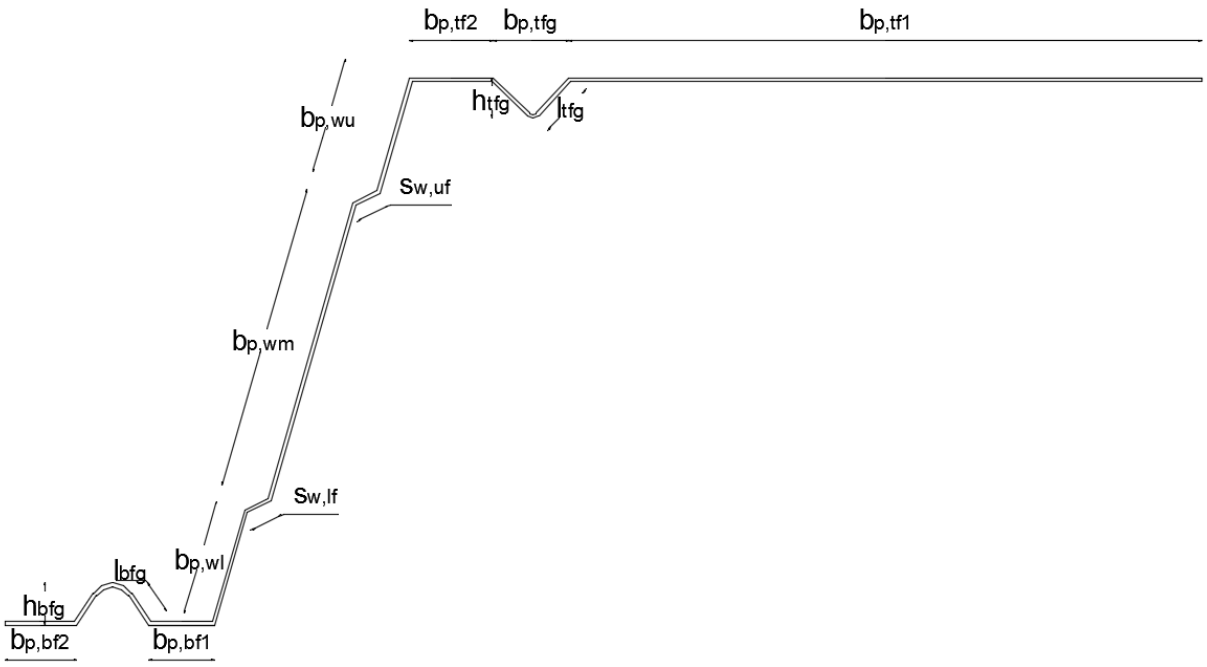

The Dimensions of the section in mm are:

h_s = 199.85 — Height of Section

t_{nom} = 0.85 — Nominal Thickness ($t_{nom} = t_{sheet}$)

b_s = 868.94 — Width of one Section

The dimensions from here are for half of the section and area in the end will be doubled.

$b_{p,tf1}$ = 231.84 ; $\bar{y}$ = 199.625 — Middle part of top flange

$b_{p,tfg}$ = 28.33 — Groove in top flange

$h_{g,tf}$ =14

$s_{g,tf}$ = 2 x 19.92 ; $\bar{y}$ = 191.535

$l_{g,tf}$ = 14.91

$b_{p,tf2}$ = 29.23 ; $\bar{y}$ = 199.625 — Outer part of top flange

$b_{p,wu}$ = 42.20 ; $\bar{y}$ = 179.054 — Upper part of web

$h_{w,uf}$ = 4.32 — Upper web fold

$s_{w,uf}$ = 9.68 ; $\bar{y}$ = 156.286

$b_{p,wm}$ = 112.67 ; $\bar{y}$ = 99.936 — Middle part of web

$h_{w,lf}$ = 4.25 — Lower web fold

$s_{w,lf}$ = 9.62 ; $\bar{y}$ = 43.674

$b_{p,wl}$ = 42.20 ; $\bar{y}$ = 20.995 — Lower part of web

$b_{p,bf1}$ = 23.36 ; $\bar{y}$ = 0.625 — Outer part of bottom flange

$b_{p,bfg}$ = 28.50 — Groove in bottom flange

$h_{g,bf}$ =15.20

$s_{g,bf}$ = 2 x 20.83 = 41.67; $\bar{y}$ = 10.914

$l_{g,tf}$ = 12.51

$b_{p,bf1}$ = 20.22 ; $\bar{y}$ = 0.625 — Outer part of bottom flange

Internal Radii and angles in the Cross-Section:

$r_{tf,g}$ = 4 ; $\emptyset_{tf,g}$ = 131 — Top flange and groove

$r_{tf,wu}$ =4; $\emptyset_{tf,wu}$= 106 — Top flange and web

$r_{bf,wl}$ =4; $\emptyset_{bf,wl}$=106 — Bottom flange and web

$r_{bf,g}$ =4 ; $\emptyset_{bf,g}$=124 — Bottom flange and groove

Properties of Gross Section with sharp corners:

Area of the gross section with sharp corners($A_{g,sc}$)

$A_{g,sc} = ts\,(b_{p1,tf} + s_{g,tf} + b_{p2,tf} + b_{p,wu} + s_{w,uf} + b_{p,wm} + s_{w,lf} + b_{p,wl} + b_{p1,bf} + s_{g,bf} + b_{p2,bf})$ x 2

$$A_{g,sc} = 1027.26\ mm^2$$

Centroid of the gross section with sharp corners($\bar{y}_{g,sc}$)

$$\bar{y}_{g,sc} = \frac{A_{p1,tf}(\bar{y}_{p1,tf}) + A_{g,tf}(\bar{y}_{g,tf}) + A_{p2,tf}(\bar{y}_{p2,tf}) + A_{p,wu}(\bar{y}_{p,wu}) + A_{w,uf}(\bar{y}_{w,uf}) + A_{p,wm}(\bar{y}_{p,wm}) + A_{w,lf}(\bar{y}_{w,lf}) + A_{p,wl}(\bar{y}_{p,wl}) + A_{p1,bf}(\bar{y}_{p1,bf}) + A_{g,bf}(\bar{y}_{g,bf}) + A_{p2,bf}(\bar{y}_{p2,bf})}{A_{g,sc}}$$

$$\bar{y}_{g,sc} = 135.53mm$$

Moment of Inertia the gross section with sharp corners($I_{g,sc}$)

$$\begin{aligned} I_{g,sc} = {} & \left[I_{p1,tf} + A_{p1,tf}\left(\bar{y}_{p1,tf} - \bar{y}_{g,sc}\right)^2\right] + \left[I_{g,tf} + A_{g,tf}\left(\bar{y}_{g,tf} - \bar{y}_{g,sc}\right)^2\right] \\ & + \left[I_{p2,tf} + A_{p2,tf}\left(\bar{y}_{p2,tf} - \bar{y}_{g,sc}\right)^2\right] + \left[I_{p,wu} + A_{p,wu}\left(\bar{y}_{p,wu} - \bar{y}_{g,sc}\right)^2\right] \\ & + \left[I_{w,uf} + A_{w,uf}\left(\bar{y}_{w,uf} - \bar{y}_{g,sc}\right)^2\right] + \left[I_{p,wm} + A_{p,wm}\left(\bar{y}_{p,wm} - \bar{y}_{g,sc}\right)^2\right] \\ & + \left[I_{w,lf} + A_{w,lf}\left(\bar{y}_{w,lf} - \bar{y}_{g,sc}\right)^2\right] + \left[I_{p,wl} + A_{p,wl}\left(\bar{y}_{p,wl} - \bar{y}_{g,sc}\right)^2\right] \\ & + \left[I_{p1,bf} + A_{p1,bf}\left(\bar{y}_{p1,bf} - \bar{y}_{g,sc}\right)^2\right] + \left[I_{g,bf} + A_{g,bf}\left(\bar{y}_{g,bf} - \bar{y}_{g,sc}\right)^2\right] \\ & + \left[I_{p2,bf} + A_{p2,bf}\left(\bar{y}_{p2,bf} - \bar{y}_{g,sc}\right)^2\right] \end{aligned}$$

$$I_{g,sc} = 6223506\ mm^4$$

Influence of Rounded Corners:

As per EN1993-1-3 clause 5.1(3), influence of rounded corners must be taken into account if the internal radius r>5t and r>0.1b_p.

For the corner between top flange and groove

$r_{tf,g}$= 4 < 5t= 7.5 & $r_{tf,g}$=4> 0.1$b_{p,tf2}$ = 2.923 Rounded Corner must be considered

For the corner between top flange and web

$r_{tf,wu}$= 4 < 5t= 7.5 & $r_{tf,wu}$=4> 0.1$b_{p,tf2}$ = 2.923 Rounded Corner must be considered

For the corner between bottom flange and web

$r_{bf,wl}$= 4 < 5t= 7.5 & $r_{bf,wl}$=4> 0.1$b_{p,bf}$= 2.264 Rounded Corner must be considered

For the corner between top flange and groove

$r_{bf,g}$= 4 < 5t= 7.5 & $r_{bf,g}$=4> 0.1$b_{p,bf}$= 2.264 Rounded Corner must be considered

To consider the influence of rounded corners, equation 5.1d of EN1993-1-3 gives the value of δ which can be used to include the influence of rounded corners.

$$\delta = 0.43 \frac{\sum_{j=1}^{n} r_j \frac{\emptyset_j}{90}}{\sum_{i=1}^{m} b_{p,i}}$$

$$\delta = 0.43 \frac{r_{tf,g} \frac{\emptyset_{tf,g}}{90} + r_{tf,wu} \frac{\emptyset_{tf,wu}}{90} + r_{bf,wl} \frac{\emptyset_{bf,wl}}{90} + r_{bf,g} \frac{\emptyset_{bf,g}}{90}}{b_{p1,tf} + b_{p2,tf} + b_{p,wu} + s_{w,uf} + b_{p,wm} + s_{w,lf} + b_{p,wl} + b_{p1,bf} + b_{p1,bf}}$$

$$\delta = 0.017$$

Properties of Gross Section with rounded corners:

The influence of rounded corner on the cross-section can be considered by reducing the properties which were calculated for the section with sharp corners using the EN1993-1-3 equations 5.1 (a&b).

Area of the gross section with rounded corners (A_g)

$$A_g = A_{g,sc}(1 - \delta)$$

$$A_g = 1812.81(1 - 0.017)$$

$$A_g = 1009.72 mm^2$$

Moment of Inertia of the gross section with rounded corners (I_g)

$$I_g = I_{g,sc}(1 - 2\delta)$$

$$I_g = 10702636(1 - 0.017)$$

$$I_g = 6011003\ mm^4$$

Calculation of Effective Cross-Section:

To calculate the effective section properties of the trapezoidal sheet, section 5.5.3.4 of EN 1993-1-3 has been used. The calculation overall consists of 3 steps:

1. Properties for the flange with intermediate stiffeners
2. Properties of web with folds

3. Interaction between flange and web stiffeners for reduction factor calculation.

Properties of Flange with Intermediate stiffeners:

To calculate the effective cross-section of the stiffener itself, section 5.5.3.3 of EN 1993-1-3 has been used. To proceed with the calculation, widths of plane elements adjacent to the stiffener are required. The cross-section of the stiffener with the adjacent elements is shown in the figure below:

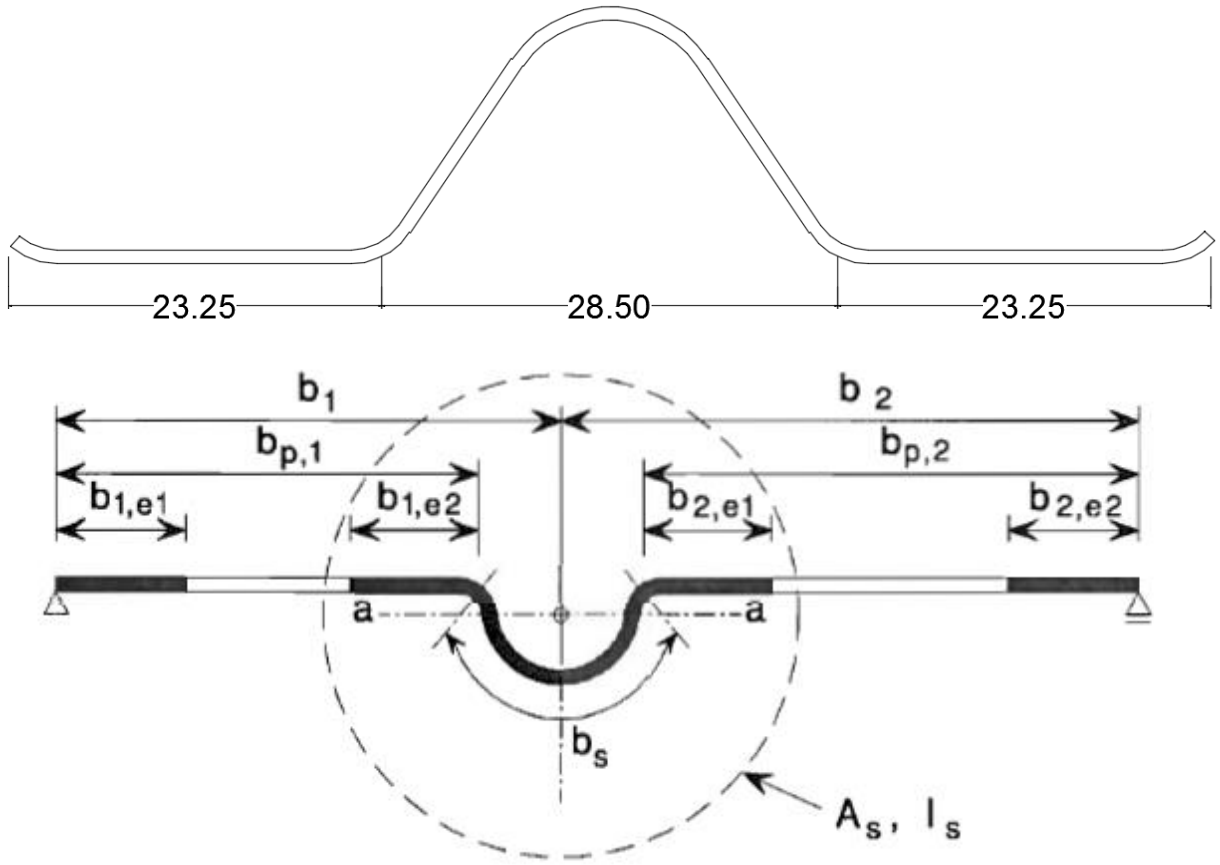

For each of the plane element adjacent to groove

$$b_{p,1} = b_{p,bf1} = 23.25$$

$$b1 = b_{\mathrm{p1,bf}} + 0.5 b_{\mathrm{p,bfg}}$$

$$b1 = 23.25 + 0.5\ x\ 28.5$$

$$b1 = 37.5$$

To calculate the effective widths of the plane elements adjacent to the stiffener, Table 4.1 of EN 1993-1-5 is used.

Since the whole of the bottom flange is under uniform compression, so

$\Psi = \frac{\sigma_2}{\sigma_1} = 1\ ;\ k_\sigma = 4$

$$\lambda_p = \frac{\frac{b_p}{t}}{28.4\varepsilon\sqrt{k_\sigma}}$$

$b_p = 23.25$

$t = 0.85$

$\varepsilon = \sqrt{235/f_{yb}} = \sqrt{235/420} = 0.748$

$$\lambda_p = \frac{\frac{b_p}{t}}{28.4\varepsilon\sqrt{k_\sigma}}$$

$$\lambda_p = 0.647$$

$$\rho = \frac{\lambda_p - 0.055\ (3 + \Psi)}{\lambda_p{}^2} \leq 1$$

$$\rho = 1$$

$$b_{eff} = \rho\ b_p$$

$$b_{eff} = 23.25$$

$$b_{e,1} = b_{e,2} = 0.5 b_{eff} = 11.625$$

The effective cross-sectional area of the flange stiffener will be:

$$A_s = t(b_{e,1} + b_{e,2} + b_s)$$

$$A_s = 0.85 * (11.625 + 11.625 + 41.67)$$

$$A_s = 55.182 mm^2$$

The centroid axis of the stiffener is:

$$\bar{y}_s = \frac{A_{\mathrm{be,1}}\left(\bar{y}_{\mathrm{be,1}}\right) + A_{\mathrm{be,2}}\left(\bar{y}_{\mathrm{be,2}}\right) + A_{\mathrm{s.bf}}(\bar{y}_{\mathrm{s.bf}})}{\mathrm{A_s}}$$

$$\bar{y}_s = \frac{9.88\ (0.425) + 9.88\ (0.425) + 35.42(8.025)}{55.182}$$

$$\bar{y}_{g,s} = 5.30mm$$

For moment of inertia, 15t will be used instead of $0.5b_{eff}$ as per Eurocode requirement

$$I_{g,s} = \left[15t * t\left(\bar{y}_{\mathrm{be},1} - \bar{y}_s\right)^2\right] + \left[15t * t\left(\bar{y}_{\mathrm{be},2} - \bar{y}_s\right)^2\right] + \left[A_{\mathrm{s.bf}}\left(\bar{y}_{\mathrm{s.bf}} - \bar{y}_s\right)^2\right]$$

$$I_{g,s} = 1806.5978mm^4$$

$$\sigma_{cr,s} = \frac{4.2k_wE}{A_s} * \sqrt{\frac{I_s t^3}{4\ b_p^2\ (2\ b_p + 3\ b_s)}}$$

For the value of k_w, slant height of web is required.

$$k_{w,o} = \sqrt{\frac{s_w + 2\ b_d}{s_w + 0.5\ b_d}}$$

$$s_w = \frac{h_s}{sin\phi_w} = \frac{199}{\sin(74)} = 207.02\ mm$$

$$b_d = 2b_p + b_s$$

$$b_d = 2 * 23.25 + 41.67 = 88.17$$

$$k_{w,o} = \sqrt{\frac{207.02 + 2 * 88.17}{207.02 + 0.5 * 88.17}}$$

$$k_{w,o} = 1.24$$

$$l_b = 3.07\sqrt[4]{\frac{I_s b_p^2\ (2\ b_p + 3\ b_s)}{t^3}}$$

$$l_b = 3.07\sqrt[4]{\frac{1806.60 * 23.25^2\ (2 * 23.25 + 3 * 41.67)}{0.85^3}}$$

$$l_b = 394.524$$

$$\frac{l_b}{s_w} = \frac{394.524}{207.02} = 1.91$$

As $\frac{l_b}{s_w} < 2$

$$k_w = k_{wo} - (k_{wo} - 1)[\frac{2l_b}{s_w} - (\frac{l_b}{s_w})^2]$$

$$k_w = 1.24 - (1.24 - 1)[\frac{394.524}{207.02} - (\frac{394.524}{207.02})^2]$$

$$k_w = 1.64$$

$$\sigma_{cr,s} = \frac{4.2 k_w E}{A_s} * \sqrt{\frac{I_s t^3}{4\, b_p^2\, (2\, b_p + 3\, b_s)}}$$

$$\sigma_{cr,s} = \frac{4.2 * 1.64 * 210000}{55.182} * \sqrt{\frac{1806.60 * 0.85^3}{4\ * 23.25^2\ (2 * 23.25 + 3 * 41.67)}}$$

$$\sigma_{cr,s} = 1429.28\ N/mm^2$$

For the web with intermediate stiffener,
Initial Calculation of the web with intermediate stiffener is based on effective section of flanges but the gross section of the webs. In this case, there is no reduction in area of flanges, so the centroid remains the same as in gross section

$e_c = 135.53$

$s_a = 42.92$ $h_a = 41.26$

$s_{sa} = 9.62$ $h_{sa} = 4.25$

$s_n = 93.36$ $h_n = 89.74$

$s_b = 112.67$ $s_{sb} = 9.68$ $s_c = 42.81$

$$s_{eff,0} = 0.76\, t \sqrt{\frac{E}{\Upsilon_{mo}\ \sigma_{com,Ed}}}$$

$$s_{eff,0} = 0.76 * 0.85 \sqrt{\frac{210000}{1 * 420}}$$

$$s_{eff,0} = 14.44$$

$$s_{eff,1} = s_{eff,0} = 14.44$$

$$s_{eff,2} = \left(1 + \frac{0.5 * 41.26}{135.53}\right) * 14.44$$

$$s_{eff,2} = 16.64$$

$$s_{eff,3} = \left(1 + \frac{0.5(\ 41.26 + 4.25)}{135.53}\right) * 14.44$$

$$s_{eff,3} = 16.87$$

$$s_{eff,n} = 1.5 * 14.44$$

$$s_{eff,n} = 21.66$$

The values are then revised

$$s_{eff,1} + s_{eff,2} \geq \ \ s_a = 42.92$$

$$14.44 + 16.64 = 31.08 < \ \ s_a = 42.92$$

$$s_{eff,3} + s_{eff,n} \geq \ \ s_n = 93.36$$

$$16.87 + 21.66 = 38.53 < \ \ s_a = 93.36$$

It means that the web is not fully active

$$s_1 = \ s_a + \ s_{sa} + s_b + 0.5(s_{sb} + s_c)$$

$$s_1 = \ 42.92 + \ 9.62 + 112.67 + 0.5(9.68 + 42.81)$$

$$s_1 = \ 191.455$$

$$s_2 = s_1 - \ s_a - \ 0.5 s_{sa}$$

$$s_2 = 191.455 - \ 42.92 - \ 0.5 * 9.62$$

$$s_2 = 143.725$$

Effective area of the stiffener is:

$$A_{sa} = t(s_{eff,2} + s_{eff,3} + s_{sa})$$

$$A_{sa} = 0.85(16.64 + 16.87 + 9.62)$$

$$A_{sa} = 36.66 mm^2$$

For the calculation of web stiffener's moment of inertia,

The centroid axis of the web stiffener is:

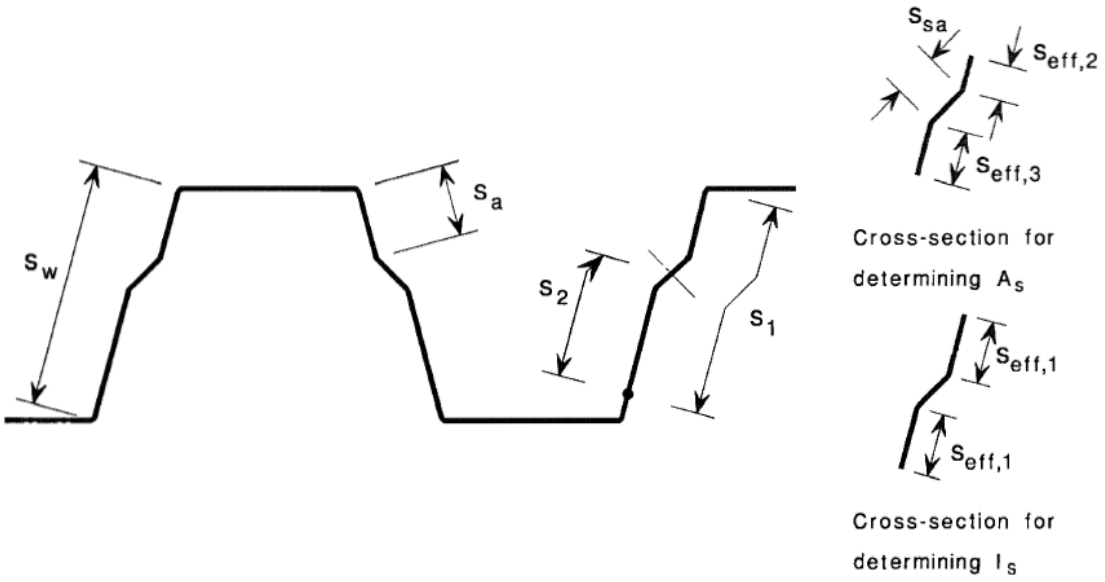

$$\bar{y}_{sa} = \frac{A_{\text{eff},1}\left(\bar{y}_{\text{eff},1}\right) + A_{\text{eff},1}\left(\bar{y}_{\text{eff},1}\right) + A_{\text{ssa}}(\bar{y}_{\text{ssa}})}{\text{A}_{\text{sa}}}$$

$$\bar{y}_{sa} = \frac{12.28\ (0.425) + 12.28\ (9.03) + 8.18(4.73)}{32.74}$$

$$\bar{y}_{g,s} = 4.74mm$$

The moment of inertia of the web stiffener is

$$I_{g,s} = \left[A_{\text{eff},1}\left(\bar{y}_{\text{eff},1} - \bar{y}_{sa}\right)^2\right] + \left[A_{\text{eff},1}\left(\bar{y}_{\text{eff},1} - \bar{y}_{sa}\right)^2\right] + \left[A_{\text{ssa}}\left(\bar{y}_{\text{ssa}} - \bar{y}_{sa}\right)^2\right]$$

$$I_{g,s} = 473.8mm^4$$

$$\sigma_{cr,s} = \frac{1.05k_f E\sqrt{I_s t^3 s_1}}{A_{sa}\ s_2(s_1 - s_2)}$$

$$\sigma_{cr,s} = \frac{1.05 * 1 * 210000\sqrt{473.8 * 0.85^3 * 191.46}}{36.66 *\ 143.73 * (191.46 - 143.73)}$$

$$\sigma_{cr,sa} = 206.94\ N/mm^2$$

$$\sigma_{cr,mod} = \frac{\sigma_{cr,s}}{\sqrt[4]{1 + [\beta_s \frac{\sigma_{cr,s}}{\sigma_{cr,sa}}]^4}}$$

$$\beta_s = \left(1 - \frac{h_a + 0.5 * h_{sa}}{e_c}\right)$$

$$\beta_s = \left(1 - \frac{41.26 + 0.5 * 4.26}{135.53}\right)$$

$$\beta_s = 0.68$$

$$\sigma_{cr,mod} = \frac{1429.28}{\sqrt[4]{1 + [0.68 * \frac{1429.28}{206.94}]^4}}$$

$$\sigma_{cr,mod} = 304.16\ N/mm^2$$

$$\bar{\lambda}_d = \sqrt{\frac{f_{yb}}{\sigma_{cr,mod}}}$$

$$\bar{\lambda}_d = \sqrt{\frac{420}{304.16}}$$

$$\bar{\lambda}_d = 1.18$$

$$for\ 0.65 < \bar{\lambda}_d < 1.38$$

$$\chi_d = 1.47 - 0.723\,\bar{\lambda}_d$$

$$\chi_d = 1.47 - 0.723 * 1.18$$

$$\chi_d = 0.62$$

The reduced effective area for the flange stiffener will be:

$$A_{s,red} = \chi_d A_s \frac{f_{yb}/\gamma_{M0}}{\sigma_{com,Ed}}$$

$$A_{s,red} = 0.62 * 55.182 * \frac{420/1}{420}$$

$$A_{s,red} = 34.213$$

$$t_{red} = t\ \frac{A_{s,red}}{A_s}$$

$$t_{red} = 0.85\ \frac{34.213}{55.182}$$

$$t_{red} = 0.527$$

The reduced effective area of the web stiffeners will be:

$$A_{sa,red} = \frac{\chi_d A_{sa}}{1 - (h_a + 0.5h_{sa})/e_c}$$

$$A_{sa,red} = \frac{0.62 * 36.66}{1 - (41.25 + 0.5 * 4.25)/135.53}$$

$$A_{sa,red} = 33.43$$

Using the reduced areas for flange and web stiffeners, total properties of the section were calculated;

$$I_{eff} = 4481600\ mm^4/\text{m}$$

$$\bar{y}_{g,s} = 149.43mm$$

$$W_{eff} = 29991.90922\ mm^4/\text{m}$$

Since the support cleats are provided; so the capacity will be checked for moment resistance only

$$M_{c,Rd} = W_{eff} * \frac{f_{yb}}{\Upsilon_{Mo}}$$

$$M_{c,Rd} = 2999.190922 * \frac{420}{1}$$

$$M_{c,Rd} = 12.60\ kN - m\ /\text{m}$$

The obtained value of 0.85mm thickness small flange section is close to Lindab value 13.26 kN-m/m.